Annual Report 1994

Chemical Structure and Dynamics

Environmental Molecular Sciences Laboratory

Pacific Northwest Laboratory
Operated by Battelle Memorial Institute
for the U.S. Department of Energy

PACIFIC NORTHWEST LABORATORY
operated by
BATTELLE MEMORIAL INSTITUTE
for the
UNITED STATES DEPARTMENT OF ENERGY
under Contract DE-AC06-76RLO 1830

Printed in the United States of America

Available to DOE and DOE contractors from the Office of Scientific and Technical Information, P.O. Box 62, Oak Ridge, TN 37831; prices available from (615) 576-8401.

Available to the public from the National Technical Information Service, U.S. Department of Commerce, 5285 Port Royal Rd., Springfield, VA 22161

DISCLAIMER

Portions of this document may be illegible in electronic image products. Images are produced from the best available original document.

PNL-10700
UC-400

Annual Report 1994
Chemical Structure and Dynamics

Prepared by
Steven D. Colson Associate Director
and the staff of the Chemical Structure
and Dynamics Program

July 1995

Prepared for the U.S. Department of Energy
under contract DE-AC06-76RLO 1830

Pacific Northwest Laboratory
Operated for the U.S. Department of Energy
by Battelle Memorial Institute

Contents

6. Miscellaneous

7. Appendix

Funding Support

[a] DOE Office of Basic Energy Sciences, Chemical Sciences Division, Fundamental Interactions Branch.

[b] PNL Laboratory Directed Research and Development (LDRD).

[c] Cooperative Research and Development Agreement (CRADA).

[d] Instrument development under the EMSL Project.

[e] Strategic Environmental Research and Development Program(SERDP).

[f] National Science Foundation.

[g] DOE Office of Environmental Restoration and Waste Management—EM-50 Characterization, Monitoring, and Sensor Technology Integrated Program.

[h] DOE Office of Nonproliferation and National Security.

[i] Atmospheric Radiation Measurement (ARM) Program, Global Climate Change Initiative.

1. Introduction

Purpose

The Chemical Structure and Dynamics program was organized as a major component of Pacific Northwest Laboratory's Environmental and Molecular Sciences Laboratory (EMSL), a state-of-the-art collaborative facility for studies of chemical structure and dynamics. Our program responds to the need for a fundamental, molecular-level understanding of chemistry at the wide variety of environmentally important interfaces by (1) extending the experimental characterization and theoretical description of chemical reactions to encompass the effects of condensed media and interfaces, and (2) developing a multidisciplinary capability for describing interfacial chemical processes within which the new knowledge generated can be brought to bear on complex phenomena in environmental chemistry and in nuclear waste processing and storage.

This research effort was initiated in 1989 and will continue to evolve over the next few years into a program of rigorous studies of fundamental molecular processes in model systems, such as well-characterized surfaces, single-component solutions, clusters, and biological molecules; and studies of complex systems found in the environment (multispecies, multiphase solutions; solid/liquid, liquid/liquid, and gas/surface interfaces; colloidal dispersions; ultrafine aerosols; and functioning biological systems).

The success of this program will result in the achievement of a quantitative understanding of chemical reactions at interfaces, and more generally in condensed media, that is comparable to that currently available for gas-phase reactions. This understanding will form the basis for the development of *a priori* theories for predictions of macroscopic chemical behavior in condensed and heterogeneous media, adding significantly to the value of field-scale environmental models, the prediction of short- and long-term nuclear waste storage stabilities, and other problems related to the primary missions of the DOE.

The group has developed research efforts in the following areas:

- Chemical structures, reaction dynamics, and kinetics in solution and at interfaces, to support DOE needs for
  - characterization, processing, and storage of mixed wastes;
  - remediation of contaminated soils and groundwater;
  - global change and other DOE needs, including nuclear nonproliferation.

- Establishment and operation of a portion of EMSL, including
  - surface/interface structure and reactions ;
  - chemical structure and reaction dynamics (clusters, reactive species & model systems);
  - time-resolved solution spectroscopy.

- Structure/function research on molecular systems, especially on problems associated with
  - surface chemistry and catalysis;
  - bioremediation;
  - high-energy processes.

- Development of state-of-the-art analytical methods for the characterization of tanks and plumes, and for detection and monitoring of trace atmospheric species.

Background

Studies of the surface chemistry at interfaces requires measurements of many chemical and physical properties within 5 to 10 Å of the interface boundary. An understanding of the interfacial chemistry can be achieved only by combining measured quantities such as chemical dynamics, structure, and bonding with theoretical analysis, to produce models consistent with the observations. This interdisciplinary approach is the heart of the EMSL concept, in which a wide variety of experimental and theoretical approaches are brought together to address complex problems of importance to the United States Department of Energy (DOE).

We have targeted condensed-phase phenomena that are relevant to chemical processes in natural and contaminated systems, including those related specifically to environmental restoration and waste storage issues at DOE sites. For example, systems have been selected to model the sorption and abiotic transformations of solutes on mineral

surfaces in soil and groundwater. Sorption and surface-catalyzed abiotic transformations are widely recognized contributors to the natural filtration capacity of soil and aquifer porous media for contaminants, and are therefore of central importance in governing contaminant transport rates and persistence. Mechanistically valid models of such phenomena at the microscopic and macroscopic scales are critically needed to predict contaminant migration on DOE sites, but are unavailable because the responsible surface chemical reactions are not completely understood.

Achievement of a quantitative understanding of chemical reaction dynamics at interfaces in condensed media is an important emerging frontier for chemical physics research. It is a challenging and demanding scientific problem requiring an understanding of the solid substrate, the solvent, and their combined effect upon the chemical reaction dynamics. It is now possible, however, to bring together diverse expertise and technology to study complex interfacial chemistry. Such a study requires integration of state-of-the-science experimental capabilities for the study of primary chemical processes, with advances in computational technology and sophisticated new theoretical models for predicting molecular structure and potential energy surfaces. Essential for the success of this program is the creation of a stimulating and interactive intellectual environment, where concepts and ideas from theoretical and experimental disciplines can be integrated to produce a comprehensive approach to the study of complex phenomena. The EMSL organization and laboratory structure are designed to provide the development of this environment through internal and external collaborations.

Chemical reactivity at environmental solid-liquid interfaces is controlled by the effects of substrate structure on the interactions between solvent and adsorbate solute molecules. In order to observe chemical changes at these interfaces, experimental methods are required to measure the changes in molecular structure and dynamics that are induced by natural and man-made surfaces. Reactions and thermodynamic properties that are enhanced at environmental interfaces include: (1) proton transfer reactions such as solute hydrolysis and acid dissociation; (2) electron transfer transformations; and (3) stability constants for adsorbate-substrate complexes. These interfacial phenomena strongly impact contaminant dynamics in soil and groundwater. However, the responsible molecular phenomena are not well understood, thereby precluding development of rigorous descriptive models. We anticipate that targeted experiments on model systems containing oxides, carbonates, and silicates in contact with solvent and solute molecules relevant to DOE sites can resolve much of the scientific ambiguity regarding interfacial reactions in geochemical systems. Such studies of interfacial chemistry will also have obvious and perhaps far-reaching consequences for our understanding of processes that affect process waste chemistry and waste form integrity when combined with the specific studies of energetic reaction mechanisms contained in the scope of this work.

The CS&D group has particular expertise in the preparation and spectroscopic analysis of molecular clusters (S. D. Colson, W. P. Hess, D. Ray, S. W. Sharpe, and L. S. Wang); ultrafast and nonlinear optical spectroscopies (D. Ray, G. R. Holtom, and X. Xie); ultrahigh resolution spectroscopy for measurements of electronic and geometric structures and dynamics (R. S. McDowell and S. W. Sharpe); surface and interface structure, chemical reaction dynamics, and kinetics (J. P. Cowin, D. M. Friedrich, S. A. Joyce, B. D. Kay and T. M. Orlando); and ion-molecule traps and storage technology (S. E. Barlow).

Approach

Experimental studies of molecular and supramolecular structures and thermodynamics are key to understanding the nature of matter, and lead to direct comparison with computational results. Kinetic and mechanistic measurements, combined with real-time dynamics measurements of atomic and molecular motions during chemical reactions, provide for a molecular-level description of chemical reactions. The anticipated results of this work are the achievement of a quantitative understanding of chemical processes at complex interfaces, the development of new techniques for the detection and measurement of species at such interfaces, and the interpretation and extrapolation of the observations in terms of models of interfacial chemistry.

Our methodology dissects complex interfacial problems into components that are subject to quantitative investigation and interpretation in terms of the component effects for solvent-reactant-substrate systems. Target solvent-reactant-surface systems have been selected for study because of their theoretical interest and applicability to DOE environmental problems. The theoretical basis for understanding the system is based upon the literature data base, augmented by new measurements on synthetic interfaces of controlled composition and structure. The interpretations are supported by the understanding of molecular processes observed via molecular dynamics and structural measurements of gas-phase clusters, on macroscopic solid surfaces, and in solution.

The interfacial chemistry work focuses on the epitaxial growth of doped water (as amorphous ice) layers on metal oxide surfaces. Within these structures, direct measurements can be made of diffusion, dissolution, bimolecular reactions, and electrochemical reactions. Extrapolation of these findings to more complex, natural systems is facilitated by theoretical models and through the results of direct liquid-phase and liquid-solid interface measurements. Using the near-field optical microscope, for example, the fate of a single molecule in solution or at an interface can be probed without averaging over the spatially and temporally inhomogeneous environments of all like molecules in the same sample.

Many of the interfacial chemistry problems facing the DOE involve mixed organic/inorganic/radioactive materials. Thus, we also need to address high-energy processes unique to this type of waste form. The primary molecular processes are ionization and dissociation and reaction of high-energy species. These processes are being studied in molecules, clusters, solutions, and at interfaces. The work on model systems (clusters, solvated molecules, surfaces and interfaces) thus has an important additional dimension: understanding the effects of the condensed phase on high-energy processes.

Isolated, gas-phase clusters of atoms that compose the actual surface are being synthesized to mimic surface structures. Spectroscopic determination of their structures is important to the evaluation of the many approximations that must be made in developing theoretical models of their chemical properties. Solvent-solvent and solvent-surface interactions are studied in a similar manner. Studies of both pure solvent and mixed solvent-substrate clusters help delineate the importance of the classes of forces required to model the solvent effects. Likewise, reactant-substrate, reactant-solvent and, potentially, solvent-reactant-substrate systems can be modeled as isolated clusters. These are very complex systems, even when cast in the form of model clusters. Our approach is to use the common practice of experimental extrapolation: small, simpler systems are subjected to quantitative theoretical and experimental analysis. This analysis forms the basis for understanding of more complex systems with the aid of approximate theories and less quantitative experimental data. For instance, while it may not be possible to get detailed structural data on solvent-reactant-substrate clusters, measurements of chemical reaction dynamics in these clusters can be modeled with approximate theories tested previously by their application to simpler systems. In the long term, we intend to deposit clusters (and other chemical species) designed to mimic reactive sites on inert substrates and study their chemical activity. This work also has the potential for producing *designer surfaces* which may be valuable as chemical sensors, or for development of unique materials for chemical separations.

Our activities in calendar 1994 are summarized in this report.

2. Reaction Mechanisms at Interfaces

Structure and Reactivity of Ice Surfaces and Interfaces

C. Huang, E. K. L. Wong,* R. S. Smith, and B. D. Kay*

Supported by Office of Basic Energy Sciences.

*Postdoctoral Research Associate.

Molecular beam scattering from surfaces is a powerful experimental tool for studying the dynamics and kinetics of the interaction of molecules with surfaces. The coupling of surface science, molecular beam, and laser technologies makes possible the measurement of total energy disposal and redistribution in gas-surface scattering. Previously these experimental methods have been employed to acquire detailed surface kinetics and state-to-state scattering measurements of molecules interacting with metallic substrates. Such experiments have resulted in a fairly detailed understanding of surface chemistry on metals. Unfortunately, we currently do not have a similar understanding of the elementary dynamical and kinetic processes occurring on ice and oxide surfaces. Such interactions are clearly important from an environmental viewpoint, since they form the molecular level basis for the complex physiochemical processes that take place on the surface of atmospheric aerosols, at the aqueous-mineral geochemical interface, and at the vapor-liquid interface. Our goal is to apply and extend molecular beam surface scattering techniques to these systems in an effort to elucidate the relevant interactions.

In this project the chemisorption and solvation kinetics and dynamics of polar molecules on multilayer ice surfaces are studied using molecular beam-surface scattering, thermal desorption (TPD and isothermal), and laser spectroscopic techniques. These experiments will help unravel the mechanism by which a strongly polar neutral molecule dissolves into an aqueous solvent and ultimately forms solvated ions. Sticking coefficients of prototypical "electrolytes" such as HCl and NH_3 on ice surfaces will be determined as a function of incident energy, angle, and surface temperature. The branching ratio between molecular vs. dissociative ("solvation") chemisorption will be probed via isotope exchange between the hydrogens of the "electrolyte" and the "solvent" substrate. In related experiments hydrophobic and hydrophilic interactions between water and various other materials will be probed using beam-generated thin films. Interlayer diffusion and phase separation will be probed using thermal desorption and surface analytic techniques.

Our initial efforts have focused on the synthesis of thin films of H_2O and D_2O ice grown on Au(111) and Ru(0001) substrates. These substrates were chosen because water wets Ru but does not wet Au. Combining molecular beam dosing with isothermal and temperature-programmed desorption techniques, we are able to grow and characterize ultrathin films (<1000 Å) of solid H_2O and D_2O. Using a molecular beam reflection technique, we have determined that the sticking coefficient is unity and independent of incident angle for surface temperatures below 130 K. Above 130 K the condensation coefficient decreases due to the onset of desorption but the trapping probability remains near unity. This is the first *direct* measurement of the condensation coefficient of gaseous water on ice surfaces. Previous indirect techniques have yielded conflicting values between 0.01 and 1 for the sticking coefficient. Figure 2.1 displays the experimentally determined condensation coefficient for three values of the incident molecular beam flux. It is clearly evident from this figure that the condensation coefficient is dependent upon both flux and substrate temperature. The dashed line represents the value of the condensation coefficient predicted by a simple kinetic model that assumes the trapping probability is unity for all substrate temperatures and the desorption kinetics follow a zero-order Arrhenius rate law. The combined temperature and flux dependence of the condensation coefficient combined with naive kinetic models is the source of previous confusion regarding the value of the water sticking coefficient on ice.

At temperatures below 140 K the initial water deposited forms a vitreous solid phase that is metastable with respect to crystalline ice. The existence of this metastable phase has been known for a long time, but the rate and mechanism by which it crystallizes is not understood. By an extensive series of careful desorption measurements (both temperature-programmed and isothermal) we were able to study the attendant crystallization kinetics quantitatively. The desorption kinetics are extremely sensitive to this phase trans-

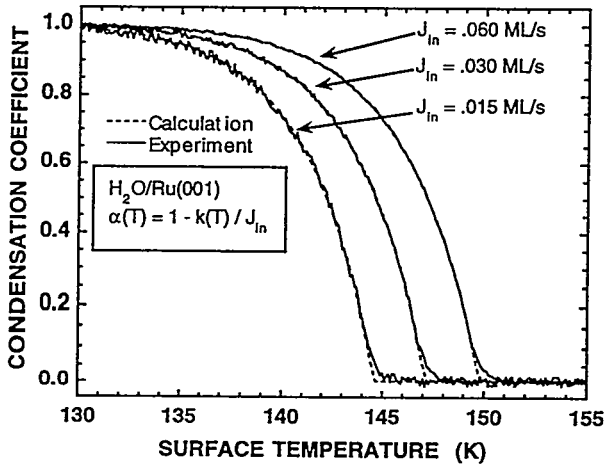

Figure 2.1. The experimentally measured condensation coefficient for water on ice as a function of substrate temperature is shown by the solid lines. These curves show that the condensation coefficient is both incident-flux and substrate temperature dependent. The dashed lines are a calculation assuming a trapping probability of unity and zero-order Arrhenius desorption kinetics.

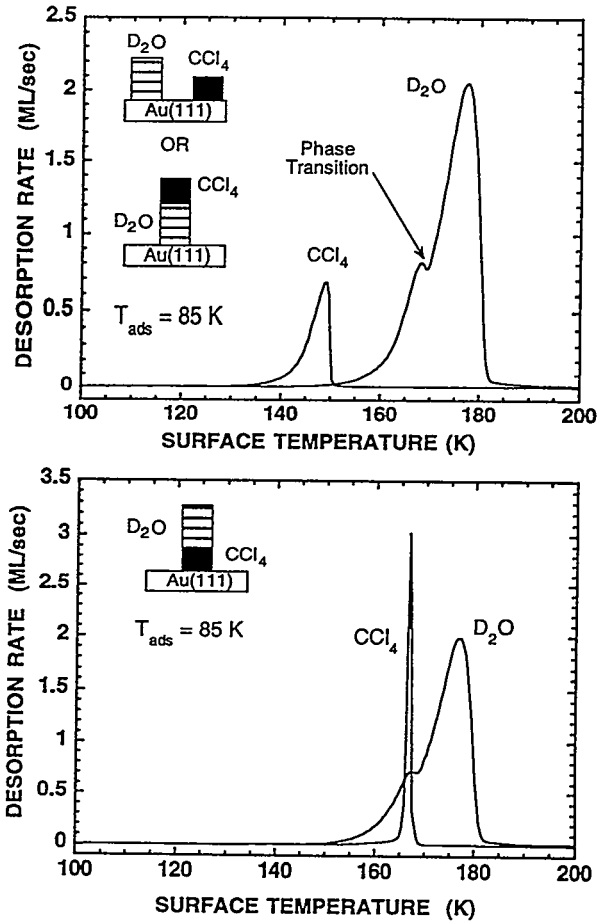

Figure 2.2. (a) Upper Panel: TPD spectra for nanoscale films of CCl_4 grown on top of amorphous ice. The spectra show the desorption of nearly all of the CCl_4 prior to any significant D_2O desorption. The "bump" in the D_2O spectrum is the result of the amorphous to crystalline phase transition. (b) Lower panel: TPD spectra for nanoscale films of amorphous ice grown on top of CCl_4. The spectra show that the CCl_4 is trapped beneath the ice until the phase transition occurs. In concert with the phase transition the CCl_4 desorbs abruptly, the "molecular volcano."

formation, since the additional free energy stabilization associated with the crystalline state must now be overcome to achieve sublimation into the vapor phase. To our knowledge, this is the first time such a transition has been observed in desorption. We observe a large isotope effect in the crystallization rate, with H_2O having a faster rate. Interestingly, the TPD spectra for films grown on Au and Ru appear surprisingly similar. However, isothermal measurements clearly indicate that the desorption kinetics are substrate-sensitive. In contrast to conventional wisdom, the desorption kinetics exhibit marked departures from zero-order behavior. Quantitative analysis of the isothermal desorption waveform yields an order of $\sim^2/_3$ for Au and $\sim^1/_5$ for Ru. We have developed a quantitative kinetic model to explain these observations.

In related experiments, we examined the desorption kinetics of multilayer films of CCl_4 and water. CCl_4 and water are immiscible, and, as such, are an ideal model system for studying hydrophobic interactions. Using molecular beams, we can create nanoscale thin films with high spatial resolution. Figure 2.2 displays TPD spectra for films composed of CCl_4 and D_2O. The upper panel (Fig. 2.2a) shows the TPD spectra for films where CCl_4 resides on top of an amorphous ice film. The resulting TPD spectra are indistinguishable from samples in which CCl_4 and D_2O are deposited in separate columns. Since the desorption rate of CCl_4 is greater than that of D_2O, its desorption is essentially complete prior to significant D_2O desorption. The "bump" in the D_2O desorption trace arises from the crystallization of amorphous ice.

As clearly demonstrated in Fig. 2.2b, CCl_4 desorption is impeded by the presence of a water overlayer and desorption occurs in dramatic fashion in

concert with the crystallization of amorphous ice. We term this dramatic effect the "molecular volcano." By examining the molecular volcano as a function of water thickness and substrate temperature we can determine a percolation threshold for the crystallization of amorphous water. In physical terms this percolation threshold arises when a connected path is formed within the water overlayer that enables the underlying CCl_4 to escape.

In an effort to further characterize the crystallization kinetics we have examined both H/D and $^{16}O/^{18}O$ isotopic exchange as a function of film thickness, temperature, and crystalline state. Surprisingly, we find complete H/D isotopic scrambling over distances up to 250 Å at temperatures as low as 150 K. The H/D isotope exchange kinetics alone cannot definitively indicate whether there is large-scale molecular motion because of the possibility of a tunneling and/or rotation exchange mechanism. The ^{18}O-labeled ice experiments shown in Fig. 2.3, however, do clearly indicate that mass transport occurs at a measurable rate within these solid films. We are currently using this experimental data to formulate a mechanistic kinetic model for the crystallization process.

Based upon the progress to date we are now able to begin a detailed study of the interaction of various molecules with well-characterized ice substrates. Initial efforts will focus on the adsorption, desorption, and reaction kinetics of CH_3OH, NH_3, and HCl with ultrathin ice films. Concurrent with these studies of model hydrophilic interactions we will continue to explore hydrophobic interactions by extending our studies of the interaction of chlorinated hydrocarbons with the ice substrates. After we demonstrate the utility of our approach to understanding solvation phenomena, we will extend the experiments to include quantum-resolved measurements of the nascent rovibrational distributions of the products which are scattered from the ice substrates. In related experiments we will explore the applicability of using this *"thin-film chemistry"* to create chemically tailored substrates that mimic the aqueous-mineral geochemical interface.

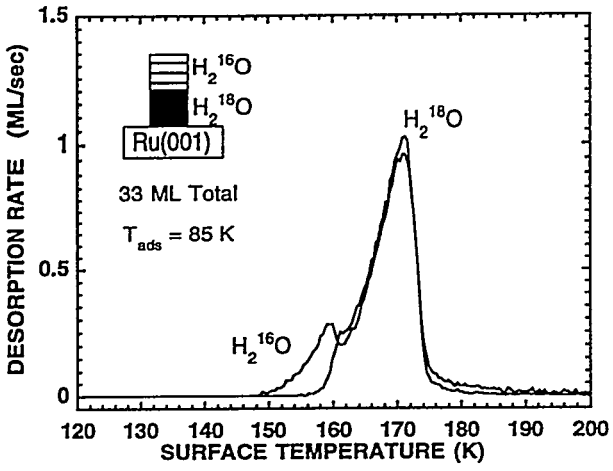

Figure 2.3. TPD spectra for films of $H_2{}^{16}O$ ice grown on top of $H_2{}^{18}O$ ice. The spectra show that prior to the phase transition the isotopically labeled ices have not mixed. After the phase transition, complete mixing is observed. These results indicate that long-range molecular diffusion occurs during the phase transition.

Chemisorption on Oxide Surfaces

C. Huang, E. K. L. Wong,* R. S. Smith, B. D. Kay, and S. A. Joyce*

Supported by Laboratory Directed Research and Development (LDRD).

*Postdoctoral Research Associate.

The objective of this program is to examine chemical phenomena occurring at model oxide surfaces. Oxide interfaces are important in the subsurface environment. Specifically, molecular-level interactions at mineral surfaces are responsible for the transport and reactivity of subsurface contaminants at Hanford. Unfortunately, our molecular-level understanding of oxide surface chemistry is severely lacking. Initial experiments will focus on the dissociative chemisorption dynamics of halogenated hydrocarbons (e.g., CCl_4, $CHCl_3$, CH_2Cl_2, CH_3Cl), H_2O, CH_3OH, NH_3, and HCl on model oxide surfaces (e.g., MgO, SiO_2, and Al_2O_3). These studies will employ variable-energy supersonic molecular beams to determine energy-, angle-, and coverage-dependent trapping and/or dissociation probabilities. In addition to using bulk single-crystal samples, a variety of techniques such as molecular beam epitaxy and/or chemical vapor deposition will be explored to grow epitaxial thin oxide films on single-crystal metallic substrates. The successful synthesis of such crystalline thin oxide films will enable the entire arsenal of electron-based surface analytical techniques to be

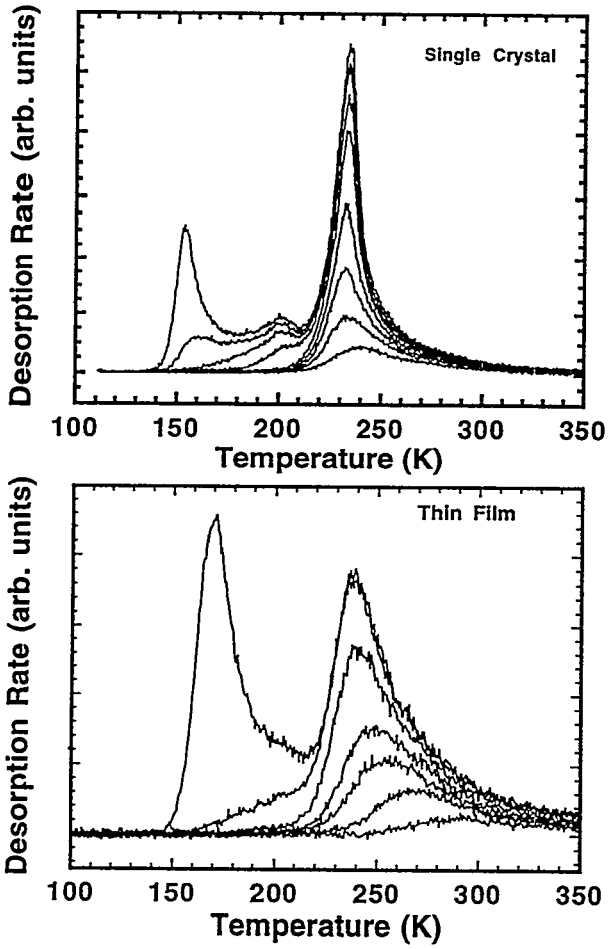

Figure 2.4. TPD spectra for D_2O desorption from bulk single-crystal MgO(100) (upper panel) and thin film MgO grown on Ru(0001) (lower panel). The high-temperature monolayer desorption feature is substrate dependent.

applied to the characterization of these nonconducting materials.

During FY94 we developed a sample mount that enables us to rapidly heat and cool bulk single-crystal samples of oxide surfaces. Figure 2.4 displays TPD spectra for D_2O desorption from bulk single-crystal MgO(100) (upper panel) and MgO thin films grown on Ru(0001) (lower panel). The thin-film results are similar to those obtained by Goodman et al. and Cowin and coworkers for MgO grown epitaxially on Mo(100), a square lattice. There are qualitative similarities between D_2O adsorption onto and desorption from the single crystal and thin film substrates. On both substrates D_2O adsorbs via precursor-mediated kinetics with a sticking coefficient near unity, and largely independent of coverage and surface temperature up to 200 K. On both substrates the desorption spectra exhibit two prominent features: a high-temperature peak (~235 K) that saturates at a coverage corresponding to approximately 1 water molecule per surface metal ion, and a nonsaturable low-temperature peak (~160 K) indicative of the formation of an ice-like multilayer. Careful examination of the high-temperature TPD feature reveals that the sub-monolayer water desorption kinetics are strongly substrate-dependent. Water desorption from the single-crystal substrate results in a TPD feature that increases with increasing exposure and has a peak at 235 K for all coverages above 0.1 monolayers. Water desorption from the thin-film substrate results in a TPD feature that increases with increasing exposure and has a peak that shifts smoothly from 290 K at low coverage to 235 K at saturation coverage.

The line shape of the TPD spectrum and how the peak temperature shifts with increasing coverage are often used to infer the molecular nature of the adsorbate. TPD peaks yielding coverage-independent maxima are indicative of first-order kinetics and suggest molecular adsorption. TPD peaks that shift to lower temperature with increasing coverage are indicative of second-order kinetics and suggest dissociative chemisorption. Based on this, we hypothesize that water adsorbed on the bulk single crystal is largely molecular in nature, while water adsorbed on the thin film is predominately dissociated. The hydroxylation of MgO by water to form $Mg(OH)_2$ is exothermic by ~15 kcal/mole, but may not occur at a measurable rate on the basal plane of MgO(100). Hydroxylation of the thin-film substrate may be more facile due to the presence of coordinatively unsaturated surface defects that catalyze the hydrolysis. Since the sticking coefficient is determined to be unity, there is no kinetic barrier to adsorption. From the data to date, we are unable to determine definitively whether the adsorption is molecular or dissociative. Current efforts are focused on examining the interaction of water with surface defects created on the bulk single crystal by rare gas ion sputtering to address this important issue.

Scanning Tunneling Microscopy of Epitaxial Oxide Films

*S. A. Joyce, J. P. Cowin, and M. C. Gallagher**

Supported by Laboratory Directed Research and Development (LDRD).

*Postdoctoral Research Associate.

Many aspects of environmental problems, from soil contamination and transport through the ground water to catalytic remediation schemes, involve the adsorption of molecules on a surface. The scanning tunneling microscope (STM) is capable of imaging solid surfaces and molecular adsorbates with atomic-scale resolution. As a real space probe, the STM can directly determine the role of surface structure, especially at defects such as steps, vacancies, etc., in the adsorption and heterogeneous chemistry of molecules on surfaces.

Unfortunately, many surfaces of relevance to environmental chemistry are unsuitable for detailed studies due to the insulating nature of many oxides, the lack of large, single-phase crystals, and/or difficulties associated with surface preparation. These problems can be obviated by using ultrathin films grown epitaxially on well-characterized, single-crystal, conducting substrates.

1. *MgO on Mo(100)*

In collaboration with M. S. Fyfield, Portland State University.

The growth of microscopically thin films on conducting substrates overcomes the electrical charging problems associated with bulk insulators. To this end we have used in-situ STM to investigate the growth and electronic properties of MgO thin films deposited on Mo(001). We have chosen the growth of magnesium oxide on molybdenum to study for a number of reasons: MgO, with a bandgap of 8 eV, is a prototypical ionic solid insulator, the epitaxial growth on Mo(100) has been demonstrated,[1] and several groups at PNL, both experimental and theoretical, have extensively studied the structure, growth, and chemistry of MgO. The films were grown by evaporating Mg metal in a background pressure of oxygen. We have successfully imaged films as thick as 25 Å, clearly demonstrating the feasibility of this method. Films were grown at substrate temperatures between 300 and 1050 K. Low-temperature growth produced smooth, uniform films with small MgO islands of between 20 to 100 Å. Annealing these films at 1100 K results in domain coalescence and a higher degree of crystalline orientation of the domain edges. Annealing, therefore, significantly reduces the number of edge defects in the films. Images of films grown at high temperature reveal nonwetting behavior with large three-dimensional islands indicating a Volmer-Weber growth mode. Figure 2.5 displays a region of MgO film grown on Mo(100) at 970 K. The rectangular-shaped islands are crystallites of MgO(100) in registry with the underlying and partially exposed Mo substrate. The total vertical relief is ~9 Å, indicating that the films are relatively smooth over macroscopic distances. In contrast to films deposited in a background pressure of oxygen, growth of Mg metal on Mo(001) was pseudomorphic at low coverage. At higher coverage we observed a transition to three-dimensional Mg hexagonal islands, which is consistent with a Stranski-Krastanov growth mode.

Figure 2.5. A 1000 Å × 1000 Å image of MgO on Mo(001) grown at 970 K. Single atomic steps are evident in the Mo substrate. The edges of the square MgO islands are oriented along the MgO(100) direction. Tunneling conditions: 3.3 V, 0.2 nA.

2. *TiO_x on W(110)*

In collaboration with C. H. F. Peden and G. S. Herman,* Materials and Interfaces.

*Postdoctoral Research Associate

Macroscopic single crystals of the rock-salt oxide, $TiO_{x\sim1}$, are not available. Long-range, periodic

structures of ultrathin film TiO_x, however, can be grown on the surface of W(110) substrates.[2] In FY94, a collaboration was begun with members of the Materials and Interfaces group to study with STM the surface structures of these epitaxial films. Films are produced by depositing Ti metal on a room temperature substrate, dosing with molecular oxygen and then annealing. STM and low-energy electron diffraction (LEED) studies reveal a rich structural "phase diagram" for this system which is sensitive to the amount of Ti deposited and to the final annealing temperature. Most of the observed diffraction patterns are quite complex and can only be reasonably interpreted as multiple scattering from both the TiO_x overlayer and the W(110) substrate. An image of a one-monolayer film of TiO_x annealed to 1350 K is shown in Fig. 2.6. The complex, mesoscopic features in the image can be understood in terms of the atomic-scale coincidences which occur between the TiO_x and the underlying substrate.

References

1. M. Wu, J. S. Corneille, J. W. He, C. A. Estrada, and D. W. Goodman, *J. Vac. Sci. Technol. A* **10**, 1467 (1992).

2. G. S. Herman and C. H. F. Peden, *J. Vac. Sci. Technol. A* **12**, 2087 (1994).

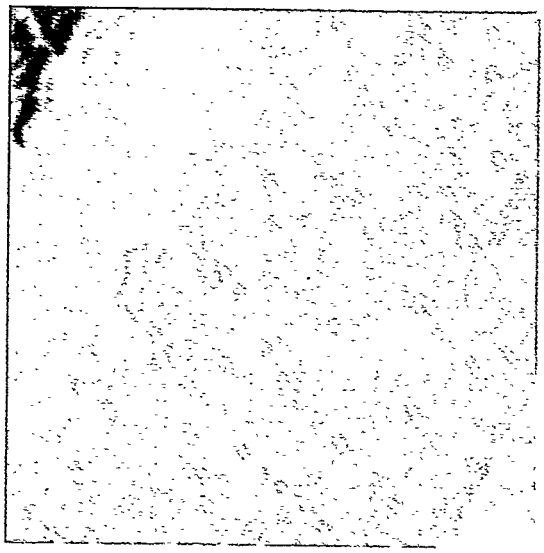

Figure 2.6. A 250 Å × 250 Å image of TiO_x on W(110). The TiO_x coverage is 1 monolayer and the annealing temperature was 1350 K. There are three steps running from the lower left to upper right. The direction along the step is [001]. Tunneling conditions: 1.6 V, 0.15 nA.

Bonding and Structure of Organic Ligands at Oxide/Water Interfaces

D. M. Friedrich, C. C. Ainsworth, and P. L. Gassman**

Supported by Laboratory Directed Research and Development (LDRD).

*Earth and Environmental Sciences Center (EESC).

The objective of this research is to examine the sorption chemistry of organic ligands at the solid-water interface by application of optical spectroscopic methods. In support of this objective, research is being performed (1) to develop state-of-the-art sensitive spectroscopic methods using laser induced fluorescence (LIF) and high-sensitivity infrared spectrometry (FTIR) in novel ways that will allow spectroscopic interrogation of organic ligands at the solid-water interface at low sorbate surface coverage (≤1%); and (2) to use these methods to identify and characterize the nature (bonding, structure, and dynamics) of interfacial organic species.

Interactions between organic ligands and minerals at the solid-water interface are integral to many processes occurring in soils and subsurface materials. These processes include contaminant transport, soil formation, and diagenesis. Often, these interactions are characterized as surface complexation reactions and are assigned a structure based on inadequate data. Under these conditions, modeling efforts are little more than exercises in curve fitting. In order to better understand and simulate important aqueous-mineral interfacial phenomena, it is crucial to obtain spectroscopic data concerning speciation, structures, and dynamics of organic ligands at the aqueous-mineral interface under controlled conditions that are still relevant to the natural environment.

The current investigations are performed using salicylic and phthalic acids (mono- and diprotic acids, respectively) as probes, and Al_2O_3 as the mineral interface. The two aromatic acids were chosen because they are both fluorophores and they are reported in the literature as model compounds for the study organic ligand surface speciation (bonding, structure) as a function of important geochemical variables (pH, ionic strength, surface loading). Al_2O_3 was chosen because of its spectroscopically benign nature (i.e., IR and UV

transmittance and weak Raman interference). Most experiments are performed in constant-temperature, dilute suspensions (1 g/l) of Al_2O_3, and low concentrations of the organic ligand (10^{-7} *M*).

Fluorescence spectra of sodium salicylate has been detected at levels of less than one salicylate ion per alumina particle. (At 10^{-7} *M* bulk concentration, 90% of the salicylate ions are adsorbed, corresponding to 0.7 molecules/particle in alumina suspension of 1 g/l rated at 100 m^2/g.) This level of sensitivity was achieved with standard xenon lamp excitation in a commercial fluorometer. This year we achieved improved levels of sensitivity and signal/noise by means of polarized UV laser excitation. Use of LIF permits lower suspension loading which, in turn, will lead to reduced levels of stray-light scattering and improved measures of polarization anisotropy (discussed below). We estimate detection limits of sorbed salicylate in alumina suspensions to be less than 10^{-10} *M* using the current LIF apparatus

A key advance from this research this year is the demonstration that fluorescence anisotropy measurements can be used to confirm and characterize the binding of organic acids to colloidal mineral surfaces in aqueous solution. The method of polarized emission is useful for determining the electronic structure and rotational dynamics of fluorophores. Polarized excitation light "photoselects" the subset of randomly oriented absorbers that have transition moments parallel to the polarization vector of the excitation light (cosine-squared distribution). If the absorbers are prevented from rotational diffusion during the fluorescence lifetime, then the emission from the photoselected subset also will be polarized. Rotational diffusion can be inhibited by using viscous solutions or by attaching the fluorophore to a slowly diffusing body in solution, such as a polymer chain or a colloidal particle. Emission anisotropy measurement have long been used to determine macromolecular dynamics such as protein folding.

Figure 2.7 summarizes the fluorescence results that suggest aqueous salicylate sorbs on colloidal alumina as at least two distinct chemical species. The fluorescence spectrum of free (non-sorbed) salicylate anion peaks at 415 nm in pH 4.5 aqueous solution. When excited at 351 nm, the fluorescence spectrum of sorbed salicylate resembles that of aqueous salicylate (415 nm). However, this fluorescence is anisotropic with a polarization ratio ($N = I_V/I_h$) of approximately 2, suggesting that the species excited at 351 nm is anionic salicylate bound (i.e., not free to rotate on the nanosecond time-scale of the fluorescence emission) at the alumina surface (Fig. 2.8). Excitation at 300 nm reveals the existence of a second, bound species. When excited at 300 nm, the fluorescence of sorbed salicylate exhibits a blue-shifted maximum (387 nm) and a diffuse shoulder (415-420 nm). Like the 415-nm fluorescence, the 387-nm fluorescence band is also polarized, indicating another bound species. The blue shift is characteristic of the emission of salicylate esters (such as methyl salicylate) in which intramolecular hydrogen bonding is prevented by protic solvents. Therefore, we tentatively assign the 387-nm fluorescence to a salicylate-aluminum surface complex (Fig. 2.8). To determine whether the surface complex is mono- or bidentate, mono- or binuclear, will require more detailed vibrational spectroscopic information.

If the adsorption of salicylate to alumina is performed at pH 6 and increasing background electrolyte ionic strength (IS), the intensity of the local maximum decreases as IS increases. This decrease is not observed at pH 4.5. The effect of IS on the intensity of the local maximum is coincident with that observed for the surface concentration of salicylate and pressure-jump relaxation events. These data suggest that there are at least two distinct surface complexes on the alumina surface: the response of the 387 nm maximum and the 415 nm maximum to IS and pH changes correlates to an inner-sphere and outer-sphere surface complex, respectively.

These results challenge current interpretations of the nature of organic acid surface complexes. Outer-sphere ionic species are thought to be rotationally and translationally labile, while our photoselection results indicate sorbed anionic salicylate is rotationally restricted. Reaction-based models of mineral dissolution by organic acid sorption have tended to emphasize covalent inner sphere surface complexes and to ignore or even discount the presence of outer sphere ions. Our results clearly indicate that a substantial fraction of the sorbed salicylate is sorbed in the ionic form. These results will require refinement of reaction-based surface complexation models to include sorbed ionic organic species.

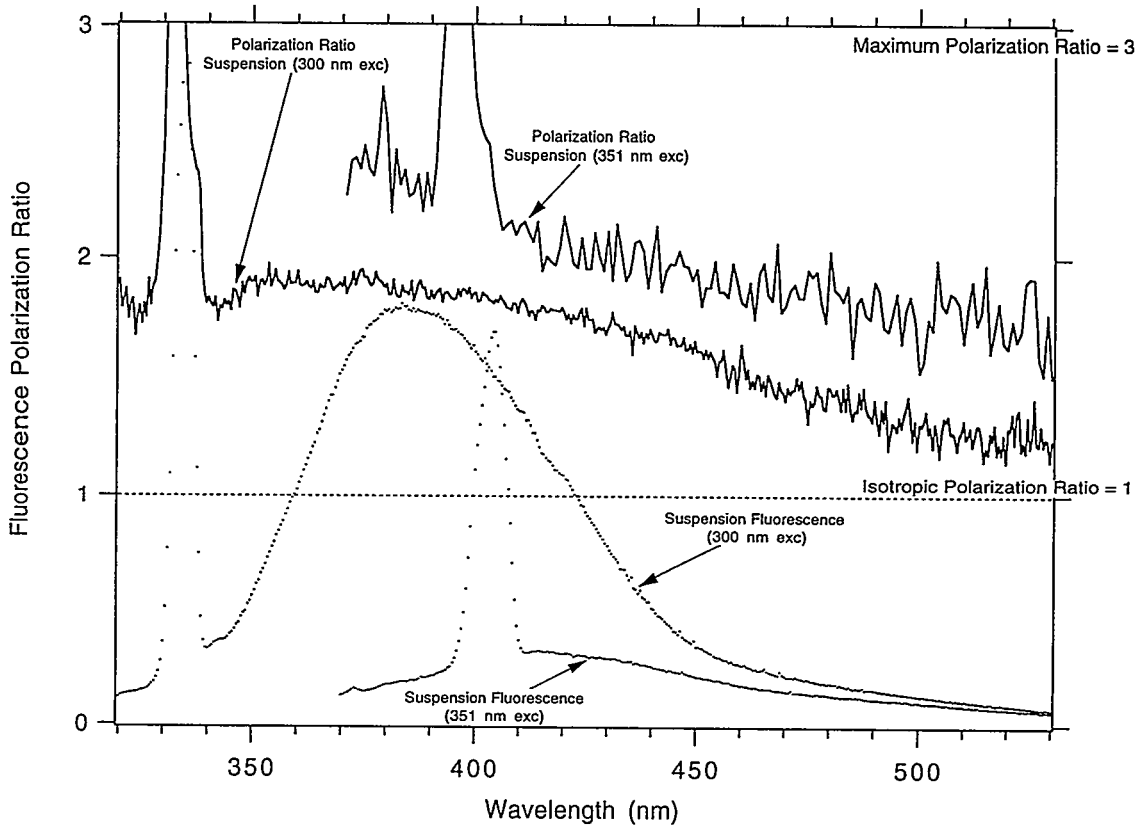

Figure 2.7. Fluorescence spectra and polarization ratio for 10^{-7} *M* sodium salicylate sorbed (90%) to alumina colloidal particles (100 m^2/g) in pH 4.5 suspension (1 g/liter). Bottom curves (·····): fluorescence excited at 300 nm and 351 nm. The fluorescence band excited at 351 nm has the same shape as solution-phase (unbound) salicylate. Upper curves (——): spectral dispersion of fluorescence polarization ratio. For a sample of randomly oriented fluorophores excited by vertically polarized light, the limits of the polarization ratio (I_v/I_h) are $0.5 \leq N \leq 3.0$. Unpolarized fluorescence from unbound, solution-phase salicylate would have unity polarization ratio. The sharp peak in each curve is due to Raman scattering from water. Fluorescence spectra are normalized to constant laser excitation intensity.

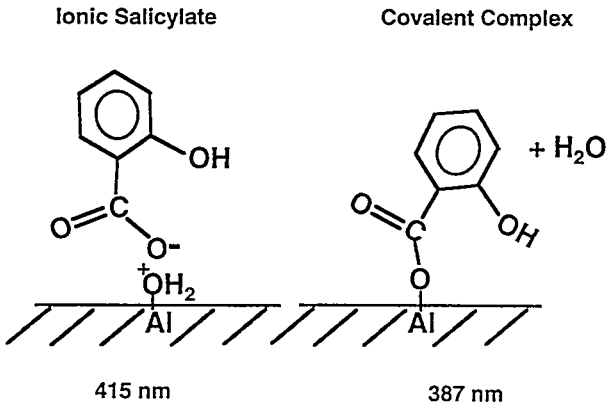

Figure 2.8. Proposed structures of sorbed salicylate. The 415-nm fluorescence band is assigned to an ionic structure. The 387-nm fluorescence band is assigned to an aluminum ester of salicylic acid that may be a mono- or bidentate or binuclear covalent surface complex.

Future work includes establishing methods to correct for the depolarizing effects of multiple light scattering in the turbid suspensions, and determining the electronic state assignment of the aluminum complex by low-temperature photoselection and quantum chemical calculations. The inner-sphere and outer-sphere salicylate species are being distinguished and characterized by measurement of fluorescence lifetimes, quantum yields, and time-resolved fluorescence anisotropy of the sorbed salicylate species.

Single-Molecule Spectroscopy and Dynamics at Interfaces

*X. S. Xie, R. C. Dunn, E. V. Allen,**
*G. R. Holtom, and G. A. Anderson**

Supported by Office of Basic Energy Sciences.
*Applied Physics Center.

Recent advances in near-field fluorescence microscopy[1] make it possible to conduct single-molecule spectroscopy at the nanometric scale in an ambient environment.[2–5] Probing molecules in specific local environments provides unprecedented and detailed information. Using time-resolved single-molecule spectroscopy we can study chemical reactions on individual molecules.

Figure 2.9 shows a typical near-field fluorescence image of single molecules (sulforhodamine 101 dispersed on a glass surface). The different intensities of the peaks are due to the different molecular orientations, which can be determined in all three dimensions. Figure 2.10 shows two room-temperature fluorescence excitation spectra of single molecules (oxazine 725 dispersed on a glass surface), obtained by scanning the wavelength of the excitation light in our near-field microscope. They show distinctly different spectral properties of the single molecules.

There are two classes of time-resolved experiments that enable us to probe single-molecule dynamics:

On the 10^{-2} to 10^{3} second time scale, one can observe single events, such as orientational motions,

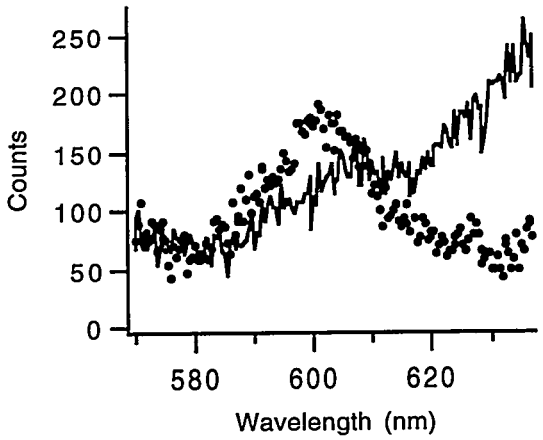

Figure 2.10. Excitation spectra of two single oxazine 725 molecules.

spectral diffusion, and photobleaching. Single-molecule events are usually characterized by abrupt jumps in experimental observables. For example, we have observed intensity fluctuations in the emission from single sulforhodamine 101 molecules dispersed on a glass surface, which are attributed to spectral diffusion (instead of rotational diffusion) of the molecules.[4]

On the picosecond to nanosecond time scale, one can study the dynamics of repetitive processes,[4] making it possible to study photo-induced chemical reactions of single molecules in specific local environments. Figure 2.11 shows the fluorescence decay of a single oxazine 725 molecule dispersed on a glass surface. This molecule undergoes a twisted intramolecular charge transfer reaction on its excited state. Interestingly, we find a distribution in the charge transfer rates for individual

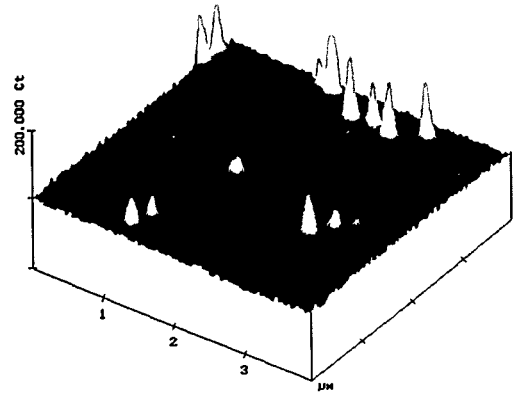

Figure 2.9. Near-field fluorescence image of single sulforhodamine 101 molecules dispersed on a glass surface.

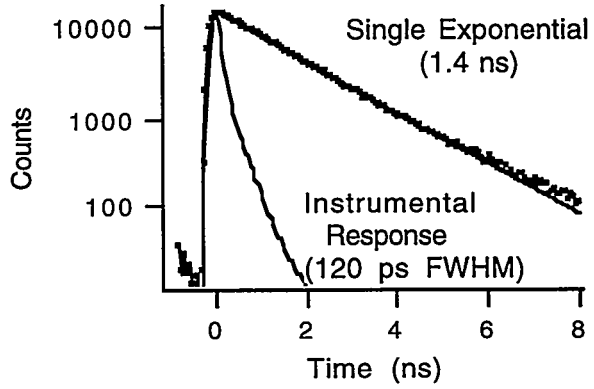

Figure 2.11. Fluorescence decay of a single oxazine 725 molecule undergoing a photo-induced charge transfer reaction.

molecules. Time-resolved fluorescence measurements on a single-molecule basis allow us to study chemical reactions at interfaces with much greater detail than has heretofore been possible.

References

1. E. Betzig and J. K. Trautman, *Science* **257**, 189 (1992).
2. E. Betzig and R. J. Chichester, *Science* **262**, 1422 (1993).
3. J. K. Trautman et al., *Nature* **369**, 40 (1994).
4. X. S. Xie and R. C. Dunn, *Science* **265**, 361 (1994).
5. W. P. Ambrose et al., *Science* **265**, 364 (1994).

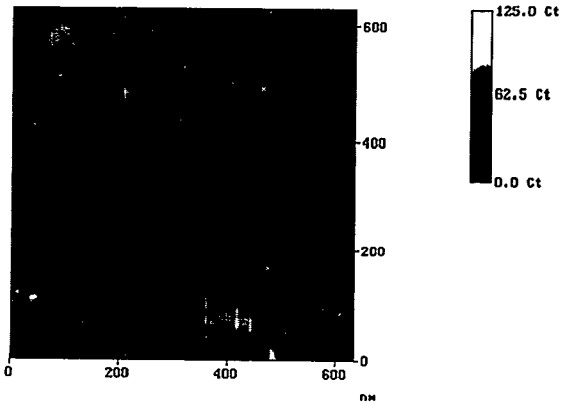

Figure 2.12. A 633 nm × 633 nm near-field fluorescence image of single proteins (allophycocyanin trimers) dispersed on a mica surface.

Photosynthetic Studies with Near-field Fluorescence Spectroscopy

R. C. Dunn, L. Mets, and X. S. Xie*

Supported by Cooperative Research and Development Agreement (CRADA).

*University of Chicago.

The high spatial and time resolution, single-molecule sensitivity, and noninvasive nature of our near-field microscope offer a powerful approach for studying biological systems. In particular, fluorescence measurements with near-field optics offer exciting possibilities for photosynthetic research, providing spectroscopic information not accessible with other high resolution scanning probe techniques such as SEM, STM, and AFM.

In our efforts to study photosynthetic proteins, we have obtained near-field fluorescence images of single allophycocyanin trimers dispersed on a mica substrate.[1–2] Allophycocyanin trimers are disc-like (11 nm × 3 nm) photosynthetic antenna proteins, each containing only six tetrapyrrole chromophores. The near-field fluorescence image shown in Fig. 2.12 has a scan size of 633 nm, the wavelength of the excitation light used. Each emission feature (FWHM 90 nm) is attributed to a single protein, limited by the size of the near-field tip. Shear-force images (not shown) obtained simultaneously with the same near-field tip determine the heights of the proteins to be 3 nm. This result demonstrates the single protein sensitivity and spatial resolving power of our near-field microscope.

The near-field technique provides a means of spectroscopically mapping the various protein complexes in the photosynthetic membrane.[2–3] In collaboration with Professor Laurens Mets at the University of Chicago, we have begun the spectroscopic mapping of the photosynthetic membrane of green plants in order to elucidate the relationship between membrane structure and biological functionality. Figures 2.13 and 2.14 show the simultaneous shear force image and near-field fluorescence image of intact thylakoid membrane fragments from green algae containing only light-harvesting complexes (*Chlamydomonas reinhardtii* PSI - PSII doubly deficient C2 strain).[3] These images enable us to correlate topographic and spectroscopic information. The four bilayer membrane pieces seen in Fig. 2.13 lay down flat on a mica surface. Their thickness is measured to be ~7 nm, consistent with those of lipid bilayer membranes. Only the two big pieces contain fluorescent chlorophyll molecules as seen in Fig. 2.14. We have also conducted a time-resolved fluorescence experiment on an intact photosynthetic membrane with the near-field microscope. Figure 2.15 shows the first fluorescence lifetime measurement done with nanometer resolution.[3] This demonstrates that electron and energy transfer dynamics can be studied on single photosynthetic proteins in the native states with this nonperturbative approach.

References

1. R. C. Dunn, E. V. Allen, S. A. Joyce, G. A. Anderson, and X. S. Xie, *Ultramicroscopy* **57**, 113 (1995).
2. X. S. Xie, E. V. Allen, G. R. Holtom, R. C. Dunn, and L. Mets, *Proc. SPIE* **2137** (*Time Resolved Laser Spectroscopy in Biochemistry IV*), 264 (1994).
3. R. C. Dunn, G. R. Holtom, L. Mets, and X. S. Xie, *J. Phys. Chem.* **98**, 3094 (1994).

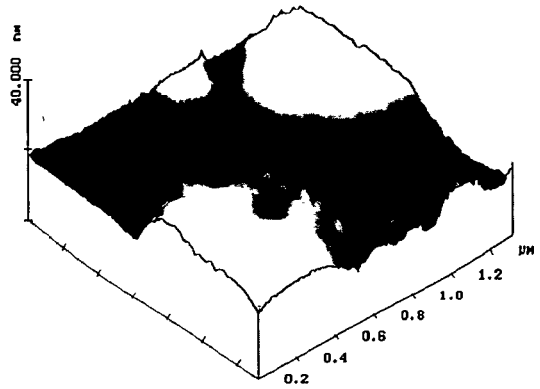

Figure 2.13. Shear force image of photosynthetic membrane fragments.

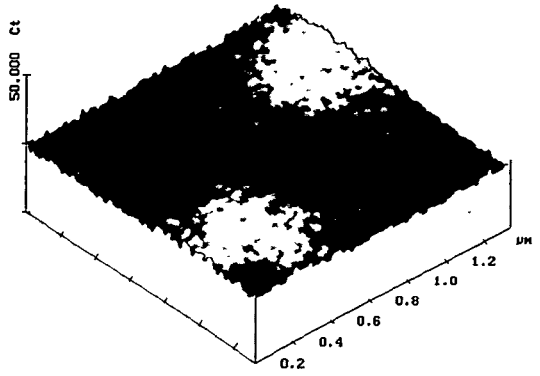

Figure 2.14. Near-field fluorescence images of photosynthetic membrane fragments, taken simultaneously with Fig. 2.13.

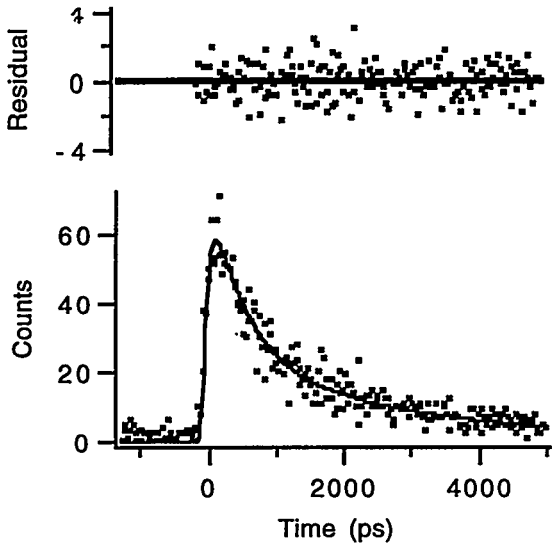

Figure 2.15. Fluorescence decay of LHC II proteins in an intact photosynthetic membrane taken with the near-field microscope. The decay is fit with a sum of exponentials with lifetimes of 450 ps (65%) and 2.7 ns (35%). The top trace shows the residual.

Structure and Dynamics of Liquid Water Molecules by Femtosecond Infrared Spectroscopy

G. R. Holtom, R. C. Crowell, and X. S. Xie

Instrument development supported by Environmental Molecular Sciences Laboratory (EMSL).

The importance of water as a universal and unique solvent for chemical and biological reactions has continued to stimulate theoretical, computational, and experimental efforts on understanding the structure and dynamics of liquid water. Liquid water has a broad absorption band in the 3-μm region due to its fundamental stretching vibrations, which are particularly sensitive to its specific hydrogen-binding structure. Graener et al.[1] have originated picosecond hole burning experiments on liquid water in this spectral region, and revealed the inhomogeneous nature of the hydrogen bonding structures. Femtosecond coherent experiments would be particularly informative about the vibrational dephasing and other dynamical properties of the system. A 50-fs pulse at 3 μm is needed in order to coherently excite the entire inhomogeneously-broadened band. However, this has been experimentally difficult due to the lack of a femtosecond source in this spectral region.

We have recently demonstrated a stable femtosecond infrared source at 3 μm using a synchronously pumped OPO,[2,3] which is suitable for performing femtosecond coherent spectroscopy in the O–H stretching region. An optical parametric oscillator synchronously pumped by a mode-locked Ti:sapphire is operated at a center frequency of 3660 cm^{-1}, providing nearly transform-limited 120-fs pulses with 0.2-nanojoule pulse energy at a repetition rate of 76 MHz.

Using this new laser source, we have made the direct observation of infrared optical free induction decay (FID) of water molecules dissolved in deuterated methylene chloride.[4] This experiment is the initial step toward our goal of understanding liquid water.

The solid line in Fig. 2.16 shows the FTIR absorption spectrum of H_2O dissolved in CD_2Cl_2. The 3600-cm^{-1} peak is assigned to the symmetric stretching and the 3684-cm^{-1} peak to the asym-

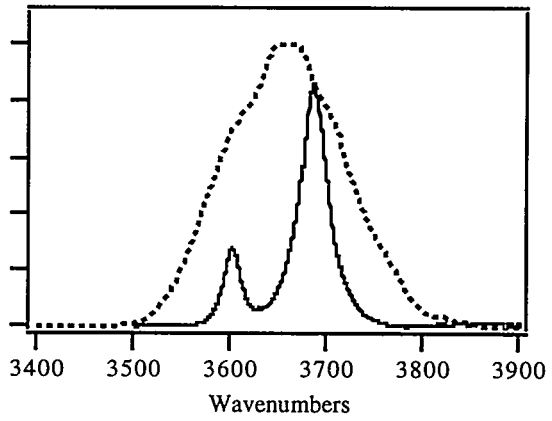

Figure 2.16. The infrared absorption spectrum of water dissolved in deuterated methylene chloride (solid line), and the infrared spectrum of the pulses from the femtosecond OPO (dashed line).

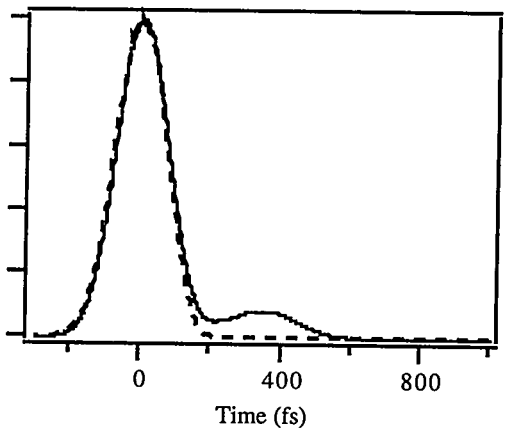

Figure 2.17. The up-converted infrared FID of water dissolved in CD_2Cl_2 (solid line) and the instrumental response (dashed line).

metric stretching of the water molecules. The IR spectrum indicates no water cluster formation at this concentration. The dashed line in Fig. 2.16 shows the spectrum of the excitation pulses from the OPO, which clearly has enough bandwidth to coherently excite the two vibrational modes of the solute water molecules.

Figure 2.17 shows the up-converted infrared FID (solid line) and the instrumental response function (cross correlation of IR and 816-nm beam, dashed line). The later has a FWHM of 180 fs. The FID first follows the instrumental function and has the distinct first recurrence at 365 fs. The 365-fs time delay corresponds to the 84-cm^{-1} splitting in the IR spectrum in Fig. 2.16. Figure 2.18 shows a logarithmic plot of the same data, which shows the subsequent beats. Such a FID is the result of the two interacting vibrational modes of water molecule radiating in a coherent manner. We have directly measured the ground-state vibrational quantum beats of water molecules at room temperature.

This initial experiment shows promise for using multiple infrared pulse sequences to conduct femtosecond nonlinear vibrational spectroscopy in order to unscramble the complex molecular interactions and dynamics in molecular liquids.

References

1. H. Graener, G. Seifert, and A. Laubereau, *Phys. Rev. Lett.* **66**, 2092 (1991).
2. R. A. Crowell, G. R. Holtom, and X. S. Xie, *Ultrafast Phenomena IX* (Springer-Verlag, Berlin, 1994), p. 156.
3. G. R. Holtom, R. A. Crowell, and X. S. Xie, "A High Repetition Rate Femtosecond Optical Parametric Oscillator-Amplifier System near 3 Microns," *J. Opt. Soc. Am. B.*, in press.
4. R. A. Crowell, G. R. Holtom, and X. S. Xie, *J. Phys. Chem.* **99**, 1840 (1995).

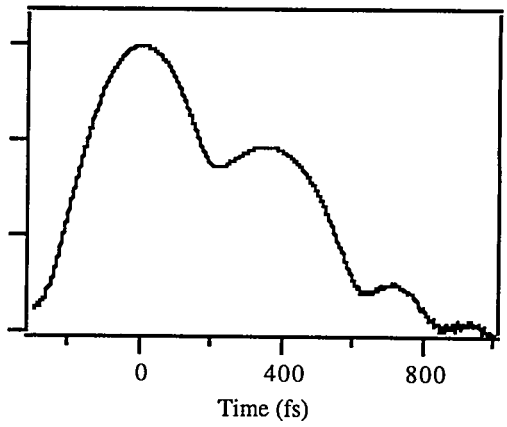

Figure 2.18. The same data as Fig. 2.17 drawn with a logarithmic scale.

Molecular Dynamics at the Water/Solid Interface

M. J. Iedema, S. A. Joyce, H. Wang, J. Biesecker,† N. Kizhakivariam,* and J. P. Cowin*

Supported by Office of Basic Energy Sciences.

*Postdoctoral Research Associate.

†Graduate student of Prof. B. Ellison, University of Colorado.

Defects at oxide surfaces can control the chemistry of many reactions and mediate contaminant transport in soils. We have studied the adsorption/desorption kinetics of water on thin single-crystal films of MgO (on a Mo(100) surface), to explore the effect of defects. Scanning tunneling microscope studies (done in collaboration with S. A. Joyce) show that several-monolayer MgO films grow nearly atomically smooth, but have domain sizes that range from about 20 Å for an unannealed 400-K grown film, to 150 Å after annealing at 1050 K. The fraction of sites bordering the edges of the domains should range from 10% to 50% in these two cases. Water desorption on these surfaces shows (Fig. 2.19) that there are two contributions to the binding/desorption of water that scale roughly in proportion to the expected fraction of edge atoms. When the thin film is grown on a 4.5° tilted (thus stepped) substrate, the water desorption on the stepped oxide also shows the effect of having more defect sites (Fig. 2.19). New work in progress uses atomic epitaxy of an intimately mixed oxide, CaO + MgO, to explore the effect of substitutional defects on water chemistry on an oxide surface.

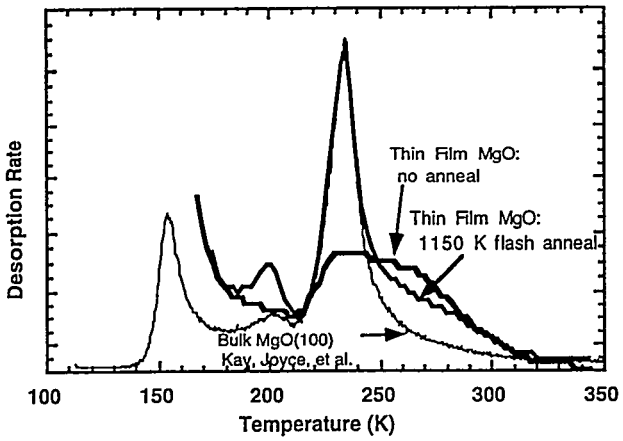

Figure 2.19. Water desorption from various MgO surfaces.

1. CCl_4 Degradation: Phosgene and Water

Photochemical degradation of CCl_4 on MgO has been studied to learn about destruction pathways of one of the more resistant chlorocarbons. Of particular interest is the production of phosgene ($OCCl_2$): it seems to be an important intermediate in photocatalytic destruction of many chlorocarbons. Figure 2.20 shows its evolution during heating of a thin-film MgO surface covered with a monolayer of CCl_4, after irradiation at 193 nm. The dry surface (curve a) shows strong binding to the intermediates of phosgene, while with a monolayer of water present, the kinetics indicate a much weaker interaction (curve b). Oxygen-18 studies indicate that the reaction mechanism differs, the oxygen coming from the MgO lattice if the water coverage is less than a monolayer, from the water if it is more. Water desorption studies allow us to predict that monolayer water films would exist in chlorocarbon scrubbing applications of MgO powders up to 700 K.

2. Ions at Interfaces

Much of the chemistry of importance in aqueous-mineral and electrochemistry involve aqueous ions. Our studies of ions at surfaces involve a col-

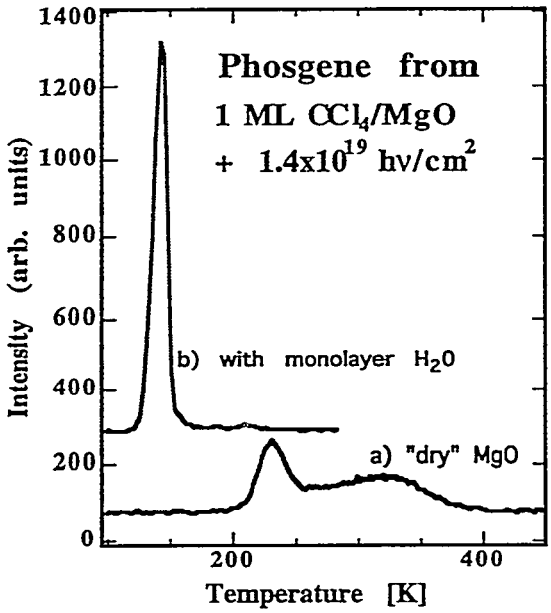

Figure 2.20. Evolution of phosgene from a monolayer of CCl_4 on a thin-film MgO surface irradiated at 193 nm.

laboration between PNL and the University of Colorado. Professor Barney Ellison and his student John Biesecker built an ion source and delivered it to PNL for joint use. We will use cryogenic temperatures (≤20 K) and molecular beam dosing to create models of aqueous interfaces with known spacing (in z) between various molecules, ions, and the surface. Unlike others, we employ a mass-selected, positive or negative molecular-ion beam, producing 10 to 50 nA of ions at several eV impact energy. This allows study of ionic surface processes for a wide range of molecular ions (NH_4^+, H_3O^+, N_2O^+, NO_3^-, ClO^-, CN^-, OH^-, etc.). We can prepare systems at equilibrium or ones which are highly metastable. Neutralization of the deposited ions make it an effective radical source. These capabilities will also allow studies of important atmospheric chemistry of aerosols, for species like ClO, ClO^-, and $NO_x^{+/-}$.

The source has recently demonstrated (for N_2O^+) narrow-energy beams at 10 nA or higher fluence, at about a volt impact energy. As the beam energy is reduced from 500 V, the current is nearly constant down to the 1-V limit. Previous attempts by others have shown strong beam losses typically starting below 50 V. Our design minimizes these losses, which are due to space-charge effects. Hydration and ion migration studies are about to commence using thin-layer water epitaxy plus ions.

The Uptake of Gases by Aqueous Solutions Probed by Surface Nonlinear Optical Spectroscopy

R. Doolen and D. Ray*

Supported by Laboratory Directed Research and Development (LDRD).

*Postdoctoral Research Associate.

The goal of this project is the direct spectroscopic measurement of the thermochemistry and kinetics of gas/liquid mass transfer across water surfaces. The detailed molecular-level data obtained from these experiments, along with molecular-scale simulations performed by staff in the Theory, Modeling, and Simulation program, will provide improved understanding of the uptake of gases by aqueous solutions, and may provide an alternative method for measuring mass accommodation coefficients of atmospherically important species.

The basic experimental approach is to measure the orientation, the adsorption isotherm, and the solvation kinetics of selected adsorbates on liquid water surfaces by surface second harmonic generation spectroscopy using a high-repetition-rate femtosecond laser and a photon-counting detection system. Surface second harmonic generation is a nonlinear laser spectroscopy that is both species-selective and intrinsically surface-selective. The basic methodology has been developed by Eisenthal and coworkers at Columbia University, but applications in environmental science have not yet been demonstrated. Analysis of the data obtained, in combination with values for the solvation energy and data from droplet uptake measurements, will yield a complete representation of a model potential energy surface for the process of mass accommodation. Measurements of the surface excess of benzaldehyde at the gas/liquid interface of aqueous solutions are in progress.

3. Radiation and Other High-Energy Processes at Environmental Interfaces

Investigation of Acetyl Chloride Photodissociation by Photofragment Imaging

S. M. Deshmukh, J. D. Myers,† S. S. Xantheas,‡ and W. P. Hess*

Supported by Office of Basic Energy Sciences.

*Postdoctoral Research Associate.
†Computing and Information Sciences.
‡Theory, Modeling and Simulation.

The photochemistry of acetyl chloride is interesting from both environmental and a fundamental chemistry perspectives. The discharge of chlorocompounds into the environment threatens stratospheric ozone, terrestrial ecosystems, and groundwater supplies.[1] The photochemistry of acetyl chloride is also important from a mechanistic viewpoint, as it appears not to follow the well-known Norrish type I reaction, which is characteristic of asymmetrically substituted aldehydes and ketones.[2] To investigate the details of acetyl chloride dissociation, we have recorded the velocity distribution of the Cl, CH_3, and CO fragments using an ion imaging technique.[3] Following excitation of CH_3COCl near the maxima of the $^1[n, \pi^*(C{=}O)]$ transition by a polarized 236-nm laser light, Cl, CH_3, and CO fragments are probed by using (2+1) multiphoton ionization (MPI). The experimental apparatus is similar to that described by Chandler.[3] Briefly, a molecular beam is directed into the extraction region of a time-of-flight (TOF) mass spectrometer and toward the center of a micro channel plate (MCP) detector. The beam is crossed at right angles with the counter-propagating photolysis and probe laser beams, roughly equidistant from the repeller and the extractor optics of the TOF spectrometer. Atomic chlorine photofragments, in the ground ($^2P_{3/2}$) and spin-orbit excited ($^2P_{1/2}$) states, are probed (ionized) using the two-photon transitions at 235.33 nm for Cl ($^2D_{3/2} \leftarrow {}^2P_{3/2}$) and at 237.8 nm for Cl* ($^2D_{3/2} \leftarrow {}^2P_{1/2}$), methyl fragments are probed using the two-photon $4p_z \leftarrow X$ transition near 286 nm, and CO fragments are probed using the two-photon B $\leftarrow$ X transition near 230 nm. Following ionization, Cl, CH_3, and CO photofragments are rapidly extracted (2800 V) from the ionization region and accelerated along the molecular beam axis to impinge upon a dual-chevron microchannel plate/phosphor-screen detector. The resultant image is a two-dimensional projection of the three-dimensional spatial distribution of the selected fragments. Although the raw images do not directly describe the three-dimensional photofragment velocity distributions, the velocity distributions may be extracted from the raw images by the use of inverse Abel transforms.[3]

Figure 3.1 displays the raw photofragment images for Cl, CH_3, and CO fragments following 236 nm excitation of acetyl chloride. The Cl ion image (Fig. 3.1(a)) clearly shows two vertically displaced lobes, and an anisotropic spatial distribution. The CO ion image (Fig. 3.1(b)) has a much more isotropic appearance ($\beta \sim 0$) than the Cl ion image. Considerable intensity appears in the center of the image, indicating a significant slow component. Similarly, the CH_3 ion image shows a largely isotropic appearance although lateral broadening is evident. Again, the methyl fragments display intensity in the central portion of the image, indicating a slow component that is momentum-matched to the CO product. Figure 3.2 displays the velocity distributions of Cl, CH_3, and CO photofragments obtained by taking the inverse Abel transform of the quadrant-averaged raw image. The full three-dimensional velocity distribution is recovered by rotation of the transformed image about the vertical symmetry axis. The speed distribution at any particular angle may be obtained by taking a radial cut of the transformed image.

The Cl atom speed distribution is angularly dependent, and yields a translational energy distribution with a mean value of 9.9 kcal/mol or 0.43 eV. The total fragment recoil energy is peaked near 18 kcal/mole, which is in good agreement with the value of 16 kcal/mole reported in the 248 nm photolysis,[2] considering the greater photon energy used here. The anisotropy parameter of the fast component, obtained from the Abel transformed image, is $\beta \approx 0.9 \pm 0.2$, corresponding to a 33% admixture of $\sin^2\theta$ distribution in the predominantly $\cos^2\theta$ angular distribution. In contrast to the Cl photofragment image, the CO image displays an isotropic spatial distribution. The speed distribution yields the half maximum value of 780 m/s at $\theta = 0°$, which is equivalent to a mean translational energy of 2.04 kcal/mol or 0.09 eV. The

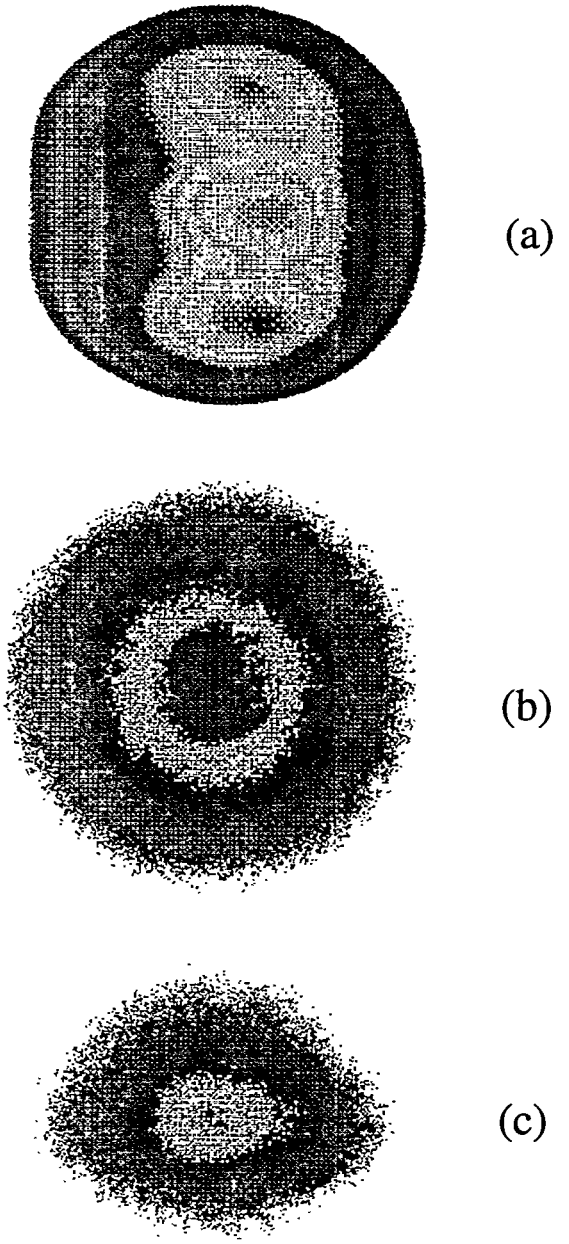

Figure 3.1. False-color photofragment images of (a) Cl, (b) CO, and (c) CH_3 products in the 236-nm dissociation of acetyl chloride. The Cl, CO, and CH_3 fragments are probed using various (2+1) MPI schemes described in the text.

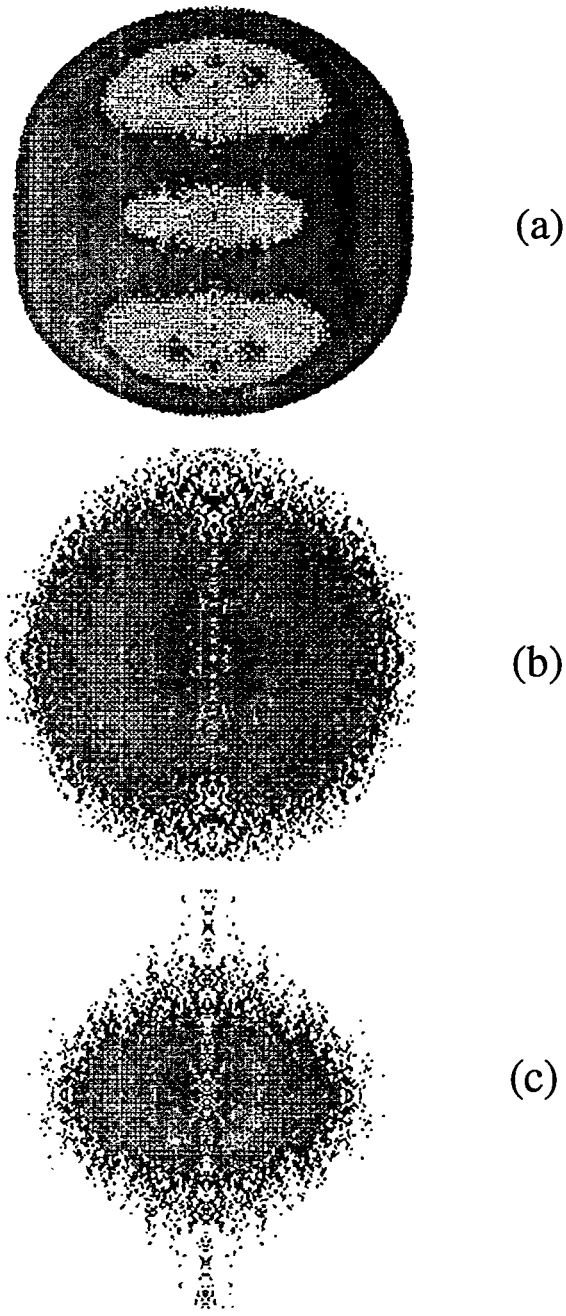

Figure 3.2. False-color images of the fragment velocity distributions produced by performing inverse Abel transforms of the (a) Cl, (b) CO, and (c) CH_3 images presented in Fig. 3.1.

mean speed of CO fragments at $\theta = 90°$ is 750 m/s. The speed distribution for CH_3 fragments yields the half-maximum value of 1450 m/s at $\theta = 0°$, which is equivalent to a mean translational energy of 3.78 kcal/mol or 0.16 eV. The mean speed of CH_3 fragments at $\theta = 90°$ is 1540 m/s. We do not observe high-velocity methyl radicals that would be indicative of primary C–C bond fission.

The dissociation of acetyl chloride at 5.25 eV, to form Cl, CH_3, and CO products occurs through a two-step process. The mechanism for acetyl chloride dissociation may be described by the reaction steps

$$CH_3COCl + h\nu \rightarrow CH_3CO^* + Cl\ /Cl^* \quad (1)$$
$$CH_3CO^* \rightarrow CH_3\ (v,J,T) + CO\ (v,J,T). \quad (2)$$

The Cl photofragment image displays distinct anisotropy that is characteristic of a prompt dissociation with a dissociation lifetime assumed to be less than a rotational period of roughly 1 ps.[4] The CO and CH_3 photofragment images display isotropic spatial distributions. The lack of anisotropy in the CH_3 and CO photofragment images indicates that the only primary dissociation channel is C–Cl bond cleavage and that the CH_3 and CO dissociation dynamics requires a subsequent kinetic step. Rotation of the CH_3CO intermediate prior to decomposition is presumably responsible for the loss of anisotropy in the secondary dissociation step.

The initial CH_3CO photoproduct is born in a distribution of excited vibronic states, of which approximately 30% decompose to form CH_3 and CO.[5] In an earlier spectroscopic study, we reported the CH_3 product internal state distribution and the translational energy distribution of Cl/Cl* fragments.[5] The CH_3 product state distribution displays very little internal excitation as the rotational distribution extends only up to $N'' = 5$, and only a small amount of excitation is detected in the lowest ν_2 umbrella vibration; the internal energy of CH_3 was found to be less than 0.02 eV.[5] Here we find that, although the CO product is not vibrationally excited, significant rotational excitation is evident from the band contour analysis. It is clear from these observations that dynamical, rather than statistical, models best explain the product state distributions.

References

1. S. Solomon, *Rev. Geophys.* **26**, 131 (1988); V. Vaida, S. Solomon, E. C. Richard, E. Ruhl, and A. Jefferson, *Nature* **342**, 405 (1989).
2. M. D. Person, P. W. Kash, and L. J. Butler, *J. Phys. Chem.* **96**, 2021 (1992); M. D. Person, P. W. Kash, and L. J. Butler, *J. Chem. Phys.* **97**, 355 (1992).
3. D. W. Handler and P. L. Houston, *J. Chem. Phys.* **87**, 1445(1987); D. W. Chandler, M. H. Janssen, S. Stolte, R. N. Strickland, J. W. Thoman Jr., and D. H. Parker, *J. Phys. Chem.* **94**, 4839 (1990).
4. M. K. Dzvonik, S. Yang, and R. Bersohn, *J. Chem. Phys.* **61**, 4408 (1974).
5. S. Deshmukh and W. P. Hess, *J. Phys. Chem.* **98**, 12535 (1994).

Theoretical Investigation of Acetyl Chloride Photodissociation

S. M. Deshmukh, J. D. Myers,† S. S. Xantheas,‡ and W. P. Hess*

Supported by Office of Basic Energy Sciences.
*Postdoctoral Research Associate.
†Computing and Information Sciences.
‡Theory, Modeling and Simulation.

Theoretical calculations were performed to assist in interpreting the experimental results obtained by an ion imaging technique during photodissociation of acetyl chloride at 236 nm. The recorded Cl images display anisotropic angular distributions, characteristic of a prompt, impulsive dissociation of the C–Cl bond. Furthermore, the experimental data suggest that a fraction (about 28%) of the CH_3CO, produced as a primary photoproduct, subsequently decomposes to form CH_3 and CO. The optimal structures of the minimum ($^2A'$) and transition state corresponding to the dissociation of the acetyl radical (CH_3CO) are shown in Fig. 3.3(a), whereas the optimal geometry of CH_3COCl ($^1A'$) is shown in Fig. 3.3(b) at the MP2/cc-pVTZ level of theory. The arrows show the displacement of the atoms along the mode corresponding to the imaginary frequency at the transition state. Internal coordinates are indicated in degrees and Å. The energy profile for the CH_3CO dissociation along the C–C reaction coordinate at the MP2/cc-pVTZ level of theory is shown in Fig. 3.4. The values of the C–C–O and H–C–H angles are indicated for each value of the C–C bond. The barrier for CH_3CO dissociation was experimentally estimated at 16.2 ± 2 kcal/mol, and theoretically predicted at 19.1 kcal/mol at the MP2/cc-pVTZ level of theory. The dissociation proceeds toward a nearly C_s pathway, i.e., the atoms O, C, C, and H_a remain nearly on the same plane. The geometry of the transition state for the acetyl radical dissociation is a more open structure with a relaxed, nearly planar CH_3 group, and a contracted C–C–O bond angle. As the C–C bond lengthens, the pyramidal methyl group slowly relaxes to near the planar structure of free methyl. The gently relaxing H–C–H angle allows the methyl radical to form without exciting the ν_2 bending vibration, and since the methyl tripod does not cock off axis during dissociation, little rotation of the methyl radicals is produced. The CO product displays no observable vibrational excitation, but significant CO rotational excitation is observed. This is consistent with the

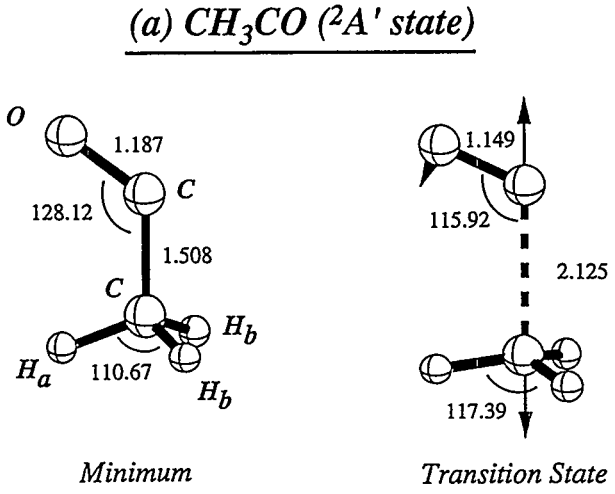

Figure 3.3. (a) Optimal structures of the minimum ($^2A'$) and transition state corresponding to the dissociation of the acetyl radical at the MP2/cc-pVTZ level of theory. The arrows show the displacement of the atoms along the mode corresponding to the imaginary frequency at the transition state. (b) Optimal geometry of CH_3COCl ($^1A'$) at the MP2/cc-pVTZ level of theory. Internal coordinates are indicated in degrees and angstroms.

calculated C=O bond contraction to near that of the free CO along the reaction path. It appears that these motions occur gently, allowing the methyl and CO fragments to transform adiabatically into ground-vibrational-state products. The rotational state distribution is also qualitatively explained by examining the differences in the ground-state acetyl chloride and transition-state acetyl structures.

Laser Interactions with an Ionic Molecular Crystal: Sodium Nitrate Ablation in the 6-eV Valence Band

R. A. Bradley Jr., E. J. Lanzendorf,† M. I. McCarthy,‡ T. M. Orlando, and W. P. Hess*

Supported by Strategic Environmental Research and Development Program (SERDP).

*Postdoctoral Research Associate.
†Graduate Student.
‡Theory, Modeling and Simulation.

Laser ablation is an important technique in an increasing number of fields including chemistry, physics, materials science, microelectronics, biology, and medicine.[1] The utility of laser ablation is derived from the diversity of materials that are amenable to the technique. The combination of laser ablation and mass spectrometry has led to the mass determination of a variety of refractory materials, including high-molecular-weight biomolecules.[2,3] Laser ablation combined with mass spectrometry (LAMS) is being developed as a diagnostic for analysis of atomic and molecular species in mixed hazardous wastes.[4] Using this approach, analysis of complex multicomponent mixtures can be performed rapidly using very little sample. Reduced sample size is highly desirable for the analysis of many hazardous wastes because it minimizes the secondary waste generated from the analytic procedures. The LAMS technique is being applied to analyze mixed wastes extracted from the underground storage tanks at the Hanford Nuclear Reservation. A major component of these tanks is sodium nitrate ($NaNO_3$), so understanding the ablation mechanisms of this material is essential to analyzing these wastes. Sodium nitrate is a wide-band-gap, insulating material that forms a molecular ionic crystal with a hexagonal unit cell of D_{3d} symmetry. We examine laser/solid interactions following resonant excitation of single-crystal sodium nitrate by measuring the translational, rotational, and vibrational energy distributions of desorbed NO.

The $NaNO_3$ crystals were excited using 5-ns pulses of 213-nm light incident on the sample at 40° to the crystal face. Neutral NO fragments are probed using 1+1 multiphoton ionization (MPI) following ablation. The positive ions produced via MPI are

detected using a time-of-flight (TOF) mass spectrometer. The relative populations of the rotational and vibrational levels ($v'' = 0$–4) of the observed NO were determined from the intensity of the P_{12} bandhead of the (0,0), (1,1), (2,2), (2,3), and (3,4) vibronic transitions. Figure 3.5 shows a typical MPI spectrum of desorbed NO. The initial NO yield was determined using a quadrupole mass spectrometer (QMS) on fresh (initially unirradiated) $NaNO_3$ samples. The neutral NO desorption yield is quantitatively different for resonant excitation of the $\pi^* \leftarrow \pi_2$ band at 213 nm as compared to nonresonant excitation at 266 nm. For freshly-cleaved samples the neutral NO yield for 213-nm excitation is approximately 1,000 times greater than for 266-nm excitation, hence it is clear that resonant excitation leads to a significant enhancement of the NO yield due to a photochemical reaction. Examination of the power dependence of the ablation process indicates that all NO production is a result of single-photon absorption at 213 nm.

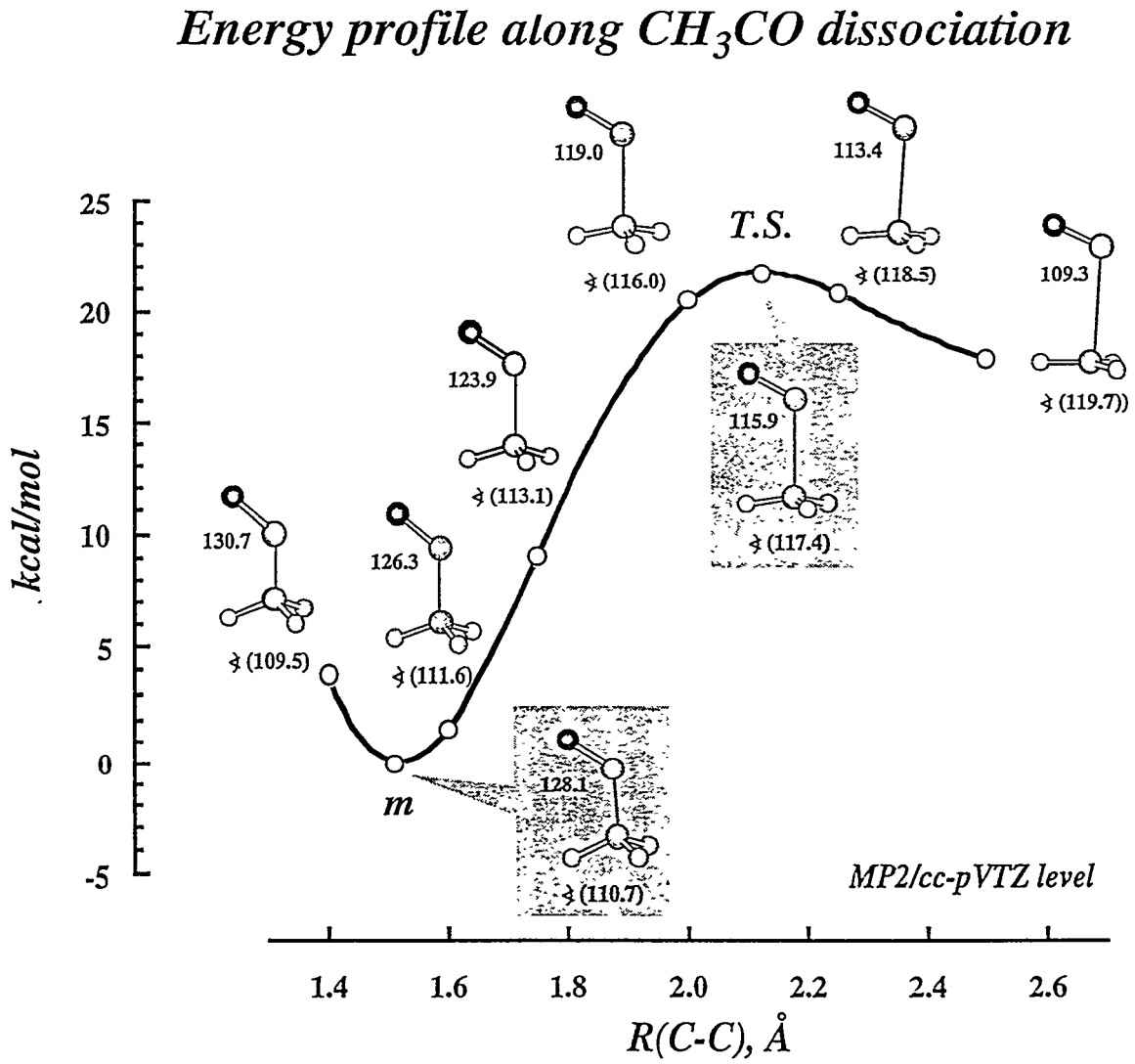

Figure 3.4. Energy profile for the CH_3CO dissociation along the C–C reaction coordinate at the MP2/cc-pVTZ level of theory. The values of the C–C–O and H–C–H angles are indicated for each value of the C–C bond. Abbreviations: m = minimum, T.S. = transition state.

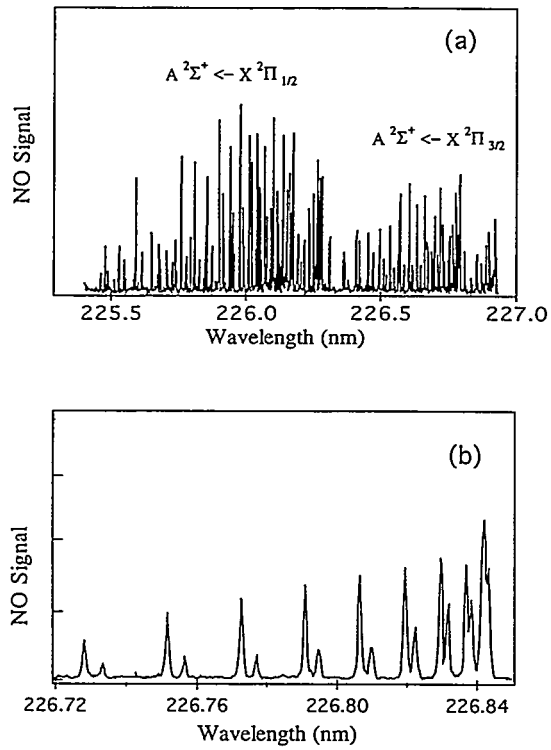

Figure 3.5. The NO rotational distribution following 213-nm excitation: (a) displays the full rotational spectrum of the (0, 0) $A\,^2\Sigma^+ \leftarrow X\,^2\Pi_{3/2,1/2}$ transition, while (b) is the power-corrected spectrum of the P_{12} rotational band, expanded from the rotational spectrum shown in (a). A Boltzmann analysis of this spectrum yields a rotational temperature of 270 ± 50 K.

The large oscillator strength of the $\pi^* \leftarrow \pi_2$ absorption band greatly enhances the ablation efficiency for resonant 213-nm excitation. We measure the neutral product yield of NO and O_2 using the QMS and find the ratio of NO to O_2 yield to be approximately 15:1, which is significantly greater than the stoichiometric ratio. No significant desorption of atomic oxygen was observed above the background level (m/z = 16) due to H_2O and O_2 cracking in the electron impact ionizer of the QMS. For low laser fluence (<2 MW/cm^2), no NO_2 or Na is observed at 213 nm within detection limits. We also observe no indication that product channels for NO_2 or O production are present.

For the NO desorbing from the surface, there is significant population in the higher vibrational states. This vibrational distribution provides a poor fit to a Boltzmann plot, and must therefore be nonthermal. The TOF spectra are fit to a half-range Maxwell-Boltzmann velocity distribution function,[5] yielding a translational temperature of 250 ± 40 K, in thermal equilibrium with the unirradiated surface. We have also investigated the rotational energy distribution of the desorbing NO from $NaNO_3$ ablation at 213 nm. A Boltzmann analysis of the spectrum displayed in Fig. 3.5 yields a rotational temperature of 270 ± 50 K for the ablated NO. Data obtained at higher temperatures indicates that the rotational temperature of the desorbing NO tracks with the substrate temperature. The observation of considerable NO vibrational excitation implies that the surface residence time of the newborn NO product is short compared with the lifetime of vibrationally-excited NO on the surface. This may be due to the poor energy match between a vibrational quanta for NO (~1900 cm^{-1}) with the Debye frequency of crystalline $NaNO_3$ (100–200 cm^{-1}). The translational and rotational state distributions however, indicate a finite residence time as these degrees of freedom are equilibrated with the surface temperature.

Photoexcitation of the $\pi^* \leftarrow \pi_2$ band in $NaNO_3$ creates excited-state nitrate anion NO_3^{-*} (a Frenkel exciton) both at the surface and in the bulk crystal. The surface dynamics of photoexcited $NaNO_3$ results from the dissociation of the NO_3^{-*} exciton at or near the surface. Since this exciton presumably self-traps at the vacuum surface interface, the subsequent dissociation mechanisms can be described in terms of the decay of a surface-bound negative ion excited state. Hence, the ablation process is actually probing the *photochemistry* of the $NaNO_3$ solid to gas interface. At or near the surface layer, direct photodissociation can occur, leading to desorption of NO. Equation (1) describes the proposed mechanism:

$$NO_3^-(s) + h\nu \rightarrow NO_3^{-*}(s) \rightarrow NO(g) + O_2^-(s) \quad (1)$$

Here the (s) indicates surface or near-surface sites, and (g) indicates escaped gas-phase species. According to this mechanism, the O_2^- product remains trapped on the surface in the defect site created by the decomposition of the nitrate ion.

To understand the energetics of $NO_3^{-*}(s)$ dissociation we must consider the stabilization of the nitrate anion by the Coulomb field of crystalline $NaNO_3$. We estimate the bulk anion stabilization to be ~7.5 eV, considerably larger than the 5.8 eV excitation energy. The anion stabilization may be

estimated from the positions of the $\pi^* \leftarrow \pi_2$ and Na^+ (3s) $\leftarrow \pi_2$ bands, the electron affinity[6] (3.9 eV) of NO_3, and by assuming that the Na^+ (3s) $\leftarrow \pi_2$ band observed at 10.5 eV in the bulk absorption spectrum, lies roughly 1 eV below the vacuum level. Therefore, single-photon excitation of bulk NO_3^{-*} is incapable of releasing a photoelectron, and energetic constraints require either O_2^- trapping, or possibly F-center formation following desorption of neutral NO.

References

1. *Laser Ablation: Mechanisms and Applications* **389** (Springer-Verlag, New York, 1991).
2. M. Karas and F. Hillenkamp, *Anal. Chem.* **60**, 2299 (1988).
3. J. Grotemeyer, and E. W. Schlag, *Acc. Chem. Res.* **22**, 399 (1989).
4. *Laser Ablation: Mechanisms and Applications—II* **288**, 626 (AIP Press: New York, 1994).
5. R. Kelly and R. Dreyfus, *Surf. Sci.* **198**, 263–276 (1988).
6. H. Yamashita and R. Kato, *J. Phys. Soc. Jpn.* **29**, 1557 (1970).

Electron- and Photon-Stimulated Surface/Interface Chemistry

T. M. Orlando, R. G. Tonkyn, G. A. Kimmel, and K. Knutsen**

Supported by Office of Basic Energy Sciences.

*Postdoctoral Research Associate.

One of the main objectives of this program is to understand the effects of ionizing radiation on condensed-phase systems by probing the detailed chemical and physical transformations induced by bombardment of molecular solids with *low-energy* (1–100 eV) electrons and vacuum ultraviolet (VUV) photons. Our interest is largely based on the fact that energetic particles lose energy primarily via the production of low-energy secondary electrons. For example, the average energy lost by a fast (~600 keV) Compton electron in a single ionization event in the condensed phase is approximately 30 eV. Thus, before degrading, such an electron can produce ~10^3–10^4 low-energy (1–100 eV) secondary electrons. We are particularly interested in probing amorphous water, since the disordered hydrogen-bonding network in amorphous ice makes this system a good model for the *liquid* state. In general, our studies are relevant to understanding the chemical transformations that occur in DOE mixed (radioactive/chemical) waste storage facilities.

1. Low-Energy Electron Stimulated Reactions in Amorphous Ice

We have measured the quantum-resolved translational and internal (vibrational and rotational) energy distributions of the D_2 desorbates produced during electron (100 eV) irradiation of D_2O amorphous ice using resonance-enhanced multiphoton ionization (REMPI) spectroscopy. This is a continuation of our initial study (*J. Chem. Phys.* **101**, 3282 (1994)), which probed the low-energy electron-stimulated production of D_2 from amorphous ice using quadrupole mass-spectrometry (QMS). The D_2 desorbates have very little translational energy (~20–50 meV), but are vibrationally (v = 0–4) and rotationally (J = 0–12) excited. The rotational state distribution of the D_2 does not change as the ice temperature increases from 88 K to 145 K. However, we find that the D_2 yield increases monotonically in this temperature range, with the yield at 145 K approximately double that at 88 K. Although the mobilities of defects, charge carriers, and radicals are known to be dependent upon temperature, these results suggest that the final states leading to D_2 production are independent of temperature. We suggest that the dominant mechanisms for production of D_2 at 100-eV incident electron energy are dissociative recombination of holes (D_2O^+ or D_3O^+) with quasi-free or trapped electrons and dissociation of excitons at the vacuum-surface interface. These dissociation events can produce D_2 directly via molecular elimination or indirectly via reactive scattering of the energetic D atom fragments.

Time-of-flight laser resonance enhanced ionization has also been used to measure the yields and kinetic energy distributions of the D (^2S), O ($^3P_2$), and O ($^1D_2$) desorbates produced during low-energy (5–50 eV) electron-beam irradiation of amorphous ice. The low-energy neutral desorption thresholds (~8–10 eV) and kinetic energy distributions demonstrate the importance of valence-level holes. Figure 3.6 shows the yields of D (^2S), O ($^3P_2$), and D_2 ($^1\Sigma_g^+$) as a function of incident electron energy. Careful examination of the threshold region indicates that the production of D (^2S) primarily involves *direct* excitation or ionization followed by very rapid geminate recombina-

tion. The yield vs. incident electron energy data can be fit well using theoretical[1] and experimental[2] data on the *ionization* efficiency of *liquid* water. Lifetime and symmetry arguments suggest that it is probable that exchange recombination events which lead to the creation of excited triplet states dominate in the production of O ($^3P_{2,1,0}$), and D_2 ($^1\Sigma_g^+$). Our results clearly demonstrate that the use of amorphous ice layers is a very good model for liquid radiolysis events. We hope to extract numbers relevant to the conventional G-values, since the total thickness of our sample is on the order of a *single* spur diameter.

We have begun a series of experiments which are directed toward understanding the role that the local structure and lattice defect sites might play in the electron-stimulated production of D_2 (H_2), O ($^3P_{2,1,0}$), O (^1D), D(^1S) and D^- from water ice. This was addressed by studying the yields of all of these products as a function of time, temperature, and phase. We produce amorphous ice at temperatures below 140 K and crystalline (glassy) ice between 150–160 K. In general, the yields of all products increase with temperature and are ~50% higher from amorphous ice. The change in yield with respect to the phase is consistent with the higher surface area, higher desorption rates, and higher electron-hole pair localization probabilities expected for the more disordered amorphous ice.

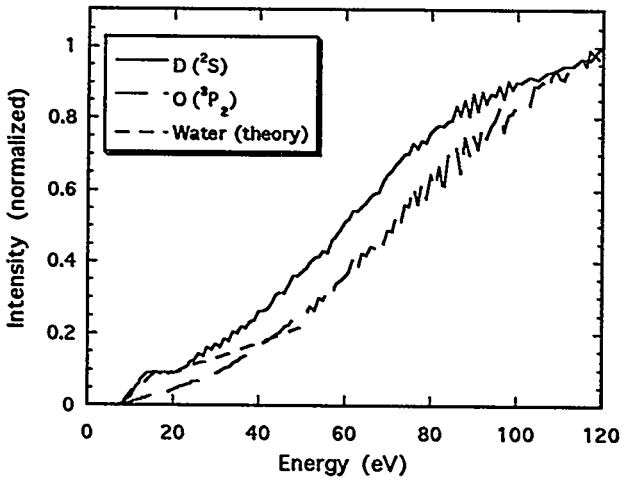

Figure 3.6. Yield of D (^{2}S), O ($^3P_2$), and D_2 ($^1\Sigma_g^+$) as a function of incident electron energy. The fit to the D_2 ($^1\Sigma_g^+$) yield is derived from calculations[1] and experimental[2] data on the ionization efficiency of liquid water. The fit to the D_2 ($^1\Sigma_g^+$) and O ($^3P_2$) data is the square of the ionization efficiency.

2. Low-Energy (5–80 eV) Electron-Stimulated Degradation of $NaNO_3$ Single Crystals

Low-energy (5–80 eV) electron-stimulated desorption of $H^+(D^+)$, $OH^+(OD^+)$, and Na^+ from solution-grown $NaNO_3$ single crystals is studied by quadrupole and time-of-flight mass spectrometry. Desorption yields, thresholds, and branching ratios are reported as a function of incident electron energy and fluence. We suggest that the $H^+(D^+)$ and $OH^+(OD^+)$ ions arise primarily from Na–H(D) and Na–OH(OD) termination sites produced during the interaction of water with surface defect sites. We associate the ~24-eV threshold for $H^+(D^+)$ desorption with hole production in the O(2σ) level and the yield increase ~33 eV with direct excitation of the Na 3s ← 2p, L_{23} exciton. We also correlate the $OH^+(OD^+)$ desorption threshold at ~33 eV with excitation of the Na 3s ← 2p, L_{23} exciton and the Na^+ threshold between ~42–46 eV with direct ionization of the Na^+ 2p level. The production and desorption of $H^+(D^+)$, $OH^+(OD^+)$, and Na^+ can be explained in terms of localized electronic excitations at surface termination (defect) sites which decay primarily via intermolecular Auger processes. Auger decay results in cation expulsion due to the repulsive Coulomb interaction, as demonstrated by the hot translational energy distribution (~4–7 eV peak energy) of the $H^+(D^+)$ desorption products. Desorption of $H^+(D^+)$ products dominate the cation desorption yields from solution-grown $NaNO_3$ crystals by a factor of ~100. We have also observed colloidal Na buildup at temperatures below 375 K using very low electron-beam fluxes (~10^{10-12} electrons/cm^2 pulse). The relevance of these results to tank-waste chemistry needs to be further explored.

We have also studied the low-energy (5–80 eV) electron-stimulated degradation of melt-grown $NaNO_3$ single crystals. Desorption yields, thresholds, and branching ratios are measured under conditions where substrate metallization and charge buildup are negligible. The major cations observed are O^+, N^+, Na^+, and NO^+, and the only anion observed is O^-. The threshold for cation production is 33 ± 1.5 eV, and there is a further increase in the Na^+ yield at ~45 eV. These thresholds are similar to those observed for solution-grown crystals, and thus we associate the threshold with the Na^+ 2p core exciton and the increase at 45 eV to ionization of the Na^+ 2p level. The core exciton and doubly-charged ion can decay via an intermolecular Auger process involving electrons

from the nitrate Π band. This decay can result in the production of NO_3^+, a reversal of the Madelung potential, and cation expulsion due to Coulomb repulsion. The major neutrals observed are NO and O_2, and the lower threshold (~20 eV) is believed to result from single-hole ionization of the 2e' nitrate bonding level. The O^- signal closely follows the O_2 and NO yield, and we suspect that the O^- signal is due to dissociative electron attachment of O_2 or NO during escape from the surface. We cannot rule out direct production of O^- via decay of self-trapped NO_3^{-*} surface excitons.

References

1. S. M. Pimblott and A. Mozumder, *J. Phys. Chem.* 95, 7291 (1991).
2. D. N. Nikogosyan, A. A. Oraevsky, and V. I. Rupasov, *Chem. Phys.* 77, 131 (1983).

Fundamental High-Energy Reaction Diagnostics/Kinetics

R. G. Tonkyn, S. E. Barlow, and T. M. Orlando

Supported by Laboratory Directed Research and Development (LDRD).

Researchers at PNL have been developing high-energy corona reactors for the destruction of hydrocarbon contaminants. These reactors, which generate low-temperature plasmas and operate at atmospheric pressure, are potentially useful in large-scale remediation efforts. However, the details of the physical and chemical parameters which govern the destruction efficiency are, at present, poorly understood. We have developed a differentially-pumped mass spectrometer system that can be used to sample virtually any plasma source. We have equipped this system with a Flowing-Afterglow and Chemical Ionization Source that allows us to sample selectively the neutrals present in the discharge region. This capability, when coupled with quadrupole mass spectrometry, allows us to sample the cation, anion, neutral, and electron number densities and hence "pick apart" the plasma for detailed studies.

To date we have utilized the Flowing-Afterglow Mass Spectrometer to probe the plasma parameters and plasma chemistry occurring in high-energy packed-bed coronas that are used to destroy halogen-containing hydrocarbon wastes such as carbon tetrachloride. Work which addresses the specific role of the packing material in enhancing the destruction efficiencies has been emphasized, since surface-interface interactions and catalytic effects are expected to enhance destruction efficiencies. The catalytic packing materials were also investigated to determine their effect on byproduct generation. These tests demonstrated the near-real-time monitoring capability of our new instrument. Soda-lime bead packing materials were well characterized at various operating conditions. The results compared well with the data generated in a larger, laboratory-scale reactor, and thus confirm the validity of the flowing-afterglow experimental results for predicting performance on larger-scale prototypes. Three catalytic materials, TiO_2, ZrO_2, and Cr_2O_3, were investigated on a preliminary basis. These materials showed improvement in destruction efficiency for CCl_4 and will be investigated further.

An important collaboration was established with Lawrence Livermore National Laboratory, to investigate areas of common interest in corona processing technology. A PNL-designed reactor and power supply were shipped to LLNL facilities and tested using LLNL control and monitoring facilities. These tests examined destruction efficiencies of NO_x and a model hydrocarbon system such as C_3H_6. These tests were performed to assess the applicability of corona technology to cold-start issues in the automotive industry, and also allowed PNL and LLNL to compare the relative merits of their respective corona technologies.

4. Cluster Models of the Condensed Phase

Structure and Bonding of Silicon Oxide Clusters

L. S. Wang, J. B. Nicholas, S. D. Colson, and J. Fan†*

Supported by Office of Basic Energy Sciences.
*Theory, Modeling and Simulation.
†Postdoctoral Research Associate.

Silicon oxide is a predominant component of the earth. Its surface chemistry plays important roles in the storage and underground transport of waste materials. At EMSL major effort is being directed to understanding the surface and interface properties of SiO_2. We have initiated a study of the structure and bonding of small silicon oxide clusters with a combined experimental and theoretical approach, using anion photoelectron spectroscopy (PES) and quantum calculations. The small, controlled sizes of these cluster systems provide not only atomic-level models to better understand the bulk surfaces and defect sites, but also are an excellent testing ground for validating theories that are intended for large and real-world systems.

A magnetic bottle time-of-flight PES spectrometer with a laser vaporization cluster source has been constructed and tested.[1] It has a mass resolution ($M/\Delta M$) of about 500 and an electron energy resolution of better than 30 meV at 1 eV kinetic energy, making it a powerful apparatus for studying clusters. Several initial experiments have been carried out on small silicon oxide and similar germanium oxide clusters. To test the abilities of the apparatus, several other experiments are also carried out, particularly on mixed Fe/C/H clusters and FeO^- and FeO_2^-. The high mass resolution and high energy resolution are amply demonstrated.

1. PES and Theoretical Studies of SiO_2^-, $Si_2O_3^-$, GeO_2^-, $Ge_2O_3^-$, $Ge_2O_2^-$, and $Si_3O_4^-$

We began with the smallest silicon oxide clusters for which accurate quantum calculations can be applied. The knowledge obtained with the smaller clusters will guide our study for the larger and more complicated ones. Quantum calculations are performed on all the clusters to determine the cluster structure and to compare with the experiments. Except for SiO_2 and GeO_2, all the other clusters already exhibit structural features reminiscent of the oxide surfaces and the bulk systems, with a tetrahedrally bonded Si in Si_3O_4 and an M_2O_2 ring in Si_2O_3, Ge_2O_3, and Ge_2O_2.

The PES spectra of SiO_2^-, $Si_2O_3^-$, GeO_2^-, and $Ge_2O_3^-$ are shown in Fig. 4.1. These spectra are taken at a 266-nm photon energy. The optimized geometries with density functional theory (DFT) are also shown in the figure. The arrows indicate the adiabatic and vertical detachment energies. The broad width of these spectra is due to the significant O–Si–O bond angle change taking place from the anion to the neutral, as shown. As expected, both the Si and Ge species have similar structures.

The Ge_2O_2 and $Ge_2O_2^-$ anions are studied both with DFT and PES at variable detachment energies.[2] We find that the Ge_2O_2 cluster is a rhombus (D_{2h}) closed-shell molecule with a large HOMO-LUMO gap. The PES spectrum of $Ge_2O_2^-$ is obtained at four detachment photon energies: 1064, 532, 355, and 266 nm (Fig. 4.2). Vibrational structure is resolved at the lowest photon energy with a single progression and a frequency of 400(60) cm^{-1}. The experimental adiabatic electron affinity is found to be 0.625(0.050) eV for Ge_2O_2. The calculated vertical and adiabatic electron affinities and the HOMO-LUMO gap are in good agreement with the experimental values. The calculated totally symmetric vibrational mode of Ge_2O_2 (335 cm^{-1}) is in reasonable agreement with the observed vibration, and represents a Ge–Ge breathing motion.

We obtained a vibrationally resolved photoelectron spectrum of $Si_3O_4^-$ (Fig. 4.3), for which a single vibrational progression is observed with a frequency of 800(50) cm^{-1}. This is the first observation of well-resolved vibrations for a relatively complicated covalent cluster, and provides important information about the cluster structure.[3] We use ab initio quantum mechanical calculations to determine the geometry of this cluster, which is found to be D_{2d} for the neutral ground state Si_3O_4, and C_{2v} for $Si_3O_4^-$. In both cases, a central Si atom is bonded to the four O atoms in a distorted tetrahedral coordination. The calculated electron affinity and vibrational frequency are in excellent agreement with the experiment.

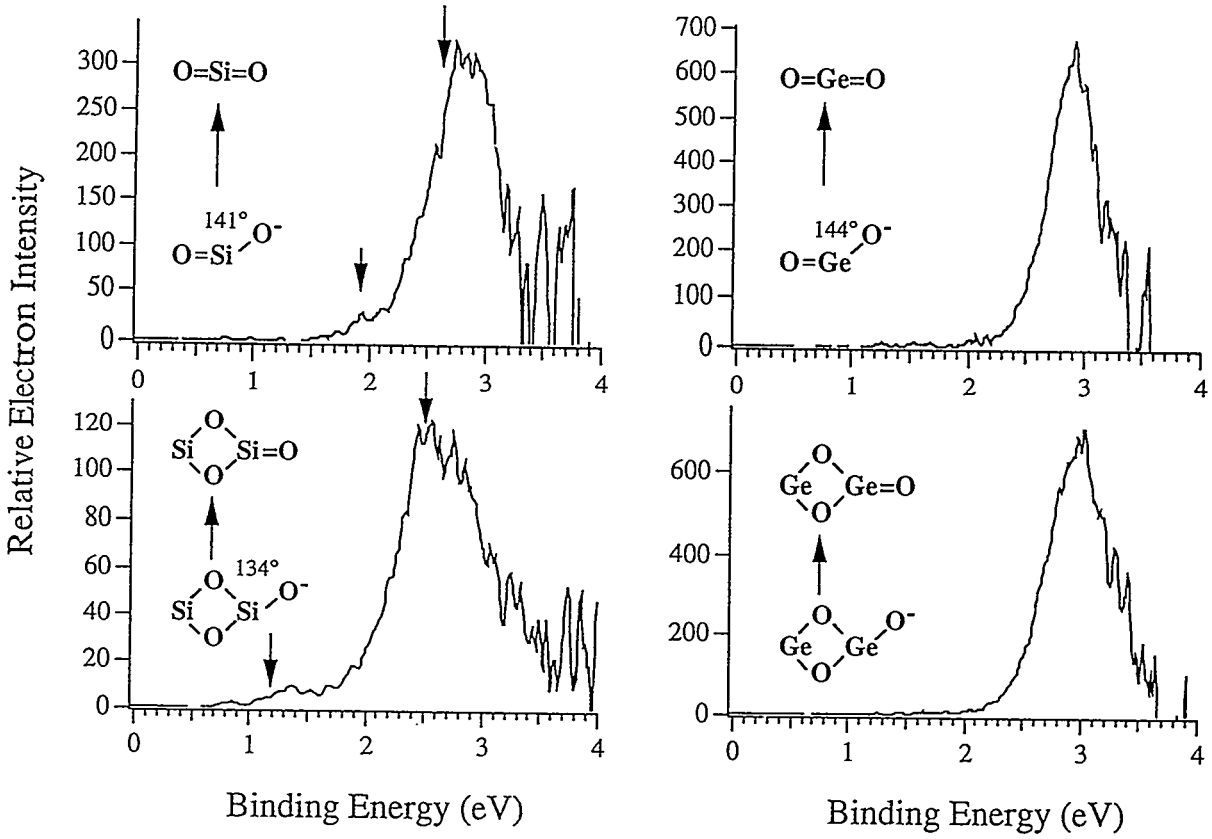

Figure 4.1. Photoelectron spectra of SiO_2^-, $Si_2O_3^-$, GeO_2^-, and $Ge_2O_3^-$ at 266-nm photon energy. The arrows indicate the calculated adiabatic and vertical electron binding energies from DFT.

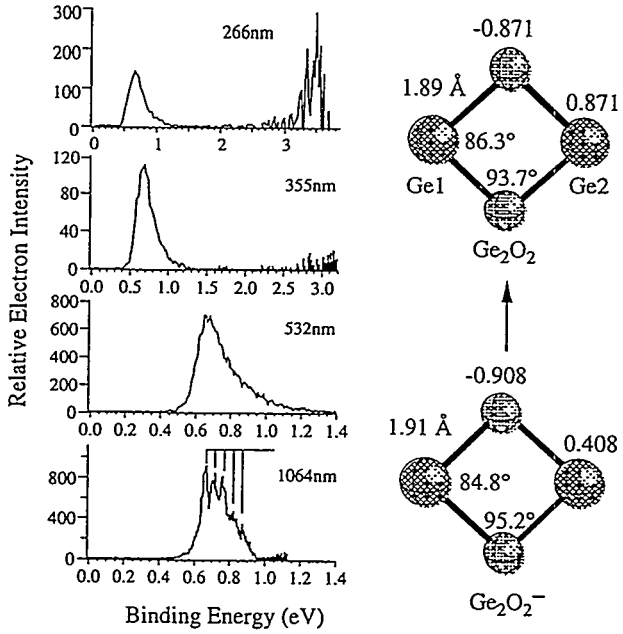

Figure 4.2 (left). The photoelectron spectra of $Ge_2O_2^-$ at four different detachment photon energies, and the DFT optimized structures and charge distributions of $Ge_2O_2^-$ and Ge_2O_2.

2. *Studies of FeC_n^- and FeC_nH^- (n = 2–4)*

Small carbon and hydrocarbon fragments are important in the surface chemistry of many heterogeneous catalysts, usually as intermediates of dehydrogenation reactions and as precursors to carbon films. Metal complexes of these fragments provide interesting models for the study of their bonding with surfaces. Toward this end, we studied complexes of several hydrocarbon fragments bonded to a single transition-metal atom in the gas phase by anion photoelectron spectroscopy (PES), which provides unique information about the electronic structure and the molecular bonding of these simple metal complexes.

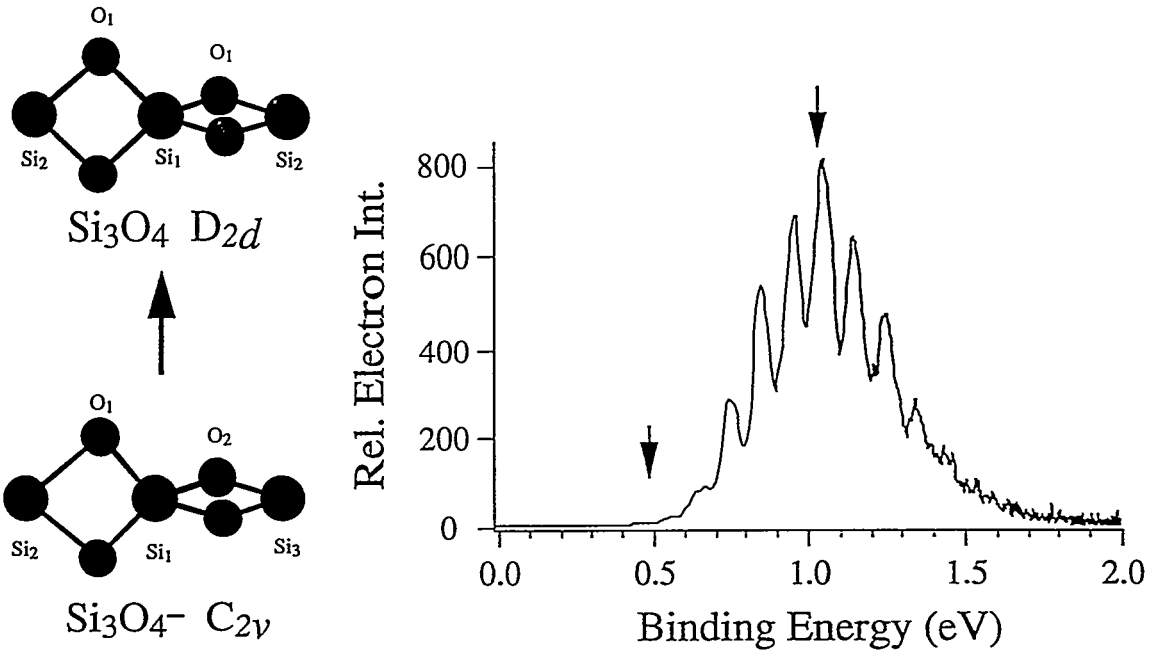

Figure 4.3. The photoelectron spectrum of $Si_3O_4^-$ at 532 nm, showing a well-evolved vibrational progression. The arrows indicate the predicted adiabatic and vertical detachment energies.

The photoelectron spectra of FeC_2^- and $FeC_2H(D)^-$ are studied at 355-nm photon energy.[4] The electron affinities of FeC_2 and $FeC_2H(D)$ are determined to be 1.91(10) eV and 1.41(5) eV, respectively. An excited state of FeC_2 at 1 eV above its ground state is also observed. Only one major detachment channel is observed for $FeC_2H(D)^-$. A vibrationally resolved spectrum at 2.33 eV photon energy for FeC_2D^- is also obtained with a Fe–C stretching progression, yielding a vibrational frequency of 500(100) cm^{-1}. The bonding between Fe and C_2 and $C_2H(D)$ is similar to that in acetylene: Fe is bonded to one C atom through a σ bond in a linear geometry, while C≡C maintains its triple bond feature as in acetylene.

We also studied FeC_n^- and FeC_nH^- (n = 3–4) at 355-nm photon energy.[5] Vibrational structures are resolved in the spectra of FeC_3^- and FeC_3H^-. The FeC_4^- spectrum is unusually broad, indicating a large equilibrium geometry change from the anion to the neutral states. The FeC_4H^- spectrum exhibits a single strong feature. Theoretical studies using DFT have been carried out to determine the structures and bonding of these clusters. All the molecules in the anion ground states are found to be linear, with the Fe atom bonded at one end. The Fe and C bonding involves strong Fe 4*s* and C *sp* interactions as well as considerable Fe 3*d* and C *p* interactions. The n = 3 species can be best characterized by the cumulenic type of bonding with FeC_3H also having an acetylenic isomer. The n = 4 species in the linear structures can be approximately described by diacetylenic type of bonding. Mulliken charge analyses indicate that the extra charge in all the anions enters mainly into the Fe 4*s* antibonding orbital, in agreement with the assignment that the threshold detachment takes place from the σ* orbital mainly between the Fe and C atoms. The vibrational structure resolved in the FeC_3^- spectrum yields a Fe–C stretching frequency of 700(150) cm^{-1} for the first excited state of FeC_3, in agreement with the Fe–C multiple bonding character.

3. Vibrationally- Resolved PES of FeO^- and FeO_2^-: Observation of Low-Spin Excited States of FeO and Determination of the Electron Affinity of FeO_2

The photoelectron spectra of FeO^- and FeO_2^- are obtained at 355-nm photon energy (Fig. 4.4).[6] Transitions to the ground state ($^5\Delta$) and three low-lying excited states ($^5\Sigma^+$, $^3\Sigma^+$, and $^3\Delta$) of FeO are observed. The two low-spin excited states found at 6770 and 8310 cm^{-1} above the ground state, respectively, have not been observed before. The two Σ states, characteristic of detachment of a non-bonding electron from the FeO^- anion, exhibit no vibrational progressions, while a vibrational progression is observed for each of the two Δ states. The two high-spin states, $^5\Delta$ and $^5\Sigma^+$, are in agreement with a previous photoelectron study.[7] The $^3\Delta$ state vibrational frequency is 800(50) cm^{-1}. The spectrum of FeO_2^- shows only one major feature with little vibrational structure at this photon energy. The electron affinity of FeO_2 is determined to be 2.358(0.030) eV.

References

1. L. S. Wang, H. S. Cheng, and J. Fan, *J. Chem. Phys.*, in press, 1995; PNL-SA-25584.

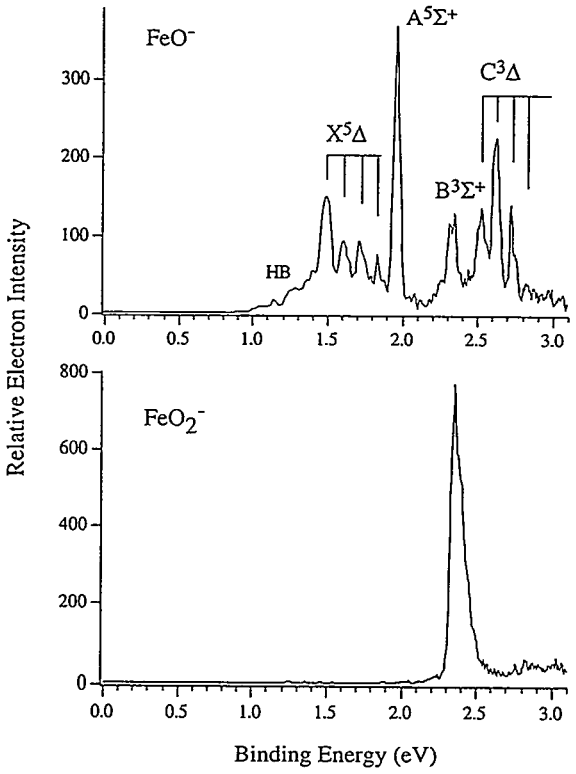

Figure 4.4. The photoelectron spectra of FeO^- and FeO_2^- at 355 nm.

2. J. B. Nicholas, J. Fan, H. Wu, S. D. Colson, and L. S. Wang, *J. Chem. Phys.*, submitted, 1995.
3. J. Fan, J. B. Nicholas, J. M. Price, S. D. Colson, and L. S. Wang, *J. Am. Chem. Soc.*, in press, 1995; PNL-SA-25585A.
4. J. Fan and L. S. Wang, *J. Phys. Chem.* **98**, 11814 (1994).
5. J. Fan, L. Lou, and L. S. Wang, *J. Chem. Phys.* **102**, 2701 (1995).
6. J. Fan and L. S. Wang, *J. Chem. Phys.*, in press, 1995.
7. P. C. Engelking and W. C. Lineberger, *J. Chem. Phys.* **66**, 5054 (1977).

Photoelectron Spectroscopy and Electronic Structure of Metal Clusters and Chemisorbed Metal-Cluster Complexes

*L. S. Wang and H. Wu**

Supported by National Science Foundation.

*Department of Physics, Washington State University.

Clusters containing two to several hundred atoms are considered to be ideal models for studying chemisorption on surfaces due to their finite sizes, which enable more rigorous theoretical calculations. Cluster chemical reactivities have been studied extensively in the past few years and have been found to be a strong function of cluster size, and can vary by orders of magnitude simply by adding or subtracting one atom. Yet it is not understood why some clusters are more reactive than others. We are interested in investigating the cluster-molecule interactions through ultraviolet photoelectron spectroscopy (PES) of size-selected negative cluster ions by probing the change of the electronic structure of a cluster upon chemisorption. This knowledge obtained from comparing PES spectra of the bare clusters with that of the cluster-adsorbate complexes should lead to detailed insight about how a molecule interacts with the cluster.

1. Photoelectron Spectroscopy of Size-Selected Transition Metal Clusters

The photoelectron spectra of size-selected Fe_n^- (n = 3–24) clusters are investigated at a photon energy of 3.49 eV.[1,2] The photoelectron spectra of

these clusters exhibit sharp features throughout this size range. The spectra for Fe_{3-8}^- show large size-dependence, with many resolved features. The spectra for Fe_{9-15}^- exhibit some similarity with each other, all with a rather sharp feature near the threshold. An abrupt spectral change occurs at Fe_{16}^-, then again at Fe_{19}^- and Fe_{23}^-. These photoelectron spectral changes coincide remarkably with changes of the cluster reactivity with H_2. Extended Hückel molecular orbital (EHMO) calculations are performed for all the clusters to aid the spectral interpretations. The calculations yield surprisingly good agreement with the experiment for clusters beyond Fe_9 when BCC (body-centered cubic) structures are assumed for Fe_{9-15} and a similarly close-packed structure with a BCC Fe_{15} core for the larger clusters. Figure 4.5 shows the PES spectra for Fe_{9-16}^- along with the EHMO results and the assumed cluster structures. The EHMO calculations allow a systematic interpretation of the sharp photoelectron spectral features in Fe_{9-15}^-, and reproduced the abrupt spectral change taking place from Fe_{15}^- to Fe_{16}^-. Most importantly, the reactivity changes of the clusters with H_2 are successfully explained based on the detailed electronic structures of the clusters, as revealed from the PES spectra and the theoretical calculations. The calculations also correctly predict the existence of magnetism in these clusters and yield reasonable values for the cluster magnetic moments.

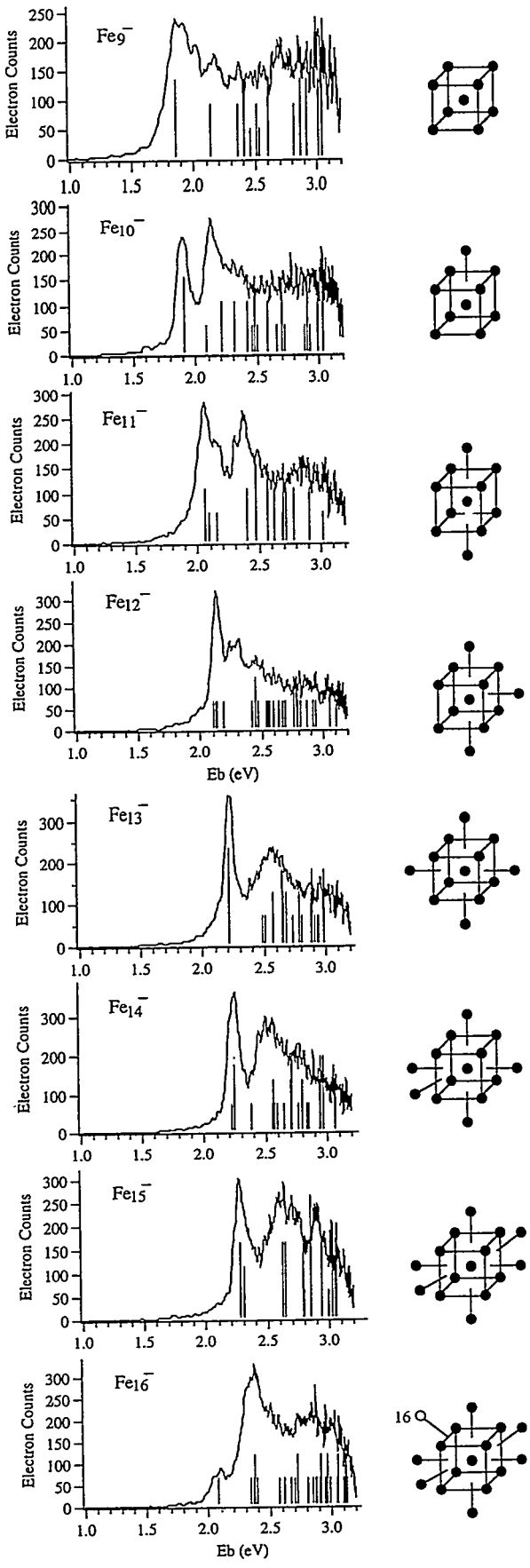

Figure 4.5 (right). Photoelectron spectra of Fe_9^- to Fe_{16}^- at 3.49-eV photon energy. The stick spectra are the extended Hückel occupied energy levels by aligning the HOMO level with the threshold feature. The stick height is proportional to the orbital degeneracy and electron occupancy. The assumed structures in the calculations are also shown.

2. Oxygen-Chemisorbed Iron Clusters

The photoelectron spectroscopy of size-selected oxygen-chemisorbed clusters, Fe_nO^- (n = 1–16), has been studied to probe the initial oxidation of the iron clusters.[3] The spectra of the pure iron clusters show rather sharp features in the whole size range, but those of the oxygen-chemisorbed ones are considerably different, with extensive sharp structures observed for n up to 6 only. The electron affinities (EAs) of both the bare and the chemisorbed clusters exhibit strong size variations. However, the first oxygenation of the iron clusters induces a systematic lowering of EA in the size range n = 9–15 (Fig. 4.6). Toward a complete molecular picture of these interesting clusters, density functional theory (DFT) calculations are performed to determine the equilibrium cluster structures, oxygen chemisorption sites, and their electronic structures. The equilibrium structures obtained for Fe_nO with n = 2–6 are shown in Fig. 4.7. For Fe_{2-4}, the O atom prefers the bridging edge site. For Fe_5, the DFT results show equal stability for both the edge site and the threefold face site. For Fe_6, the O atom prefers the threefold face site.

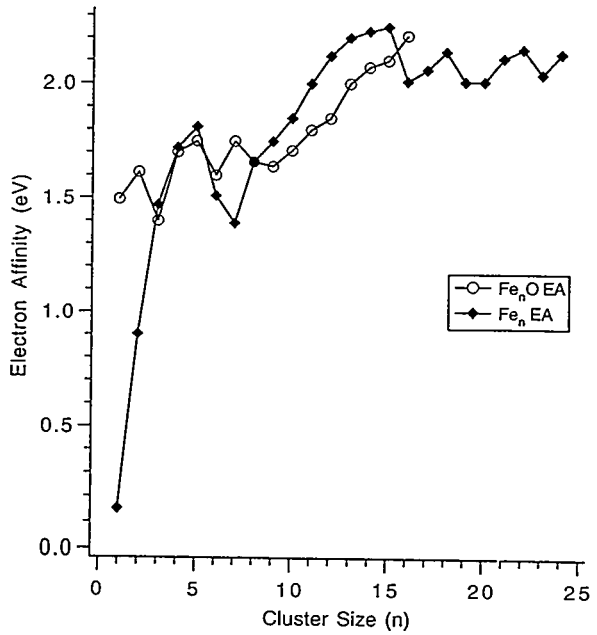

Figure 4.6. The electron affinities of pure iron clusters and oxygen-chemisorbed iron clusters.

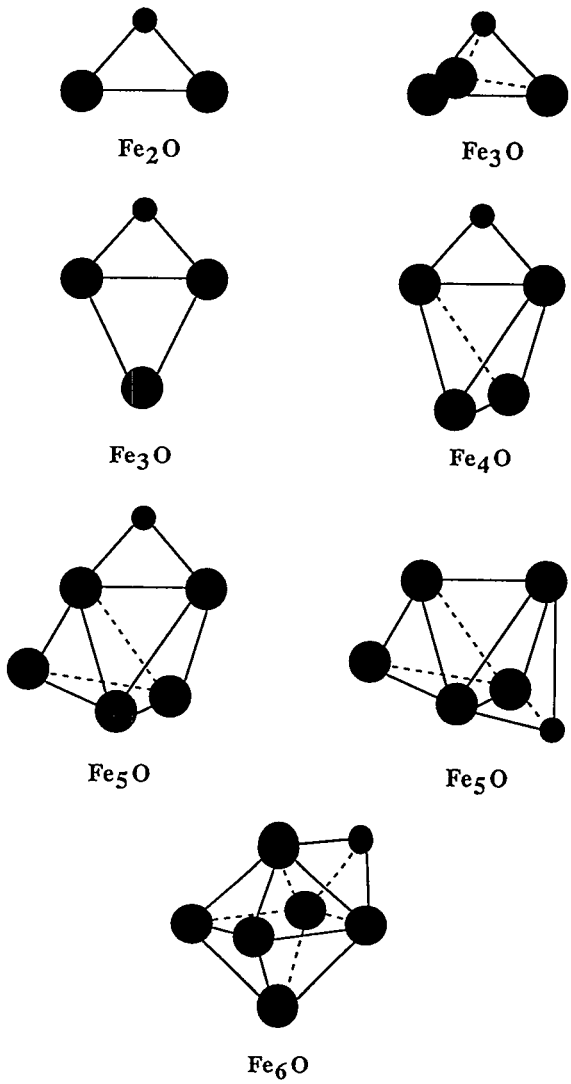

Figure 4.7. Structures of a few small oxygen-chemisorbed iron clusters from density functional theory calculations.

3. Study of Iron-Carbon Mixed Clusters, FeC_n (n = 2–5): A Possible Linear to Cyclic Transition from FeC_3 to FeC_4

Small carbon clusters have been studied over the past few decades and continue to be a fertile current research topic due to their importance in many disciplines. The current interest in carbon clusters is fueled by the discovery and characterization of fullerenes. The field of fullerene science now includes the study of metallo-fullerenes[4] and carbon nanotubes.[5] The formation of metallo-fullerenes was discovered soon after the discovery of C_{60} itself. However, their formation seems to be highly selective: only the alkali, alkali-earth, and

rare-earth elements are found to form metallofullerenes easily. No transition metals have been found to form metallo-fullerenes. Carbon nanotubes have been found to form in the arc synthesis of fullerenes. The introduction of a transition metal into the arc synthesis of fullerenes has been found to catalyze single nanotube formation with the tube diameters down to that of C_{60} itself.[6] To understand the metallo-fullerene formation and the catalytic roles of the transition metals in the carbon nanotube formation requires detailed knowledge about the basic interactions between carbon and the transition metals. Carbon has been found to form metallo-carbohedrenes (met-cars), a series of stable molecules with transition metals.[7] The met-cars may have important materials applications—as catalysts, for example. However, the mechanisms for the formation of met-cars and their basic physical and chemical properties are not understood. A detailed characterization of the met-car formation mechanism will require a thorough understanding of the small metal-carbon mixed clusters and how their structure and bonding evolve as the cluster size increases.

We studied small Fe/C mixed clusters, FeC_n^- (n = 2–5) by anion photoelectron spectroscopy at 3.49-eV photon energy.[8] The spectra of FeC_2^- and FeC_3^- show well-resolved features and are consistent with linear-to-linear detachment transitions. The FeC_4^- spectrum is quite broad, suggesting large geometry change from the anion to the neutral. Since FeC_4^- is known to be linear,[9] our data suggest that neutral FeC_4 may have a cyclic structure. The spectrum of FeC_5^- exhibits both sharp and broad features, consistent with the existence of both a linear and a cyclic isomer. A linear-to-cyclic structural transition is thus suggested to take place for the neutral FeC_n clusters from $n = 3$ to 4: for $n < 4$ they are linear and for $n \geq 4$ they can be both linear and cyclic. This is similar to the linear-to-cyclic transition occurring for pure carbon clusters from n = 9 to 10, but at a much smaller cluster size due to the presence of the Fe atom.

References

1. L. S. Wang, H. S. Cheng, and J. Fan, *Chem. Phys. Lett.*, in press, 1995.
2. L. S. Wang, H. S. Cheng, and J. Fan, *J. Chem. Phys.*, in press, 1995.
3. L. S. Wang, J. Fan, and L. Lou, *Surf. Rev. Lett.*, in press, 1995.
4. Y. Cai, T. Guo, C. Jin, R. E. Haufler, L. Chibante, J. Fure, L. H. Wang, J. M. Alford, and R. E. Smalley, *J. Phys. Chem.* **95**, 7564 (1991).
5. S. Iijima, *Nature* **354**, 56 (1991).
6. S. Iijima and T. Ichihashi, *Nature* **363**, 603 (1993); D. S. Bethune, C. H. Kiang, M. S. de Vries, G. Gorman, R. Savoy, J. Vaquez, and R. Beyers, *Nature* **363**, 605 (1993).
7. B. C. Guo, K. P. Kerns, and A. W. Castleman, Jr., *Science* **255**, 1411 (1992).
8. L. S. Wang, *Surf. Rev. Lett.*, in press, 1995.
9. G. von Helden, N. G. Gotts, P. Maitre, M. T. Bowers, *Chem. Phys. Lett.* **227**, 601 (1994).

High-Resolution Spectroscopy of Molecules and Clusters

S. W. Sharpe, T. A. Blake, and S. Xu*

Supported by Office of Basic Energy Sciences.

*Postdoctoral Research Associate.

Infrared spectroscopy is one of several powerful techniques that the physical chemist can call upon for studying the behavior of matter on an atomic scale. But high-resolution gas-phase infrared spectroscopic techniques have traditionally been plagued by a number of problems, including spectral congestion, Doppler broadening, and pressure broadening. Spectral congestion is related to the number of quantum states populated at a given temperature and dictated by Maxwell-Boltzmann statistics. Doppler broadening is related to temperature through the kinetic energy relationship, but also involves the random three-dimensional motion of the gas molecules. Pressure broadening is related to temperature through the collisional frequency of the molecules, which in turn depends on the density and velocity of the sample. By cooling and reducing the pressure of a gas sample these three effects may be minimized, but at the expense of drastically reduced signals.

A relatively new technique which takes advantage of the properties of rapidly expanding a gaseous sample into a moderate vacuum has been used in our laboratory for the last year. A gas is expanded through a slit orifice which measures 5 inches in length by 1/6000 of an inch wide. The ensuing ribbon of gas expands at supersonic velocities and in the process, molecules entrained in this ribbon are cooled to a few degrees above absolute zero

without condensing. In addition, the random three-dimensional motion of the gas molecules are changed to a two-dimensional flow with little velocity component in the plane of expansion but perpendicular to the mass flow. If infrared laser light is used to interrogate the gas molecules through the plane of expansion, spectral congestion, Doppler broadening, and pressure broadening are all reduced significantly. By exploiting the virtues of supersonic expansions, we have recently obtained high-resolution infrared absorption spectra of a number of important molecules and cluster species.

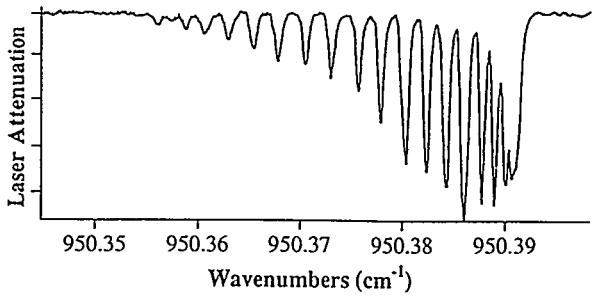

Figure 4.8. A representative spectrum of the NH_3-Ar dimer corresponding to the Q branch of the Π_s ($j = 1, k = 0$) $\leftarrow \Sigma_a$ ($j = 0, k = 0$) transition.

Ammonia-Argon Dimer

Small aggregates or clusters of weakly bonded molecules and atoms have been the focus of research efforts for nearly three decades. Their existence is suspected in interstellar space (e.g., NH_3–H_2), they may be implicated in the infrared atmospheric continuum (e.g., water dimer), they are prototypes for both the liquid and condensed phases, and they provide an exacting test of theory and modeling. The NH_3–Ar dimer was first observed by microwave/radiofrequency techniques in 1984. Since then numerous papers have appeared discussing both detailed experimental and modeling efforts. The ammonia-argon dimer is a prototypical cluster exhibiting free internal rotation of the NH_3 subunit and tunneling due to the ammonia inversion or "umbrella" mode. In addition, NH_3–Ar exists in both ortho and para states due to the three equivalent hydrogens. Currently, there is little experimental information on the states involving ammonia inversion in this dimer. This information is critical to developing a more complete potential energy surface.

We have recorded extensive experimental data on the NH_3–Ar dimer by probing the umbrella mode near 950 cm^{-1} with tunable semiconductor diode lasers. We have observed and cataloged several hundred lines corresponding to various levels of internal rotation; a portion of this spectrum is shown in Fig. 4.8. This data is being analyzed jointly by PNL and researchers at NIST (Gerry Fraser and Alan Pine).

Cation-Ether Complexes in the Gas Phase: Bond Dissociation Energies and Equilibrium Structures of $Li^+[O(CH_3)_2]_x$, $x = 1$–4

M. B. More, E. D. Glendening,† D. Ray, D. Feller,† and P. B. Armentrout**

Supported by Office of Basic Energy Sciences.

*Department of Chemistry, University of Utah.
†Theory, Modeling, and Simulation.

Non-covalent interactions between ions and neutral molecules are of fundamental importance to molecular recognition and related phenomena in condensed phases. The importance of these interactions is illustrated by the selectivity of macrocyclic ligands (e.g., crown ethers) toward alkali cations in aqueous solution. Crown-ether cation complexes are interesting not only from a fundamental point of view, but also because of their possible utility in advanced chemical separations methods currently under development to reduce the present inventory of high-level radioactive waste. Computational methods that possess the capability to predict the selectivity of a macrocyclic ligand for a given cation in a variety of environments would be useful tools in the development of advanced separations technologies, but such methods do not currently exist. Accurate models of the relevant non-covalent interactions are prerequisite to the development of such methods. One approach to understanding these non-covalent interactions is the study of ion-molecule complexes in the gas phase. Measurements and calculations on the isolated complexes allow the

separation of intrinsic effects from effects due to solvation and solvent-induced phenomena. Obtaining accurate data on complexes of cations with simple ethers, and determining the level of theory required to accurately model these complexes are the first steps toward developing accurate models of the interaction between cations and polyethers.

The present work was undertaken to extend the thermochemical database on ML_x^+ complexes and to test and validate the experimental and theoretical methods employed. Dimethyl ether (DME) was selected as the ligand, as it may be considered the simplest functional subunit of an aliphatic polyether. Accurate experimental determinations of the bond dissociation energies of the $(DME)_xLi^+$–DME complexes facilitate assessment of the level of *ab initio* theory required to describe accurately the non-covalent interactions in the complexes. Also, the results of the calculations (vibrational frequencies and geometries) are used to provide a more accurate analysis of the experimental results. An understanding of the thermochemical results is aided by the application of natural energy decomposition analysis (NEDA) to the calculated wavefunctions. The work presented here represents the first steps in a synergistic program to develop a predictive model of the non-covalent interactions between cations and polyethers. Work in progress extends this first investigation to other metals and more complicated ligands, such as the crown ethers.

The bond dissociation energies, equilibrium structures and harmonic vibrational frequencies of $Li^+[O(CH_3)_2]_x$, x = 1–4, were determined. Bond dissociation energies were determined experimentally by analysis of the thresholds for the collision-induced dissociation of $Li^+[O(CH_3)_2]_x$, x = 1–4, by xenon (measured at the University of Utah using guided ion-beam mass spectrometry) and theoretically by *ab initio* electronic structure calculations at RHF and MP2 levels of theory. In all cases, the lowest-energy dissociation channel observed experimentally, and the primary product, is endothermic loss of one ether molecule. The cross-section thresholds are interpreted to yield 0- and 298-K bond energies after accounting for the effects of multiple ion-molecule collisions, internal energy of the complexes, and unimolecular decay rates. Both experimental and theoretical results are in good agreement with previous experimental results for $Li^+[O(CH_3)_2]$. Agreement between experiment and theory is also very good for x = 2–4, where the experimental bond energies are 12 ± 6, 10 ± 7, and –2 ± 10 kJ/mol, respectively, lower than theory. The calculated equilibrium structures of the complexes exhibit the importance of electrostatic interactions. Natural energy decomposition analysis of the calculated wavefunctions indicates charge transfer is also important in these complexes.

Spectroscopy and Dynamics of Molecular Clusters

A. H. Bahnmaier,† V. A. Venturo,* A. G. Joly, J. M. Price,‡ and D. Ray*

Supported by Office of Basic Energy Sciences.
*Postdoctoral Research Associate.
†Supported by Deutsche Forschungsgemeinschaft (DFG).
‡Computing and Information Sciences.

The synthesis of clusters in molecular beams affords the opportunity to create model systems exhibiting a rich variety of chemical phenomena. The application of techniques of laser spectroscopy and mass spectrometry to size-selected cluster beams facilitates rigorous studies of fundamental properties (both static and dynamic) of these model systems. The goal of this project is to examine the relationships between cluster structure (geometric and electronic) and function (reaction dynamics and kinetics) in molecular and ionic clusters. Comparison of the experimental results with predictions of emerging theoretical models is an important component of this project.

A photoionization-based version of rotational coherence spectroscopy (RCS) was implemented and used to measure psec time-resolved rotational coherence transients of fluorene and fluorene–Ar. RCS is a time-domain spectroscopic technique that yields the rotational constants of an absorber to an accuracy of <1%, without requiring precise measurement or detailed analysis of individual eigenstates. A software package for simulation and analysis of rotational coherence transients (accessible via the Internet) was developed in collaboration with J. M. Price (Computer and Information Sciences, EMSL). Fluorescence-based implementations of RCS have been used extensively by Felker and coworkers at UCLA and Topp and coworkers

at the University of Pennsylvania to study the geometric structures of small clusters (dimers and trimers) that are amenable to size-selective photoexcitation. Photoionization-based implementations allow the use of time-of-flight mass spectrometry to effect mass selection and extend the range of applicability of RCS to larger and/or photochemically active clusters.

5. Analytical Methods Development

Molecular Speciation of Waste Tank Contents

S. D. Colson, S. E. Barlow, J. P. Cowin, M. E. Geusic, N. G. Gotts,† R. S. McDowell, and B. M. Wise‡*

Supported by Office of Environmental Restoration and Waste Management—EM-50 Characterization, Monitoring, and Sensor Technology Integrated Program.

*Materials and Chemical Sciences Center.
†Postdoctoral Research Associate.
‡EMSL, Materials and Interfaces.

Current chemical analysis of Hanford waste tank cores relies heavily on traditional wet-chemistry techniques. This frequently requires significant pretreatment, which generates additional unwanted mixed-waste materials. In addition, current technologies provide limited data on chemical constituents as a function of core depth in the tank, preventing managers and staff of the TWRS programs from obtaining detailed information on the amounts and distribution of chemical constituents within the tanks. The current wet chemistry analysis techniques are very time consuming (up to six months to analyze and report) and expensive (often in excess of $500K per core) to execute. Hot-cell chemical analysis process throughput is now a major time/cost factor in meeting the schedule for analysis of Hanford tank core samples. As promising pretreatment methods are scaled up, definitive information is needed on those tank wastes for which the process proves ineffective (to understand why), and to provide a basis for further process technology development, if necessary. Addressing these needs in existing and/or future plants can have multimillion dollar cost impacts.

The combined impact of these needs is to drive the development of analytical methods that can provide rapid results; be automated to handle high sampling rates with as little associated sample preprocessing as possible; provide simultaneous results on a number of analytes, reducing time and costs; reduce the reliance on traditional, time-consuming, and more costly analyses; and can be deployed for operation outside the development laboratory (to hot cells and on-line in waste processing facilities). Laser ablation mass spectrometry (LA/MS) responds to these needs and in addition provides microsampling to allow depth profiling, and provides direct elemental and molecular species analysis to support TWRS methods development and subsequent on-line process analysis and control.

The LA/MS method being developed for analysis of waste tank samples is part of a larger, jointly-funded EM-50/EM-30 program to accelerate the characterization of the Hanford waste storage tanks. This method depends upon three key steps:

(1) The ablation of solid material to form small particles;

(2) The entrainment of these particles in a carrier gas and their transport via a small tube to a low-radioactivity area; and

(3) The chemical analysis of these particles by mass spectrometry.

Our challenge was to optimize this method to analyze for the chemical species present in the waste material. Other portions of this program have shown that only aerosol particles in the micron to tenths-of-micron size are efficiently transported. Hence, several of our objectives focus on the methods for the production of aerosol particles of this size that quantitatively represent the chemical speciation distribution of the waste material. A second major component of our work focused on the chemical analysis of the aerosol particles themselves. The third element of the program is data analysis (of both elemental and chemical speciation data) via chemometric methods to enhance LA/MS as a screening tool in itself and when used in conjunction with other methods such as Raman and infrared spectroscopies. The chemometrics studies showed that standard pattern recognition techniques can adequately classify waste tank samples.

The molecular speciation project established that the sampling methods proposed will yield accurate sample fingerprints, and identified two methods for analysis that we will employ in parallel. One analyzes the aerosol stream by injecting it directly into a mass spectrometer, where it is analyzed following laser ionization. This unit yields results in seconds. A second instrument, which gives complementary results, will capture the aerosol material and analyze it in batch modes via secondary ion mass spectrometry (SIMS), with sev-

eral minutes to an hour turnaround time. Estimated sensitivity limits are generally at the few parts-per-million level.

Rovibrational Spectroscopy of Carbon Tetrachloride

S. Xu, R. S. McDowell, and S. W. Sharpe*

Supported by Office of Nonproliferation and National Security.

*Postdoctoral Research Associate.

Carbon tetrachloride was once widely used as a refrigerant, solvent, and degreaser, and waste CCl_4 constitutes a significant fraction of the cleanup problem at the Hanford reservation and other industrial sites. In the atmosphere, CCl_4 acts as both a greenhouse gas and a source of ozone-depleting free Cl atoms. There is interest in long-range detection and analysis of CCl_4, both for environmental applications and for monitoring of industrial compliance with ES&H regulations. The design of laser systems for such purposes requires a detailed knowledge of the rotational-vibrational infrared spectrum of the molecule.

Rather surprisingly, no high-resolution infrared spectra or rotational analysis of CCl_4 has ever been reported, in part because of an extremely dense rotational-vibrational spectrum in the gas phase. This results from several factors, including the presence of five naturally occurring and overlapping isotopomers, each of which has its own unique spectral features with slightly displaced vibrational origins. In addition, the congestion of rovibrational lines in room-temperature spectra of CCl_4 is exacerbated by the large vibrational partition function ($Q_{vib} \approx 6.02$ at 300 K, so only 16.6% of the molecules are in the ground vibrational state, and hot bands dominate the spectrum), and the small rotational constant (the most populated rotational level at 300 K is $J = 60$). Finally, the levels ν_3 (799 cm^{-1}) and $\nu_1 + \nu_4$ (774 cm^{-1}) are in Fermi resonance, so the combination $\nu_1 + \nu_4$ is much stronger than would otherwise be expected and both bands have mixed character.

We have obtained high-resolution rotationally resolved infrared spectra of the spherical-top rotor $C^{35}Cl_4$ (in samples of natural isotopic composition) both in static cells by FTIR spectroscopy (ν_4 and $\nu_1 + \nu_4$) and in a supersonically cooled expansion with tunable diode lasers (ν_3). For the ν_3 fundamental, quantum assignments were made for individual transitions from $P(20)$ to $R(24)$, and the partially resolved Q branch was matched with synthesized spectra. The bands ν_4 and $\nu_1 + \nu_4$ exhibit much reduced manifold splitting, and scalar fits were made to the $R(24)$–$R(70)$ and $P(38)$–$R(56)$ frequencies, respectively. The $\nu_3/(\nu_1 + \nu_4)$ Fermi diad yields Coriolis constants $\zeta_3 = 0.621$ and $\zeta_4' = -0.145$ that satisfy the harmonic sum rule, but are perturbed by the Fermi resonance and are inconsistent with intramolecular force fields previously reported based on isotope shifts in matrix spectra. The true bending-mode Coriolis constant $\zeta_4 = -0.414$, obtained from analysis of the isolated and unperturbed ν_4 band, agrees well with the isotope shifts.

Consideration of these Coriolis constants has led to some generalizations involving vibrational motions in all tetrahedral XY_4 molecules, for which the higher-frequency infrared-active fundamental ν_3 is a nearly pure stretch. Construction of a vector-displacement normal-mode model yields a simple formula for the Coriolis constants that agrees well with those observed over a wide range of central-atom/ligand mass ratios, from CCl_4 ($m_X/m_Y = 0.34$) to SnH_4 ($m_X/m_Y = 115$), and that can indicate when a perturbation is affecting a measured constant: $\zeta_3 \approx 4/[3(m_X/m_Y) + 4]$.

The detailed spectral data and spectroscopic and molecular constants obtained for CCl_4 enable us to model the absorption for various atmospheric conditions. We have identified several promising analytical frequencies, based on Q-branch features in the 12.5–13 μm region that are relatively free of atmospheric interference. Intensity measurements are in progress so that we can quantify the detection limits.

Rovibrational Analysis of Chlorine Nitrate

T. A. Blake, S. Xu, and S. W. Sharpe*

Supported by Atmospheric Radiation Measurement (ARM) Program, Global Climate Change Initiative; and by Laboratory Directed Research and Development (LDRD).

*Postdoctoral Research Associate.

Chlorine nitrate is an important reservoir species in stratospheric chemistry: it sequesters the reactive molecules ClO and NO_2, both of which participate in catalytic cycles that destroy stratospheric ozone. Ozone degradation proceeds via a catalytic process involving atomic chlorine, which can be produced by the photodissociation of Freons (e.g., CF_2Cl_2). Chlorine nitrate has been postulated to act as a reservoir for atomic chlorine and may be important in terminating this catalytic cycle. These processes can be summarized as follows:

$$CF_2Cl_2 + h\nu \rightarrow CF_2Cl + Cl$$
$$O_3 + Cl \rightarrow ClO + O_2$$
$$NO_2 + ClO + M \rightarrow ClONO_2 + M^{\dagger}.$$

Monitoring the chlorine budget of the stratosphere has become an important goal of atmospheric scientists. Chlorine nitrate has been detected by ground-based and balloon-borne infrared spectrometers and by an infrared emission spectrometer on board the Upper Atmospheric Research Satellite. Reducing the data from these instruments to determine the concentration of chlorine nitrate has been, however, problematic. The ν_4 fundamental band in the vicinity of 780 cm^{-1} is typically used for the atmospheric detection of chlorine nitrate because it is of moderate intensity and is unobscured by strong absorptions from other molecules. Uncertainties in the absolute absorption cross section and the spectroscopic constants of the excited vibrational state have led to systematic errors as large as 50% in the concentration measurements of this molecule. Laboratory measurements of the ν_4 band have encountered two difficulties: (1) chlorine nitrate is an unstable molecule that decomposes to ClO and NO_2 when in contact with glass or metal components; and (2) the molecule has an extremely congested rovibrational spectrum due to its small rotational constants, the ^{35}Cl and ^{37}Cl isotopic species whose bands lie within 2 cm^{-1} of one another, and hot bands that have significant population even at stratospheric temperatures of 195 K.

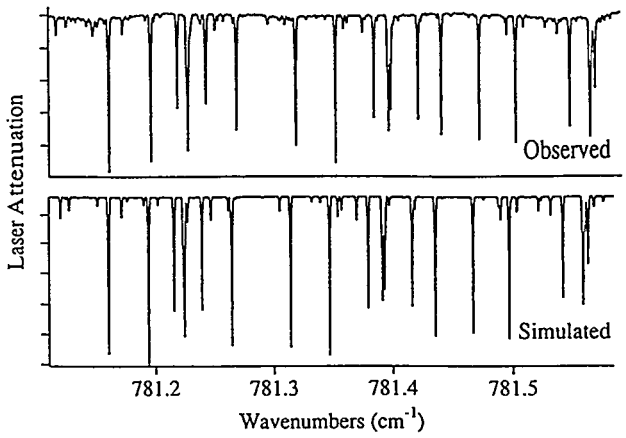

Figure 5.1. Spectrum of chlorine nitrate obtained in the supersonic expansion at approximately 7 K (lower trace). The upper trace is a simulation based on molecular constants obtained at PNL.

Previously reported infrared spectra of $ClONO_2$ are not of sufficiently high resolution and/or quality to allow for an unambiguous rovibrational assignment of the observed transitions.

For the development of rapid, reliable techniques for identifying and quantifying $ClONO_2$, an infrared "road map" and accurate upper-state molecular constants are needed. We have obtained such spectra by seeding chlorine nitrate in a pulsed jet of argon, thus obtaining the rotationally resolved spectrum of the ν_4 fundamental band using tunable infrared diode lasers. The near-perpendicular crossing of the laser and molecular beam yields sub-Doppler resolution, which, combined with a jet rotational temperature of approximately 7 K, gives a rotationally resolved and greatly simplified spectrum of the *P* and *R* branches of both the ^{35}Cl and ^{37}Cl isotopomers (Fig. 5.1). Over 800 transitions from the ^{35}Cl and 450 transitions from the ^{37}Cl isotopomers were measured, assigned, and fit to a model Hamiltonian to provide spectroscopic constants with MHz precision for the excited state of the band. Careful measurements were also made of the intensities of several transitions to give an estimate of the *a* and *b* inertial axis vibrational transition moments for the planar molecule. Subsequent calculations have provided absorption cross sections for individual transitions throughout the band.

The spectroscopic constants and intensity data produced by this research should provide a significant step forward in the analysis of chlorine nitrate field measurements.

Trace Detection of Gaseous Species

*S. W. Sharpe, T. A. Blake, and J. F. Kelly**

Supported by Office of Nonproliferation and National Security.

*Materials and Chemical Sciences Center.

Infrared spectroscopy forms the basis for a suite of analytical techniques that are highly specific and extremely sensitive, and can be directly applied to atmospheric and process monitoring. Tunable infrared diode lasers posses a number of unique properties that make them ideal devices for use in ultra-trace detection of gas-phase molecules. Currently, lead-salt diodes are available for semicontinuous coverage of 3,000 to 300 cm^{-1}. These devices can be frequency-tuned at extremely high rates, allowing a 3-cm^{-1} region to be covered in less than 0.001 second. In addition, diode lasers have extremely low noise. The high tuning rate, low noise, and intense spectral brightness allow the researcher to approach and in some cases reach the shot limit, which is the theoretical limit for laser absorption detection schemes.

We are currently involved in a number of projects requiring rapid (~1 second), real-time trace detection of gases at the parts-per-trillion (ppt) level, for both anthropogenic and naturally occurring infrared-active molecules. An example is the quantitative monitoring of nitrous oxide and its isotopomers that may be associated with fugitive emissions from underground high-level storage tanks found on many DOE sites. The technique takes advantage of the rapid tuning capabilities of diode lasers and involves scanning the laser over many absorption features. This allows us to measure the concentration of several molecules (or isotopomers) simultaneously. In addition, both speciation and detectivity are greatly enhanced by preparing low-pressure, Doppler limited samples. Parts-per-trillion detection of multicomponent (multi-isotopomer) systems can currently be obtained in under 1 second; Fig. 5.2 illustrates such an analytical scan, showing that we can accurately determine isotopic ratios of $^{14}N_2{}^{16}O$ and its isotopomers.

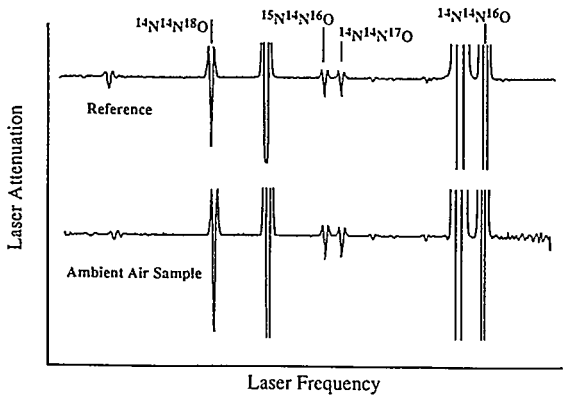

Figure 5.2. Spectrum of nitrous oxide in ambient air taken in ~1 second. Note the weaker features, which are due to minor isotopomers of N_2O containing $^{18,17}O$ and ^{15}N.

A second project involves the development of a portable device for diagnosis of human pathologies by breath analysis. In this application, we are interested in monitoring for specific biomarkers that appear only when the patient has a specific pathology or disease. These biomarkers could be a direct consequence of a pathology such as the presence of elevated ketone concentrations in the breath of diabetics. Alternatively, a stable isotopically tagged species could be introduced either by injection or ingestion. This tagged species would be metabolized only by a specific bacterium and give a unique signature in the breath.

This instrument is based on a Herriot Cell Sniffer for quantitative detection of gas-phase samples. Although the Sniffer is highly specific to a particular effluent, it can be configured for detection of almost any infrared-active molecular species. Extremely high sensitivity (i.e., sub-ppb) and excellent speciation are obtained by combining a highly-monochromatic laser source with a long optical path length, low-pressure, Doppler-limited sampling system. The device consists of a mid- or near-infrared tunable diode laser that is repeatedly ramped over a specific spectral region known to contain rotational-vibrational transitions of the target molecule. Sample is continuously admitted to the Sniffer absorption cell, which is maintained at a pressure of 30 torr or less to remove pressure-broadening effects. Ultimate spectral resolution is limited by Doppler broadening and will depend upon temperature and molecular weight of the effluent molecule, but will typically be on the order of 150 MHz (i.e., 0.005 cm^{-1}). The Sniffer cell is based on a Herriot multipass design and contains a pair of spherical mirrors separated by 55 cm, which create a 100-meter folded optical path for increased optical depth.

6. Miscellaneous

Generation of Sub-Picosecond Infrared Laser Pulses

Gary R. Holtom

Instrument development supported by Environmental Molecular Sciences Laboratory (EMSL).

Our research on chemical dynamics of hydrogen-bonded liquids requires a reliable, powerful mid-infrared source, where development has been slower than in the visible region. Based on recent advances in the technology for generating ultrafast laser pulses, we have developed the laser systems needed to make possible a new generation of experiments in chemical physics.

Our starting point is the well-developed solid-state laser systems based on titanium-doped sapphire, a very reliable and powerful source of near-infrared radiation. The challenge is to convert the output to the mid-infrared, for which we use optical parametric oscillators (OPOs) and amplifiers. The synchronously-pumped OPO is in effect a solid-state dye laser. These devices are efficient and stable, and operate in spectral regions at much longer wavelength than dyes. We can generate pulses less than 100 fs long from about 1 μm to longer than 4 μm, with average powers of hundreds of milliwatts. In addition, we are developing amplifier technologies to produce microjoule energies over this range, at repetition rates much greater than available with dye-laser technology.

This work involves characterizing new nonlinear crystals, applying new methods in shaping and characterizing ultrafast light pulses, and solving optical, mechanical, and electrical problems to create a reliable laser source for every day use in chemical physics experiments.

Non-neutral Plasma Physics for Applications to Cyclotron Resonance Mass Spectroscopy

A. J. Peurrung, S. E. Barlow, and R. T. Kouzes†*

Supported by Office of Basic Energy Sciences and Laboratory Directed Research and Development (LDRD).

*EMSL Materials and Chemical Sciences Center.
†EMSL Computing and Information Sciences.

We have undertaken a literature search and review of the non-neutral plasma as an experimental medium. We have provided an introduction to the field of non-neutral plasma physics and especially its application to cyclotron resonance mass spectrometry. Beginning with fundamental concepts and definitions, we progress to characterization of the equilibrium state, transport to equilibrium, and finally modes and waves supported by an un-neutralized charge cloud. The emphasis throughout is placed on an intuitive presentation of the physics with relevance specifically to mass spectrometry, and numerous citations are provided to the literature.

The field of non-neutral plasma physics has its genesis in investigations earlier in this century for vacuum-tube technology and electron- and ion-beam development. Later the field was subsumed into general plasma physics. More recently, non-neutral plasma physics has emerged as a discipline in its own right, and it continues to provide support in a wide variety of areas, for example, free-electron lasers, ion and electron beams, Tokamak reactors, and fluid mechanics.

Non-neutral plasma physics experiments and theory have begun in the last decade to focus on phenomena on "ion traps." These devices provide three-dimensional, stable confinement of gas-phase ions, generally of one charge sign or the other. Two particular types of trap are in common use: the Paul trap, which uses DC and RF electric fields to confine ions; and the Penning trap, which employs DC electric and magnetic fields to confine ions. Penning traps have also undergone extensive investigation and development by physical and analytical chemists in the form of Fourier Transform Mass Spectrometry (FT/MS) and Fourier Transform Ion Cyclotron Resonance (FT/ICR).

Since until recently non-neutral plasma physics was viewed as a minor sub-discipline of plasma physics, it produced little introductory literature of its own, and recent developments were largely unknown to the broader scientific community. Further, non-neutral plasma physicists have been slow to recognize the existence of a broader audience for their work. Our review attempts to bridge this communication gap by showing that much of the physics can be understood and applied without a detailed knowledge of broader issues and techniques of plasma physics. FT/MS often makes use of phenomena that are as yet little studied by non-neutral plasma physicists. This means that useful two-way communication between these heretofore separate communities may be expected to benefit both sides.

7. Appendix

Chemical Structure and Dynamics Staff

Associate Director, EMSL

Steven D. Colson

B.S. Utah State University, 1963; Ph.D. California Institute of Technology, 1968; Postdoctoral Fellow, National Research Council (Ottawa) 1968; Assistant Professor to Professor of Chemistry, Yale University, 1968–1989; joined PNL as Associate Director for Chemical Structure and Dynamics June 1989. Research interests: photochemistry, photophysics, and molecular dynamics; electronic structures of molecules; processes at the molecule/surface interface.

Program Manager

Robin S. (Rod) McDowell

B.A. Haverford College 1956; Ph.D. M.I.T. 1960; Staff Member, Assistant Group Leader, and Laboratory Fellow, Los Alamos National Laboratory, 1960–1991; joined PNL as Program Manager for Chemical Structure and Dynamics April 1991. Research interests: infrared and Raman spectroscopy applied to molecular structure and bonding; molecular dynamics and force fields; statistical mechanics; infrared analytical techniques.

Staff

Stephan E. Barlow

B.A. Southern Oregon State College 1976; Ph.D. University of Colorado 1984, Postdoctoral Fellow 1984–1989; Senior Instructor in Chemistry, University of Denver 1989–1991; joined PNL June 1991. Research interests: development and application of mass spectrometric techniques to gas-phase chemical kinetics, reaction mechanisms, and structure.

James P. Cowin

B.S. Case Western Reserve University 1974; Ph.D. University of Chicago 1981; Postdoctoral Fellow, University of Toronto, 1981–1983; Assistant Professor of Chemistry, University of California, Santa Barbara, 1983–1990; joined PNL July 1990. Research interests: molecular motions at interfaces, especially energy and charge transfer, bond formation dynamics, and light-stimulated surface reactions.

Donald M. Friedrich

B.S. University of Michigan 1966; Ph.D. Cornell University 1973; Associate Professor of Chemistry, Hope College, 1975–1985; joined PNL August 1985. Research interests: determining the mechanisms by which solvent molecules and surface structures interact at solid/liquid interfaces to control sorbate reactions such as complexation, electron-transfer, proton-transfer, and hydrogen-bonding.

Wayne P. Hess

B.A. University of Colorado 1981; M.S. University of Oregon 1983; Ph.D. University of Colorado 1988; Postdoctoral Fellow, Sandia Livermore Combustion Research Facility 1988–1990; joined PNL January 1990. Research interests: modeling condensed phase chemistry through the study of energetic reactive processes in molecular solids and thin films (dissociation and fragmentation, electronic and vibrational energy transfer), using laser-induced desorption and ablation of adsorbed molecules and solid surfaces.

Gary R. Holtom

B.A. Pfeiffer College 1969; Ph.D. University of California, Berkeley, 1978; Postdoctoral Fellow, Wesleyan University 1978–1979; Head of Laser Operations, University of Pennsylvania Regional Laser and Biotechnology Laboratory 1979–1989; joined PNL September 1989. Research interests: short-pulse laser spectroscopy; condensed-phase photochemistry, in particular the dynamics of electronically-excited organic molecules.

Stephen A. Joyce

B.S. Boston College 1982; Ph.D. M.I.T. 1987; Postdoctoral Fellow, National Institute of Standards and Technology, 1987–1989; Sandia National Laboratories, 1989–1991; joined PNL October 1991. Research interests: scanning probe microscopies for studying molecularly-resolved chemistry on solid surfaces.

Bruce D. Kay

B.S. University of Illinois 1976; Ph.D. University of Colorado 1982; Senior Member of the Technical Staff, Sandia National Laboratories, 1982–1991; joined PNL November 1991. Research interests: chemical dynamics and kinetics of molecular processes occurring at the gas-surface interface; dissociative chemisorption of halogenated hydrocarbons on model oxide surfaces; quantum-resolved H-

atom reactive scattering from halogenated surfaces; trapping and "solvation" of ions and molecules on multilayer ice surfaces.

Thomas M. Orlando
B.S. Southampton College 1982; Ph.D. State University of New York at Stony Brook 1988, Postdoctoral Fellow 1988–1989; Postdoctoral Fellow, Sandia National Laboratory 1989–1991; joined PNL September 1991. Research interests: non-thermal interfacial reaction dynamics; electron, photon, and hyperthermal ion-beam induced surface chemistry; dissociative electron attachment; laser spectroscopy.

Douglas Ray
B.A. Kalamazoo College 1979; Ph.D. University of California, Berkeley, 1985; Postdoctoral Fellow, Joint Institute for Laboratory Astrophysics, 1985–1990; joined PNL June 1990. Research interests: the experimental study of dynamical processes in clusters and at liquid interfaces using techniques of laser spectroscopy and mass spectrometry.

Steven W. Sharpe
B.S. University of Bridgeport 1979; Ph.D. State University of New York at Stony Brook 1986; Postdoctoral Fellow, University of Southern California 1987–1990; joined PNL May 1990. Research interests: high-resolution molecular spectroscopy.

Lai-Sheng Wang
B.S. Wuhan University 1982; Ph.D. University of California, Berkeley, 1989; Postdoctoral Fellow, Rice University, 1990–1992; joint Washington State University/PNL appointment January 1993. Research interests: physical and chemical properties of metal and semiconductor clusters using techniques of molecular-beam and photoelectron spectroscopy; using clusters as model systems to study surface and interfacial phenomena.

Xiaoliang (Sunney) Xie
B.S. Peking University 1984; Ph.D. University of California at San Diego 1990; Postdoctoral Fellow, University of Chicago 1990–1991; joined PNL January 1992. Research interests: chemical physics in liquids and in biological systems, using ultrafast laser techniques; molecular-level understanding of chemical reactions at interfaces and biological membranes, using near-field single-molecule spectroscopy.

Research Scientists

Thomas A. Blake
B.S. University of Bridgeport 1981; Ph.D. Wesleyan University 1989; Postdoctoral Fellow, University of Washington 1988–1991, NASA Ames Research Center 1991–1994; joined PNL September 1994.

Martin J. Iedema
B.S. University of Southern California 1988; Technician, Mt. Wilson Observatory 1987–1990; joined PNL September 1990.

Alan G. Joly
B.S. University of Rochester 1985; Ph.D. M.I.T. 1990; Postdoctoral Fellow, PNL, 1990–1993; joined PNL staff June 1993.

R. Scott Smith
B.S. Northern Arizona University 1983; Ph.D. University of Utah 1988; Postdoctoral Fellow, University of Arizona 1988–1990, PNL 1990–1992; joined PNL staff October 1992.

Russell G. Tonkyn
B.A. Reed College 1978; Ph.D. University of Wisconsin 1988; Postdoctoral Fellow, Brookhaven National Laboratory 1988–1991, PNL 1991–1992; joined PNL staff November 1992.

Technical Specialist

Greg A. Ritter
B.S. Oregon Institute of Technology 1991.

Operations Administrator

Denise A. Motsenbocker

Office Support

Cynthia A. Irwin
Brenda K. Neeley

Postdoctoral Fellows

Albert H. Bahnmaier
Ph.D. University of Ulm 1993.

Richard A. Bradley Jr.
B.A. Reed College 1986; Ph.D. University of Oregon 1992.

Robert A. Crowell II
B.S. University of California, Riverside, 1987, Ph.D. 1992, Postdoctoral Fellow 1992–1993.

Subhash M. Deshmukh
Ph.D. Wayne State University 1989; Postdoctoral Fellow, Tulane University 1989–1993.

Robert Doolen
B.S. University of New Mexico 1989; Ph.D. University of California, San Diego, 1994.

Robert C. Dunn
B.S. California State University, Sacramento, 1988; M.S. University of California, San Diego, 1990, Ph.D. 1992.

Jiawen Fan
B.S. Jinan University 1982, M.S. 1985; M.S. Washington State University 1989, Ph.D. 1991, Postdoctoral Fellow 1992–1993.

Mark C. Gallagher
B.Sc. University of Calgary 1982; Ph.D. University of Alberta 1990; Postdoctoral Fellow, Pennsylvania State University 1990–1993.

Kristine German
B.A. Carleton College 1983; M.S. University of California, Riverside, 1989, Ph.D. 1993.

Nigel G. Gotts
B.Sc. University of Sussex 1987, D.Phil. 1991; Postdoctoral Fellow, University of California, Santa Barbara, 1992–1994.

Chen (Chris) Huang
B.S. Xiamen University 1982; M.A. University of California, Santa Barbara, 1987, Ph.D. 1990, Postdoctoral Fellow 1990–1993.

Gregory A. Kimmel
B.S. Cornell University 1984, Ph.D. 1992.

Naushad Kizhakevariam
B.Tech. Indian Institute of Technology 1985; Ph.D. University of Washington 1991; Postdoctoral Fellow, Purdue University, 1991–1994.

Karen Knutsen
B.A. Linfield College 1981; Ph.D. University of Colorado 1992.

Horst B. Lueck
Ph.D. Technische Universität Berlin 1992.

Brian L. Maschhoff
B.S. University of New Mexico 1981; Ph.D. University of Arizona 1988; Postdoctoral Fellow, Rutgers University 1988–1991.

Vincent A. Venturo
B.S. Rutgers University 1985; M.S. University of California, Berkeley, 1988; Ph.D. University of California at Los Angeles 1993.

Eric K. L. Wong
B.S. University of Oregon 1985, Ph.D. 1992.

Songlin Xu
B.S. Xiamen University 1982, M.S. 1985; Ph.D. University of Kansas 1993.

Xinliang Zhou
B.S. Sun Yat-Sen University 1983; Ph.D. University of Texas at Austin 1989, Postdoctoral Fellow 1989–1992.

Graduate Students

John Biesecker
Axel R. Hebecker
Richard Webb
Hongbin Wu

Publications and Presentations

Publications

A. H. Bahnmaier, T. Engst, H. Jones, and S. D. Colson, "Rotationally Resolved Spectroscopy of the C–X Band of $^{15}NH_3$ by Infrared-Ultraviolet Double Resonance," *Mol. Phys.* **82,** 1203 (1994).

S. D. Colson and T. H. Dunning, "Understanding Nature's Solvent: Water," *Science* **265,** 43 (1994).

S. D. Colson and S. W. Sharpe, "Novel Techniques for Detection of Atmospheric Pollutants," *Laser Focus World* **30,** 22 (1994) (Interview).

R. A. Crowell, G. R. Holtom, and X. S. Xie, "Liquid Water Dynamics Probed by Femtosecond Infrared Spectroscopy," *Ultrafast Phenomena IX,* (Springer-Verlag, 1994), p. 156.

R. A. Crowell, G. R. Holtom, and X. S. Xie, "The Infrared Free Induction Decay of Liquid Water Molecules," *J. Phys. Chem.* **99,** 1840 (1995).

S. Deshmukh and W. P. Hess, "Cl (^2P_j) Fine Structure Quantum Yields from UV Dissociation of PCl_3, CCl_4, $CHCl_3$, and Cl_2 in a Supersonic Jet," *J. Photochem. Photobiol. A* **80,** 17 (1994).

S. Deshmukh and W. P. Hess, "Photodissociation of Acetyl Chloride: Cl and CH_3 Quantum Yields and Energy Distributions," *J. Chem. Phys.* **100,** 6429 (1994).

S. Deshmukh, J. D. Myers, S. S. Xantheas, and W. P. Hess, "Investigation of Acetyl Chloride Dissociation by Photofragment Imaging," *J. Phys. Chem.* **98,** 12535 (1994).

R. C. Dunn, G. R. Holtom, L. Mets, and X. S. Xie, "Near-Field Fluorescence Imaging and Florescence Lifetime Measurements of Light Harvesting Complexes in Intact Photosynthetic Membranes," *J. Phys. Chem.* **98,** 3094 (1994).

R. C. Dunn, E. V. Allen, S. A. Joyce, G. A. Anderson, and X. S. Xie, "Near-field Fluorescent Imaging of Single Proteins," *Ultramicroscopy* **57,** 113 (1995).

R. C. Dunn and X. S. Xie, "Characterization of the Temporal Behavior of Ultrashort Pulses Emerging from a Near-field Fiber Probe," *Ultramicroscopy* **57,** 169 (1995).

J. Fan and L. S. Wang, "A Study of FeC_2 and FeC_2H by Anion Photoelectron Spectroscopy," *J. Phys. Chem.* **98,** 11814 (1994).

J. Fan, L. Lou, and L. S. Wang, "FeC_n^- and FeC_nH^- (n = 3,4): A Photoelectron Spectroscopic and Density Functional Study," *J. Chem. Phys.* **102,** 2701 (1995).

B. Jackson, M. Persson, and B. D. Kay, "Quantum Mechanical Study of H(g) + Cl–Au(111): Eley-Rideal Mechanism," *J. Chem. Phys.* **100,** 7687 (1994).

J. F. Kelly and R. S. McDowell, "Environmental Analysis (Optical Spectroscopy)," *Encyclopedia of Energy Technology and the Environment* (John Wiley, 1995), 1268–1292.

G. A. Kimmel, T. M. Orlando, C. Venzia, and L. Sanche, "Low-Energy (5–50 eV) Electron-Stimulated Production of Molecular Hydrogen from Amorphous Water Ice," *J. Chem. Phys.* **101,** 3282 (1994).

R. Knochenmuss, D. Ray, and W. P. Hess, "Electronic Absorption Spectra of Large Benzene·Ar_n Clusters," *J. Chem. Phys.* **100,** 44 (1994).

R. D. Knochenmuss and D. E. Smith, "Time and Internal Energy Dependent Fluorescence Spectra of Naphthol-Water Clusters," *J. Chem. Phys.* **101,** 7327 (1994).

B. L. Maschhoff and J. P. Cowin, "Corrected Electrostatic Interaction Model for Dipoles Adsorbed on a Metal Surface," *J. Chem. Phys.* **101,** 8138 (1994).

M. O. Trulson, H. B. Lueck, and D. M. Friedrich, "Performance of a Spatial-Filter Equipped Single Monochromator for Raman Spectroscopy," *Appl. Spectrosc.* **48,** 720–723 (1994).

L. S. Wang, J. Fan, X. S. Xie, E. V. Allen, G. R. Holtom, R. C. Dunn, and L. Mets, "Near-Field Fluorescence Microscopy and Spectroscopy: Applications to Single Chromophores, Single Proteins and Photosynthetic Membranes," *Proc. SPIE* **2137** (*Time Resolved Laser Spectry. in Biochem. IV*), 264 (1994).

L. S. Wang and J. Fan, "A Study of FeC_2 and FeC_2H by Anion Photoelectron Spectroscopy," *J. Phys. Chem.* **98,** 11814 (1994).

X. S. Xie and R. C. Dunn, "Probing Single Molecule Dynamics," *Science* **265**, 361 (1994).

X. S. Xie, G. R. Holtom, L. Mets, and R. C. Dunn, "Near-Field Time-Resolved Spectroscopy on Single Molecules and Photosynthetic Membranes," *Ultrafast Phenomena IX* (Springer-Verlag, 1994), p. 124.

In Press and Submitted

C. C. Ainsworth, D. M. Friedrich, and P. L. Gassman, "Fluorescence Spectroscopy of Salicylate–Al_2O_3 Surface Complexes," in preparation.

R. A. Bradley Jr., E. Lanzendorf, M. I. McCarthy, K. Peterson, T. M. Orlando, and W. P. Hess, "Laser Interactions with an Ionic Molecular Crystal: Sodium Nitrate Ablation in the 6 eV Valence Band," *J. Phys. Chem.*, in press.

B. M. Britt, J. L. McHale, and D. M. Friedrich, "Application of Time-Dependent Raman Theory to Raman Excitation Profiles of Hexamethylbenzene-Tetracyanoethylene Electron Donor-Acceptor Complex," submitted to *J. Phys. Chem.*

J. Fan and L. S. Wang, "Photoelectron Spectroscopy of FeO^- and FeO_2^-: Observation of Low-Spin Excited States of FeO and Determination of the Electron Affinity of FeO_2," *J. Chem. Phys.*, in press.

J. Fan, J. B. Nicholas, J. M. Price, S. D. Colson, and L. S. Wang, "$Si_3O_4^-$: Vibrationally Resolved Photoelectron Spectrum and Ab Initio Calculations," accepted by *J. Am. Chem. Soc.*, Communication.

G. R. Holtom, R. A. Crowell, and X. S. Xie, "A High Repetition Rate Femtosecond Optical Parametric Oscillator-Amplifier System near 3 Microns," *J. Opt. Soc. Am. B.*, in press.

G. A. Kimmel, R. G. Tonkyn, and T. M. Orlando, "Kinetic and Internal Energy Distributions of Molecular Hydrogen Produced from Amorphous Ice by Impact of 100 eV Electrons," *Nucl. Instr. and Meth. in Phys. Res. B.*, in press.

G. A. Kimmel and T. M. Orlando, "Low-Energy (5–150 eV) Electron Interactions with Amorphous Ice," submitted to *Nature.*

K. Knutsen and T. M. Orlando, "Low-Energy (10–80 eV) Electron-Stimulated Desorption of $H^+(D^+)$, $OH^+(OD^+)$, and Na^+ from Solution Grown $NaNO_3$ Crystals," submitted to *Surf. Sci.*

J. E. Murphy, J. F. Kelly, T. M. Orlando, B. Bushaw, and R. J. Miller, "Multistate Perturbations Between Rydberg and Valence States in NO," *J. Chem. Phys.*, in press.

J. B. Nicholas, J. Fan, H. Wu, S. D. Colson, and L. S. Wang, "A Combined Density Functional Theoretical and Photoelectron Spectroscopic Study of Ge_2O_2," submitted to *J. Chem. Phys.*

A. J. Peurrung, S. E. Barlow, and R. T. Kouzes, "Coupled Gyrators: A Paradigm for Space-Charge Effects in Cyclotron Mass Spectrometry," *Non-Neutral Plasma Physics II* (AIP Conference Proceedings 331), in press.

A. Peurrung, J. P. Cowin, S. E. Barlow, G. Teeter, and T. M. Orlando, "Space-Charge Induced Acceleration of Ions Emitted by Laser-Irradiated Surfaces, submitted to *J. Appl. Phys.*

D. Ray, M. B. More, E. D. Glendening, D. Feller, and P. B. Armentrout, "Cation-ether complexes in the gas phase: bond dissociation energies and equilibrium structures of $Li^+[O(CH_3)_2]_x$, x = 1–4," in preparation.

R. J. Speedy, P. G. Debenedetti, C. Huang, R. S. Smith, and B. D. Kay, "The Entropy of Glassy Water," *Proceedings of 12th International Conference on the Properties of Water and Steam*, Orlando, Fla., September 12–16, 1994. Begell House, in press.

L. S. Wang, H. S. Cheng, and J. Fan, "Probing the Electronic Structure of Small Iron Clusters," *Chem. Phys. Lett.*, in press.

L. S. Wang, J. Fan, and L. Lou, "Iron Clusters and Oxygen-Chemisorbed Iron Clusters," *Surf. Rev. Lett.*, in press.

L. S. Wang, "Study of Iron-Carbon Mixed Clusters, FeC_n (n = 2–5): A Possible Linear To Cyclic Transition From FeC_3 to FeC_4," *Surf. Rev. Lett.*, in press.

L. S. Wang, H.. S. Cheng, and J. Fan, "Photoelectron Spectroscopy of Size-Selected Transition Metal Clusters: Fe_n^-, n = 3–24," accepted by *J. Chem. Phys.*

X. S. Xie, and R. C. Dunn, "Single Molecule Microscopy and Spectroscopy," *Zoological Studies*, in press.

X. S. Xie and R. C. Dunn, "Near-Field Single Molecule Spectroscopy," *Proc. SPIE* **2385** *(Advanced Optical Methods for Ultrasensitive Detection)*, in press.

S. Xu, R. S. McDowell, S. W. Sharpe, and B. J. Krohn, "Rovibrational Spectroscopy of $C^{35}Cl_4$," *J. Mol. Spectrosc.*, in press.

Presentations

C. C. Ainsworth, D. M. Friedrich, and P. L. Gassman, "Fluorescence Spectroscopy of Salicylate-Al_2O_3 Surface Complexes," American Society of Agronomy, Mineral-Organic Interactions Session, Seattle, Nov. 16–17, 1994.

R. A. Crowell, G. R. Holtom, and X. S. Xie, "Direct Observation of Infrared Free Induction Decay of Liquid Water Molecules with a Femtosecond OPO at 3 Microns" (Poster), Ultrafast Phenomena IX, Dana Point, Cal., May 2–6, 1994.

R. A. Crowell, G. R. Holtom, and X. S. Xie, "Femtosecond Coherent Spectroscopy of Liquid Water Molecules," CLEO/IQEC '94, Anaheim, Cal., May 8–13, 1994.

R. A. Crowell, G. R. Holtom, and X. S. Xie, "Femtosecond Infrared Spectroscopy of Water" (Poster), Gordon Research Conference on Vibrational Spectroscopy, Wolfeboro, N.H., Aug. 14–21, 1994.

R. A. Crowell, G. R. Holtom and X. S. Xie, "Dynamics of Liquid Water Molecules Probed by Femtosecond Infrared Spectroscopy," 208th ACS Meeting, Washington, D.C., Aug. 21–26, 1994.

R. C. Dunn and X. S. Xie, "Dynamics of Single Molecules at Glass Surfaces Probed by Near-field Spectroscopy," 208th ACS Meeting, Washington, D.C., Aug. 21–26, 1994.

R. C. Dunn, E. V. Allen, L. Mets, and X. S. Xie, "Biological Applications of Near-field Microscopy," 38th Annual Biophysical Meeting, San Francisco, Feb. 12–16, 1994.

R. C. Dunn, G. R. Holtom, and X. S. Xie, "Fluorescence Spectroscopy on a Single Molecule Basis," CLEO/IQEC '94, Anaheim, Cal., May 8–13, 1994.

R. C. Dunn, L. Mets, and X. S. Xie, "Application of Near-Field Single Molecule Spectroscopy to Photosynthetic Systems" (Poster), Gordon Conference on Photosynthesis: Biophysical Aspects, New Hampton, N.H., Aug. 7–12, 1994.

R. C. Dunn, G. R. Holtom, G. A. Anderson, E. V. Allen, L. Mets, and X. S. Xie, "Fluorescence Imaging and Time Resolved Spectroscopy using Near-field Optics," ILS-X/OAS Annual Meeting, Dallas, Oct. 2–7, 1994.

D. M. Friedrich, "Intramolecular Charge Transfer Dynamics Probed by Femtosecond Transient Absorption Spectroscopy and Resonance Raman Spectroscopy," University of Oregon, April 7, 1994.

D. M. Friedrich, "Fluorescence Spectroscopy of Salicylate-dAl_2O_3 Surface Complexes," PNL LDRD Symposium, December 1, 1994.

M. S. Fyfield, M. C. Gallagher, J. P. Cowin, and S. A. Joyce, "STM of Thin Film MgO Grown on Mo(001)," Pacific Northwest AVS Meeting, Troutdale, Oregon, Sept. 1994.

M. C. Gallagher, M. S. Fyfield, J. P. Cowin, and S. A. Joyce, "STM of Thin Film MgO Grown on Mo(001)," National AVS Meeting, Denver, Oct. 1994.

A. Hebecker, K. A. Zachariasse, H. B. Lueck and D. M. Friedrich, "Identification of the S1- and S2-Electronic States of Donor-Acceptor-Substituted Aromatic Compounds (D-Ar-A) by Resonance Raman Spectroscopy," Jan. 26–28, 1994.

W. P. Hess, "Optical Technologies Involved in Environmental Characterization and Monitoring," SPIE–The International Society for Optical Engineering, OE/LASE Meeting, Los Angeles, January 1994.

W. P. Hess, "An Investigation of Acetyl Chloride Dissociation by Photofragment Imaging" and "Electronic Absorption Spectra of Large Benzene·Ar_n Clusters," Western Spectroscopy Association Conference, Asilomar, Cal., January 26–28, 1994.

W. P. Hess, "Investigation of Acetyl Chloride Dissociation by Photofragment Imaging," Workshop on Imaging Methods in Molecular Structure and Dynamics, Neve Ilan, Israel, June 1994.

W. P. Hess, "Laser Ablation of Sodium Nitrate in the 6 eV Band," Physical Chemistry Seminar, Weizmann Institute of Science, Rehovot, Israel, June 1994.

W. P. Hess, "Laser Ablation of Sodium Nitrate in the 6 eV Band," Physical Chemistry Seminar, Hebrew University, Jerusalem, Israel, June 1994.

W. P. Hess, "Laser Interactions with an Ionic Molecular Crystal: Sodium Nitrate Ablation in the 6 eV Valence Band," Gordon Conference on Laser Surface Interactions, Colby-Sawyer College, New London, N.H., August, 1994.

W. P. Hess, "Investigation of Acetyl Chloride Dissociation by Photofragment Imaging," American Chemical Society National Meeting, Washington D.C., August, 1994.

G. R. Holtom, R. A. Crowell, and X. S. Xie, "A Noncritically Phase Matched Femtosecond Optical Parametric Oscillator near 3 Microns," CLEO/IQEC '94, Anaheim, Cal., May 8–13, 1994.

G. R. Holtom, R. A. Crowell, and X. S. Xie, "Design of a High-Repetition-Rate Femtosecond Optical Parametric Oscillator-Amplifier System Operating Near 3 Microns," ILS-X/OAS Annual Meeting, Dallas, Oct. 2–7, 1994.

C. Huang, E. K. L Wong, R. S. Smith, and B. D. Kay, "Adsorption, Desorption and Phase Transformation Kinetics of Multilayer H_2O and D_2O on Au(111) and Ru(0001) Surfaces," Molecular Processes at Solid Surfaces Symposium, 207th American Chemical Society National Meeting, San Diego, Cal., March 13–18, 1994.

C. Huang, E. K. L Wong, R. S. Smith, and B. D. Kay, "Adsorption, Desorption and Phase Transformation Kinetics of Multilayer H_2O and D_2O on Au(111) and Ru(0001) Surfaces," Gordon Conference on Interactions of Water with Solid Surfaces, Plymouth, N.H., July 17–22, 1994.

C. Huang, E. K. L Wong, R. S. Smith, and B. D. Kay, "Adsorption, Desorption and Phase Transformation Kinetics of Multilayer H_2O and D_2O on Au(111) and Ru(0001) Surfaces," Gordon Conference on Water and Aqueous Solutions, Plymouth, N.H., August 7–12, 1994.

C. Huang, E. K. L Wong, R. S. Smith, and B. D. Kay, "Adsorption and Desorption of Multilayer Water on Hydrophilic and Hydrophobic Surfaces," 1994 Pacific Northwest American Vacuum Society Meeting, Troutdale, Ore., Sept. 15–16,1994.

C. Huang, E. K. L Wong, R. S. Smith, and B. D. Kay, "Adsorption, Desorption and Phase Transformation Kinetics of Multilayer H_2O and D_2O on Au(111) and Ru(0001) Surfaces," 41st National American Vacuum Society Meeting, Denver, Oct. 24–28, 1994.

A. G. Joly and D. M. Friedrich, "Intramolecular Charge Transfer Dynamics Probed by Femtosecond Transient Absorption Spectroscopy," Jan. 26–28, 1994.

B. D. Kay, "State-to-State Inelastic and Reactive Gas-Surface Scattering," SPIE National Symposium on Laser Techniques in Surface Science, Los Angeles, January 27–29, 1994.

B. D. Kay, "Adsorption, Desorption and Phase Transformation Kinetics of Multilayer H_2O and D_2O on Au(111) and Ru(0001) Surfaces," Surface Science Seminar, University of Washington, Seattle, April 29, 1994. (Invited.)

B. D. Kay, "Structure and Reactivity of Amorphous and Crystalline Ice Surfaces and Interfaces," Ninth Department of Energy Basic Energy Sciences Catalysis and Surface Science Meeting, Oconomowoc, Wis., May 24–27, 1994. (Invited.)

B. D. Kay, "Adsorption, Desorption and Phase Transformation Kinetics of Multilayer H_2O and D_2O on Au(111) and Ru(0001) Surfaces," Chemistry Division Seminar, Argonne National Laboratory, Argonne Ill., May 31, 1994. (Invited.)

B. D. Kay, "Adsorption, Desorption and Phase Transformation Kinetics in Nanoscale Ice Films," Telluride Workshop on Chemical Physics and the Atmosphere, Telluride, Col. August 1–5, 1994. (Invited.)

B. D. Kay, "Adsorption, Desorption and Phase Transformation Kinetics in Nanoscale Ice Films," Physics Department Seminar, Washington State University, Pullman, Sept. 27, 1994. (Invited.)

B. D. Kay, "Adsorption, Desorption and Phase Transformation Kinetics in Nanoscale Ice Films," Chemical Physics Seminar, University of Colorado, Boulder, Oct. 28, 1994. (Invited.)

G. A. Kimmel, R. G. Tonkyn, and T. M. Orlando, "Low-Energy (5–80 eV) Electron-Stimulated Production of Molecular Hydrogen from Amorphous Water," Interaction of Water with Solid Surfaces Gordon Research Conference, Plymouth, N.H., July 17–22, 1994.

G. A. Kimmel, R. G. Tonkyn, and T. M. Orlando, "Low-Energy (5–80 eV) Electron-Stimulated Production of Molecular Hydrogen from Amorphous Water," Desorption Induced by Electronic Transitions (DIET) VI, Krakow, Poland, Sept. 26–29, 1994.

G. A. Kimmel, R. G. Tonkyn, and T. M. Orlando, "Low-Energy Electron-Stimulated Production of Molecular Hydrogen from Amorphous Water Ice," 41st National American Vacuum Society Symposium, Denver, Oct. 24–28, 1994.

K. Knutsen, G. A. Kimmel, and T. M. Orlando, "Low-Energy (5–80 eV) Electron Stimulated Destruction of $NaNO_3$ Crystals," Pacific Northwest American Vacuum Society Symposium, Troutdale, Oregon, Sept. 13–16, 1994.

K. Knutsen, G. A. Kimmel, T. M. Orlando, "Low-Energy (5–80 eV) Electron-Stimulated Degradation of $NaNO_3$ Single Crystals," Desorption Induced by Electronic Transitions (DIET) VI, Krakow, Poland, Sept. 26–29, 1994.

H. B. Lueck, D. M. Friedrich, and A. R. Hebecker, "Fluorescence Anisotropy Study on the Electronic Structure of Aminobenzonitrile Charge Transfer Systems Accompanied by INDO Calculations," Western Spectroscopy Association, Asilomar, Cal., Jan. 26–28, 1994.

R. S. McDowell, S. W. Sharpe, and J. F. Kelly, "Infrared Signatures for Remote Sensing," Interim Technical Review, CALIOPE Program, Lawrence Livermore National Laboratory, Livermore, Cal., April 26–28, 1994.

T. M. Orlando, "Electron-Stimulated Reactive Scattering in Amorphous Water Ice," American Chemical Society National Meeting, San Diego, March 13–18, 1994. (Invited.)

T. M. Orlando, "Low-Energy (5–50 eV) Electron-Stimulated Reactive Scattering in Amorphous Water Ice," Chemical Physics Colloquium, University of Oregon, Eugene, April 18, 1994. (Invited.)

T. M. Orlando, "Low-Energy Electron Stimulated Production of Molecular Hydrogen from Amorphous Water Ice," Dept. of Physics, University of Washington, Seattle, May 10, 1994. (Invited.)

T. M. Orlando, "Electron-Stimulated Production of Molecular Hydrogen from Amorphous Water," Dept. Nuclear Medicine and Radiobiology, University of Sherbrooke, Sherbrooke, Canada, July 5, 1994. (Invited.)

T. M. Orlando, "Low-Energy (5–50 eV) Electron Stimulated Production of Molecular Hydrogen from Amorphous Water Ice," Radiation Chemistry Gordon Research Conference, Salve Regina University, Providence, R.I., July 17–22, 1994. (Invited.)

T. M. Orlando, "Quantum-Resolved Studies of Electron-Stimulated Reactions in Amorphous and Crystalline Water Ice," Physical Chemistry Colloquium, University of Basel, Switzerland, Sept. 13, 1994. (Invited.)

T. M. Orlando, "Quantum-Resolved Studies of Electron-Stimulated Production of Molecular Hydrogen from Amorphous and Crystalline Water Ice," Chemical Physics Colloquium, University of Colorado, Boulder, Oct. 21, 1994. (Invited.)

A. J. Peurrung, S. E. Barlow, and R. T. Kouzes, "Non Neutral Plasmas in Mass Spectrometry," 1994 Non-Neutral Plasma Workshop, Berkeley, Cal., July 18, 1994.

R. S. Smith, C. Huang, E. K. L Wong, and B. D. Kay, "Adsorption, Desorption, Mixing and Solvation Kinetics of Mixed Methanol and Water Multilayer Ices," Gordon Conference on Water and Aqueous Solutions, Plymouth, N.H., Aug. 7–12, 1994.

R. S. Smith, C. Huang, E. K. L Wong, and B. D. Kay, "Crystallization and Isotope Exchange Kinetics of Amorphous Multilayer D_2O and H_2O Ice Films on Au(111) and Ru(0001)," 1994 Pacific Northwest American Vacuum Society Meeting, Troutdale, Ore., Sept. 15–16,1994.

R. S. Smith, C. Huang, E. K. L Wong, and B. D. Kay, "Adsorption, Desorption, Mixing and Solvation Kinetics of Mixed Methanol and Water Multilayer Ices," 41st National American Vacuum Society Meeting, Denver, Oct. 24–28, 1994.

M. O. Trulson, J. P. LaFemina, and D. M. Friedrich, "Dynamics of the ^1L_a State of p-(N,N-dimethylamino)-benzonitrile (p-DMABN) from Resonance Raman Spectroscopy," Western Spectroscopy Association, Asilomar, Cal., Jan. 26–28, 1994.

X. S. Xie and R. C. Dunn, "Fluorescence Spectroscopy on a Single Molecule Basis with a Near-field Spectrometer," Laser Applications to Chemical Analysis, 4th Topical Meeting, Jackson Hole, Wyo., Mar. 8–11, 1994.

X. S. Xie and R. C. Dunn, "Single Molecule Spectroscopy with a Near-field Fluorescence Microscope," 207th ACS meeting, San Diego, Mar. 13–18, 1994.

X. S. Xie, R. C. Dunn, G. R. Holtom, and L. Mets, "Near-field Time-Resolved Fluorescence Spectroscopy on Single Proteins: Application to Photosynthetic Membranes," Ultrafast Phenomena IX, Dana Point, Cal., May 2–6, 1994.

X. S. Xie and R. C. Dunn, "Near-field Time-Resolved Fluorescence Spectroscopy of Single Molecules," Spectral Hole-burning and Related Spectroscopies: Science and Applications, 4th Topical Meeting, Tokyo, Japan, Aug. 24–26, 1994. (Invited.)

X. S. Xie, "Probing Single Molecule Dynamics," Chemical Physics Institute 14th Annual Retreat, University of Oregon, Charleston, Ore., Sept. 11–13, 1994. (Invited.)

X. S Xie and R. C. Dunn, "Probing Single Molecule Dynamics," ILS-X/OAS Annual Meeting, Dallas, Oct. 2–7, 1994.

X. S. Xie, "Probing Single Molecule Dynamics," Washington State University, Physics Department, Pullman, Dec. 6, 1994.

S. Xu, R. S. McDowell, and S. W. Sharpe, "Rovibrational Spectroscopy of Carbon Tetrachloride," (Poster), Gordon Research Conference on Vibrational Spectroscopy, Wolfeboro, N.H., Aug. 14–19, 1994.

Collaborations

Outside Collaborations

Molecular Dynamics at the Water/Solid Interface
University of Colorado (B. Ellison)
EMSL Contact: J. P. Cowin

Electronic Structure of Substituent-Perturbed Benzenes by Deep UV Resonance Raman Spectroscopy
University of Oregon (B. S. Hudson and H. Lueck)
EMSL Contact: D. M. Friedrich

Raman Excitation Profiles of Electron Donor-Acceptor Complexes
University of Idaho (J. L. McHale)
EMSL Contact: D. M. Friedrich

Laser Raman Study of Uranyl Surface Complex Speciation
Oregon State University (G. Turner)
EMSL Contact: D. M. Friedrich

Laser Ablation Characterization of Solids
Washington State University (J. T. Dickinson, R. Webb, and K. Peterson)
EMSL Contact: W. P. Hess

Photochemistry of Thin Molecular Films
University of Utah (C. Wight)
EMSL Contact: W. P. Hess

Quantum-Resolved Reactive Gas-Surface Scattering
University of Massachusetts (Bret Jackson)
EMSL Contact: B. D. Kay

Metastability of Glassy Water and its Relation to Liquid Water
University of Wellington, N.Z. (Robin Speedy) and Princeton University (Pablo Debenedetti)
EMSL Contact: B. D. Kay

Optical Properties and Porosity of Vapor Deposited Ice Films
University of Colorado (Steven M. George)
EMSL Contact: B. D. Kay

Desorption and Phase Transformation Kinetics in Amorphous Ice
Chalmers University, Göteborg, Sweden (Bengt Kasemo)
EMSL Contact: B. D. Kay

Rovibrational Analysis of High-Symmetry Molecules
Los Alamos National Laboratory (Burton J. Krohn)
EMSL Contact: R. S. McDowell

Thermal-Electron/Water Chemistry
University of Sherbrooke (L. Sanche)
EMSL Contact: T. M. Orlando

Gas-Phase Cation–Ether Complexes
University of Utah (P. Armentrout)
EMSL Contact: D. Ray

Rovibrational Spectral Analysis of Molecular Clusters
National Institute for Standards and Technology (G. Fraser and A. Pine)
EMSL Contact: S. W. Sharpe

Quantum Chemistry Calculations on Metal Clusters
Air Products and Chemicals, Inc., Allentown, Pa. (H. S. Chen)
EMSL Contact: L. S. Wang

Spectroscopy and Structure of Metal Clusters
Washington State University (H. Wu)
EMSL Contact: L. S. Wang

Density Functional Calculations on Metal Clusters
Rice University (L. Lou)
EMSL Contact: L. S. Wang

Spectroscopic Mapping of Photosynthetic Membranes
University of Chicago (L. Mets)
EMSL Contact: X. S. Xie

Theoretical Modeling of Molecule-Metal Interactions in Near-Field Spectroscopy
Portland State University (P. Leung)
EMSL Contact: X. S. Xie

Theory of Nonlinear Infrared Spectroscopy of Hydrogen-Bonded Systems
Hong Kong University of Science and Technology (G. Yan)
EMSL Contact: X. S. Xie

Collaborations within PNL

Waste Tank Speciation Methods
Applied Physics Center (J. S. Hartman) and Materials and Chemical Sciences Center (M. L. Alexander)
CS&D Contacts: S. D. Colson and R. S. McDowell.

Bonding and Structure of Organic Ligands at Oxide/Water Interfaces
Earth and Environmental Sciences Center (C. C. Ainsworth)
CS&D Contact: D. M. Friedrich

Lanthanide Carbonate Speciation by Laser-Induced Fluorescence
Earth and Environmental Sciences Center (L. Rao and A. R. Felmy)
CS&D Contact: D. M. Friedrich

Studies of Laser/Solid Interactions
EMSL Theory, Modeling, and Simulation (M. I. McCarthy, S. S. Xantheas, and J. D. Myers)
CS&D Contact: W. P. Hess

Structure of TiO Thin Films
EMSL Materials and Interfaces (C. H. F. Peden)
CS&D Contact: S. A. Joyce

Physics and Chemistry of Ceramic Surfaces.
Materials and Chemical Sciences Center (B. C. Bunker)
CS&D Contact: S. A. Joyce

Physics and Chemistry of Ceramic Surfaces
Materials and Chemical Sciences Center (B. C. Bunker)
CS&D Contact: B. D. Kay

Gas-Phase Cation-Ether Complexes
EMSL Theory, Modeling, and Simulation (D. Feller and E. Glendening)
CS&D Contact: D. Ray

Spectroscopy and Dynamics of Molecular Clusters
EMSL Computing and Information Sciences (J. M. Price)
CS&D Contact: D. Ray

Spectroscopic Techniques for Atmospheric Monitoring
Materials and Chemical Sciences Center (J. F. Kelly)
CS&D Contacts: S. W. Sharpe and R. S. McDowell

Finite Difference Time-Domain Modeling of the Molecule-Probe Interaction in Near-Field Spectroscopy
Earth and Environmental Sciences Center (X. Bian)
CS&D Contact: X. S. Xie

Distribution

No. of Copies

OFFSITE

2 DOE/Office of Scientific and Technical Information

A. C. Albrecht
Department of Chemistry
Cornell University
Ithaca, NY 14853

J. Almloff
Department of Chemistry
University of Minnesota
207 Pleasant Street S.E.
Minneapolis, MN 55455

R. J. Anderson
Sandia National Laboratories
Livermore, CA 94550

S. L. Anderson
Department of Chemistry
State University of New York
Stony Brook, NY 11794

P. B. Armentrout
Department of Chemistry
University of Utah
2020 Henry Eyring Bldg.
Salt Lake City, UT 84112

G. H. Atkinson
Department of Chemistry
University of Arizona
Tucson, AZ 85721

D. Auerbach
Department K31-802
IBM Almaden Research Center
650 Harry Road
San Jose, CA 95120-6099

No. of Copies

Y. K. Bae
SRI International
333 Ravenswood Avenue
Menlo Park, CA 94025

P. Barbara
Department of Chemistry
University of Minnesota
207 Pleasant Street SE
Minneapolis, MN 55455

N. F. Barr
Office of Health and Environmental Research
Office of Energy Research
U.S. Department of Energy
Washington, D.C. 20545

C. W. Bauschlicher, Jr.
NASA Ames Research Center
RTC-230-3
Moffett Field, CA 94035

R. A. Beaudet
Department of Chemistry
University of Southern California
Los Angeles, CA 90089-0482

R. Beck
Department of Chemistry
University of Washington
Seattle, WA 98195

B. Bederson
Department of Physics
New York University
Washington Square
New York, NY 10003

T. P. Beebe, Jr.
Department of Chemistry
University of Utah
Salt Lake City, UT 84112

No. of Copies

S. M. Benson
Mail Stop 50E
Lawrence Berkeley Laboratory
1 Cyclotron Road
Berkeley, CA 94720

B. J. Berne
Department of Chemistry
Box 755 Havemeyer Hall
Columbia University
New York, NY 10027

E. Bernstein
Department of Chemistry
Colorado State University
Fort Collins, CO 80523

R. Stephen Berry
Department of Chemistry
University of Chicago
5735 South Ellis Avenue
Chicago, IL 60637

V. E. Bondybey
Insitut fur Physicalische Und
Theor. Chemie der
Technischen Univsersitat Munchen
D-8046 Garching b. Muchen
Deutschland - West Germany

M. Bowers
Department of Chemistry
University of California - Santa Barbara
Santa Barbara, CA 93106

B. Bozlee
Department of Chemistry
Whitman College
Walla Walla, WA 99362

J. Bradley
Exxon Research and Engineering Co.
Corporate Research
Route 22 East
Clinton Township
Annandale, NJ 08801

No. of Copies

M. Broido
ER-72, G-155, GTN
U.S. Department of Energy
19901 Germantown Road
Germantown, MD 20874

J. M. Brown
Physical Chemistry Laboratory
Oxford University
S. Parks Road
Oxford OX1 3QZ
UK

P. Brucat
Department of Chemistry
University of Florida
Gainsville, FL 32611

R. L. Byer
Department of Applied Physics
Stanford University
Stanford, CA 94305

P. R. Callis
Department of Chemistry
Montana State University
Bozeman, MT 59717

C. Campbell
Department of Chemistry, BG-10
University of Washington
Seattle, WA 98195

M. Cardillo
AT&T Bell Laboratories
600 Mountain Avenue
Murray Hill, NJ 07974

K. L. Carleton
Physical Sciences International
20 New England Business Center
Andover, MA 01810

A. W. Castleman
Department of Chemistry
152 Davey Laboratory
Pennsylvania State University
University Park, PA 16802

No. of Copies

R. R. Cavanagh
NIST
Center for Chemical Physics
Room B-268, Building 221
Gaithersburg, MD 20899

S. T. Ceyer
Department of Chemistry
Massachusetts Institute of Technology
Cambridge, MA 02139

B. T. Chait
Faculty for Chemistry
Rockefeller University
1230 York Avenue
New York, NY 10021

T. Chuang
IBM Almaden Research Center
650 Harry Road
San Jose, CA 95120

J. Chung
Department of Mechanical & Materials Engineering
Washington State University
Pullman, WA 99164

M. J. Coggiola
Program Manager, Collision Processes
SRI International
333 Ravenswood Avenue
Menlo Park, CA 94025

D. Cox
Exxon Research and Engineering Co.
Corporate Research, LH378
Route 22 East
Clinton Township
Annandale, NJ 08801

F. F. Crim
Department of Chemistry
University of Wisconsin
Madison, WI 53706

No. of Copies

G. A. Crosby
Department of Chemistry 1987
Washington State University
Pullman, WA 99164-4630

C. Crowe
Department of Mechanical & Materials Engineering
Washington State University
Pullman, WA 99164

R. F. Curl
Department of Chemistry
Rice University
Houston, TX 77251-1892

R. C. Dahlman
Office of Health and Environmental Research
Office of Energy Research
U.S. Department of Energy
Washington, D.C. 20545

H. Dai
Department of Chemistry
University of Pennsylvania
Philadelphia, PA 19104

J. G. Dash
Department of Physics, FM-15
University of Washington
Seattle, WA 98195

A. E. Depristo
Ames Laboratory
Iowa State University
Ames, IA 50011

T. Dickinson
Department of Physics
Washington State University
Pullman, WA 99164

G. P. Drobny
Department of Chemistry
University of Washington
Seattle, WA 98195

No. of Copies

J. R. Durig
Department of Chemistry
University of South Carolina
Columbia, SC 29208

T. R. Dyke
Department of Chemistry
University of Oregon
Eugene, OR 97403

C. E. Dykstra
School of Chemical Sciences
505 South Mathews Avenue
University of Illinois
Urbana, IL 61801

G. B. Ellison
Department of Chemistry
University of Colorado
Boulder, CO 80309

M. El-Sayed
Department of Chemistry
Georgia Institute of Technology
225 North Ave.
Atlanta, GA 30332

T. Engel, Chairman
Department of Chemistry, BG-10
University of Washington
Seattle, WA 98195

P. C. Engelking
Department of Chemistry
University of Oregon
Eugene, OR 97403

K. Ervin
Department of Chemistry
University of Nevada - Reno
Reno, NV 89557

P. Esherick
Division 1164
Sandia National Laboratory
Albuquerque, NM 87165

No. of Copies

E. Eyring
Department of Chemistry
University of Utah
Salt Lake City, UT 84112

J. Farley
Department of Physics
University of Nevada - Las Vegas
4505 Maryland Parkway
Las Vegas, NV 89154

P. M. Felker
Department of Chemistry
405 Hilgarde Avenue
University of California
Los Angeles, CA 90024-1569

R. W. Field
Department of Chemistry, Room 6-219
Massachusetts Institute of Technology
Cambridge, MA 02139

G. Fisk
Supervisor, Combustion Chemistry Division
Division 8353
Sandia National Laboratories
Livermore, CA 94550

G. Fleming
Department of Chemistry
University of Chicago
5735 S. Ellis Ave.
Chicago, IL 60637

R. T. Fletcher
Department of Chemistry
University of Idaho
Moscow, ID 83843

R. J. Fletterick
Biochemistry and Biophysics Department
University of California - San Francisco
San Francisco, CA 94143-0448

No. of Copies

C. W. Frank
EM-50, 7A-049
Office of Technology Development
Office of Environmental Management
U.S. Department of Energy
Forrestal Building
1000 Independence Avenue, S.W.
Washington, D.C. 20585

H. Frauenfelder
Department of Physics
University of Illinois
110 West Green Street
Urbana, IL 61801

M. E. Frazier
Office of Health and Environmental Research
Office of Energy Research
U.S. Department of Energy
Washington, D.C. 20545

B. Freiser
Department of Chemistry
Purdue University
West Lafayette, IN 47907

T. E. Furtak
Colorado School of Mines
Physics Department
Golden, CO 80401

J. H. Futrell
Chairman
Chemistry and Biochemistry
University of Delaware
Newark, DE 19716

J. W. Gadzuk
Surface Science Division - Theory
National Institute of Standards & Technology
Gaithersburg, MD 20899

No. of Copies

J. F. Garvey
Department of Chemistry
Acheson Hall State University of New York at Buffalo
Buffalo, NY 14214

R. Gentry
Department of Chemistry
University of Minnesota
Minneapolis, MN 55455

S. M. George
Department of Chemistry
University of Colorado
Boulder, CO 80309

T. F. George
Office of the Provost
Washington State University
Pullman, WA 99164-4660

D. Gerrity
Department of Chemistry
Reed College
3203 S.E. Woodstock
Portland, OR 97202

J. L. Gland
Department of Chemistry
H. H. Dow Building
2300 Hayward
Ann Arbor, MI 48109

W. A. Goddard III
Division of Chemistry and Chemical Engineering
California Institute of Technology
Pasadena, CA 99125

D. W. Goodman
Department of Chemistry
Texas A&M University
College Station, TX 77843

No. of Copies

L. Goodman
Department of Chemistry
Rutgers University
Wright-Rieman Laboratories
New Brunswick, NJ 08903

T. E. Gough
Department of Chemistry
University of Victoria
P.O. Box 3055
Victoria, BC V8W 3PG
Canada

E. R. Grant
Department of Chemistry
Purdue University
West Lafayette, IN 47909

R. B. Greegor
The Boeing Company
P.O. Box 3939
Seattle, WA 98124

R. B. Green
Associated Western Universities
723 The Parkway, Suite 100
Richland, WA 99352-4234

R. Griffin
Department of Chemistry
Massachusetts Institute of Technology
Cambridge, MA 02139

T. Gustafson
Department of Chemistry
Ohio State University
Columbus, OH 43210

P. Hackett
Steacie Institute for Molecular Sciences
National Research Council
Ottawa K1A0R6
Canada

A. T. Hagler
Biosym Technologies
10065A Barnes Canyon Road
San Diego, CA 92121

No. of Copies

H. Hamilton
Department of Mechanical & Materials Engineering
Washington State University
Pullman, WA 99164

K. G. Hancock
Division of Chemistry
National Science Foundation
1800 G Street, NW
Washington, D.C. 20550

D. M. Hanson
Department of Chemistry
SUNY Stony Brook
Stony Brook, NY 11794

C. Harris
Chemistry Department
University of California
Berkeley, CA 94720

W. C. Harris
Science & Technology Center Development
National Science Foundation
Washington, D.C. 20550

D. Haueisen, Chair
Department of Physics & Engineering
Pacific Lutheran University
Tacoma, WA 98447

P. J. Hay
T12, Mail Stop B268
Los Alamos National Laboratory
Los Alamos, NM 87545

R. Haydock
Materials Science Institute
14 Science 1
University of Oregon
Eugene, OR 97403

No. of Copies

A. J. Haymet
Department of Chemistry
University of Utah
Salt Lake City, UT 84112

E. J. Heller
Department of Chemistry
University of Washington
Seattle, WA 98195

V. E. Henrich
Department of Applied Physics
Yale University
P.O. Box 2157
New Haven, CT 06520

J. W. Hepburn
University of Waterloo
Waterloo, Ont. N2L 3G1
Canada

W. Hetherington
Department of Physics
Oregon State University
Corvallis, OR 97333

B. Hichwa
Director, Technical Development
OCLI, M.S. 121-1
2789 North Point Parkway
Santa Rosa, CA 95407

K. W. Hipps
Department of Chemistry
Washington State University
Pullman, WA 99164-4630

D. Hogland
Washington State University
Pullman, WA 99164

J. B. Hopkins
Department of Chemistry
Louisiana State University
Baton Rouge, LA 70803

No. of Copies

J. T. Hougen
Senior NBS Fellow
Molecular Spectroscopy Division
U.S. Department of Commerence
National Institute of Standards
& Technology (NIST)
Gaithersburg, MD 20899

B. Hudson
Department of Chemistry
Chemical Physics Institute
Room 189 Science II
University of Oregon
Eugene, OR 97403-1253

K. C. Janda
Department of Chemistry
University of California - Irvine
Irvine, CA 92619

J. Jellinek
Chemistry Division
Argonne National Laboratory
Argonne, IL 60439

M. Johnson
Department of Chemistry
Yale University
P.O. Box 6666
New Haven, CT 06511

P. M. Johnson
Department of Chemistry
SUNY Stony Brook
Stony Brook, NY 11794

H. Jones
University of ULM
POB 4066
D-7900 Ulm
Germany

P. Jones
Spectra Technology
2755 Northup Way
Bellevue, WA 98004-1495

No. of Copies

C. D. Jorgensen
Office of Health and Environmental Research
Office of Energy Research
U.S. Department of Energy
Washington, D.C. 20545

H. Kapteyn
Department of Physics
Washington State University
Pullman, WA 99164-4630

B. Kay
Sandia National Laboratory
Albuquerque, NM 87165

D. F. Kelley
Department of Chemistry
Colorado State University
Fort Collins, CO 80523

S. D. Kevan
Department of Physics
University of Oregon
120 Willamette Hall
Eugene, OR 97403

W. H. Kirchhoff
Division of Chemical Sciences
Office of Basic Energy Sciences
ER-141, G-343
U.S. Department of Energy
Washington, D.C. 20545

T. A. Kitchens
Office of Scientific Computing
Office of Energy Research
U.S. Department of Energy
Washington, D.C. 20545

D. Kitson
Biosym Technologies
10065A Barnes Canyon Road
San Diego, CA 92121

No. of Copies

W. Klemperer
Department of Chemistry
Harvard University
12 Oxford St
Cambridge, MA 02138

D. S. Kliger
Dean of Science
Department of Chemistry
University of California
Santa Cruz, CA 95064

J. Knee
Department of Chemistry
Wesleyan University
Middletown, CT 06459

M. Koch
Dow Chemical U.S.A.
1897 Building
Analytical Sciences Laboratory
Midland, MI 48667

B. Kohler
Department of Chemistry
University of California, Riverside
Riverside, CA 92521

R. Kopelman
Department of Chemistry
University of Michigan
Ann Arbor, MI 48109

K. Krogh-Jesperson
Department of Chemistry
Rutgers University
New Brunswick, NJ 08903

R. L. Kuczkowski
Department of Chemistry
University of Michigan
Ann Arbor, MI 48109-1055

A. C. Kummel
Department of Chemistry
University of California - San Diego
La Jolla, CA 92093

No. of Copies

M. Kuzyk
Department of Physics
Washington State University
Pullman, WA 99164-4630

P. P. Lambropoulos
Department of Physics
University of Southern California
Los Angeles, CA 90089-0484

M. Lapp
Supervisor, Division 8342
High Temperature Interfaces
Sandia National Laboratories
Livermore, CA 94550

A. H. Laufer
Division of Chemical Sciences
Office of Basic Energy Sciences
ER-141, G-340A
U.S. Department of Energy
Washington, D.C. 20545

S. Leach
Universite de Paris-Sud
Lab de Photophys Moleculaire
Batiment 213
91405 Orsay Cedex
France

T. J. Lee
NASA Ames Research Center
Moffett Field, CA 94035

Y. T. Lee
Department of Chemistry
University of California - Berkeley
Berkeley, CA 94720

S. R. Leone
Department of Chemistry and Joint
Institute for Laboratory Astrophysics
Boulder, CO 80309-0440

No. of Copies

S. Leutwyler
Institut fur Anorganische, Analytische
und Physikalisce Chemie
Universitat Bern
Freiestrasse 3
CH-3000 Bern 9
SWITZERLAND

D. H. Levy
University of Chicago
5735 South Ellis Avenue
Chicago, IL 60637

S.C.T. Lien
EM-54
Office of Environmental Management
U.S. Department of Energy
12800 Middlebrook Rd.
Germantown, MD 20874

E. C. Lim
Department of Chemistry
University of Akron
Akron, OH 44325

W. C. Lineberger
Department of Chemistry and Joint
Institute for Laboratory Astrophysics
University of Colorado
Campus Box 215
Boulder, CO 80309-0440

W. C. Luth
Engineering and Geosciences Division
Office of Basic Energy Sciences
Office of Energy Research
U.S. Department of Energy
Washington, D.C. 20545

F. W. Lytle
MS 2T-05XAFS
The Boeing Company
P.O. Box 3939
Seattle, WA 98124

No. of Copies

D. Magde
Department of Chemistry
B-014
University of California - San Diego
LaJolla, CA 92093-0314

R. S. Marianelli
ER-14, G-336
U.S. Department of Energy
19901 Germantown Road
Germantown, MD 20874

W. J. Marinelli
Group Leader, Thermophysical Sciences
Physical Sciences International
20 New England Business Center
Andover, MA 01810

R. A. Mathies
Department of Chemistry
University of California
Berkeley, CA 94720

B. W. Matthews
Institute of Molecular Biology
University of Oregon
Eugene, OR 97403-1229

U. Mazur
Department of Chemistry
Washington State University
Pullman, WA 99164-4630

W. W. McClain
Department of Chemistry 75
Wayne State University
Detroit, MI 48202

J. McHale
Department of Chemistry
University of Idaho
Moscow, ID 83843

B. V. McKoy
California Institute of Technology
Pasadena, CA 91125

No. of Copies

R. D. Mead
Spectra Technology
2755 Northup Way
Bellevue, WA 98004-1495

H. Metiu
Chemistry Department
University of California
Santa Barbara, CA 93106

J. C. Miller
Chem Physics Section
Oak Ridge National Laboratory
P.O. Box 2008
Oak Ridge, TN 37831-6125

R. L. Miller
Department of Chemistry
University of North Carolina/Chapel Hill
CB#3290
Chapel Hill, NC 27599-3290

T. Miller
Department of Chemistry
Ohio State University
120 W. 18th Avenue
Columbus, OH 43210

W. S. Millman
Office of Basic Energy Sciences
U.S. Department of Energy
Washington, D.C. 20545

T. J. Morin
Chemical Engineering Department
University of Idaho
Moscow, ID 83843

M. D. Morse
Department of Chemistry
University of Utah
Salt Lake City, UT 84112

J. Muenter
Department of Chemistry
University of Rochester
404 Hutchinson Hall, River Campus
Rochester, NY 14627

No. of Copies

K. Muller-Dethlefs
Chemis Department
Technische Universitast Müncheu
Lichten Bergstrasse 4
Garching BIE Munchen D-8046
Germany

M. Murnane
Department of Physics
Washington State University
Pullman, WA 99164-4630

A. B. Myers
Department of Chemistry
University of Rochester
404 Hutchinson Hall, River Campus
Rochester, NY 14627

D. Nesbitt
University of Colorado
Joint Institute for Laboratory Astrophysics
Campus Box 440
Boulder, CO 80309-0440

T. L. Netzel
Georgia State University
Atlanta, GA 30303

D. Neumark
Department of Chemistry
University of California - Berkeley
Berkeley, CA 94720

T. Oka
Department of Chemistry
University of Chicago
Chicago, IL 60637

M. Okumura
Department of Chemistry
Mail Code 127-72
Cal Tech
Pasadena, CA 91125

No. of Copies

A. A. Patrinos
ER-74, E-156/GTN
U.S. Department of Energy
19901 Germantown Road
Germantown, MD 20874

M. Philpott
IBM Almaden Research Center
650 Harry Rd.
San Jose, CA 95120

D. M. Poutsma
Oak Ridge National Laboratory
MS-6182, Building 4500N
P.O. Box 2008
Oak Ridge, TN 37831-6182

D. Pratt
Department of Chemistry
University of Pittsburgh
Parkman Ave & University Dr
Pittsburgh, PA 15260

H. E. Radford
Center for Astrophysics
60 Garden St.
Cambridge, MA 02138

D. A. Ramsay
NRC Canada/100 Sussex Dr.
Ottawa
Ontario KlA OR6
Canada

M. R. Riches
ER-74, G-141/GTN
U.S. Department of Energy
19901 Germantown Road
Germantown, MD 20874

S. Riley
Argonne
9400 South Cass Avenue
Argonne, IL 60439

No. of Copies

G. W. Robinson
Texas Tech University
Lubbock, TX 79409

R. J. Saykally
Department of Chemistry
University of California - Berkeley
419 Lattimer Hall, #1460
Berkeley, CA 94720

E. Schlag
Chemis Department
Technische Universitast München
Lichten Bergstrasse 4
Garching BIE München D-8046
Germany

T. J. Sears
Chemistry Department
Brookhaven National Laboratory
33 Louis St.
Upton, NY 11973-9999

G. Scoles
Department of Chemistry
Princeton University
Princeton, NJ 08544

H. Sellers
National Center for Supercomputing Applications
University of Illinois
405 North Matthews Avenue
Urban, IL 61801

J. M. Shreeve
Department of Chemistry
University of Idaho
Moscow, ID 83843

M. W. Shupe
EM-541, 464/TREV
U.S. Department of Energy
12800 Middlebrook Road
Germantown, MD 20874

No. of Copies

J. D. Simon
Department of Chemistry, B-032
University of California - San Diego
La Jolla, CA 92093

T. Slanger
Molecular Physics Laboratory
SRI International
333 Ravenswood Avenue
Menlo Park, CA 94025

R. E. Smalley
Department of Chemistry
Rice University
P.O. Box 1892
Houston, TX 77251

D. A. Smith
Health Effects & Life Sciences Research Division
Office of Health and Environmental Research
Office of Energy Research
U.S. Department of Energy
Washington, D.C. 20545

M. A. Smith
Department of Chemistry
University of Arizona
Tucson, AZ 85721

F. H. Stillinger
D. K. Stillinger
AT&T Bell Laboratories
Murray Hill, NJ 07974

P. C. Stair
Department of Chemistry
Northwestern University
2145 Sheridan Road
Evanston, IL 60208-3113

R. M. Stratt
Department of Chemistry
Brown University
324 Brook Street, Box H
Providence, RI 02912

No. of Copies

E. M. Stuve
Department of Chemical Engineering
University of Washington BF-10
Seattle, WA 98195

J. A. Syage
Propulsion & Environmental Science Lab - M5-754
Aerospace Corporation
P.O. Box 92957
Los Angeles, CA 90009-92957

I. Thomas
ER-13, J-317/GTN
U.S. Department of Energy
19901 Germantown Road
Germantown, MD 20874

T. Torgersen
Engineering & Geosciences Division
Office of Basic Energy Sciences
Office of Energy Research
U.S. Department of Energy
Washington, D.C. 20545

S. Traina
Agronomy Department
Ohio State University
2021 Coffey Road
Columbus, OH 43210

F. P. Tully
Div. 8353
Combustion Research Facility
Sandia National Laboratories
Livermore, CA 94551-0969

J. Tully
AT&T Bell Laboratories
600 Mountain Avenue
Murray Hill, NJ 07974

V. Vaida
Department of Chemistry
University of Colorado
Boulder, CO 80309

No. of Copies

S. P. Walch
NASA Ames Research Center
Moffett Field, CA 94035

E. A. Walters
Department of Chemistry
University of New Mexico
Albuquerque, NM 87131

F. B. Wampler
Mail Stop J515
Los Alamos National Laboratory
P.O. Box 1663
Los Alamos, NM 87545

R. O. Watts
School of Chemistry
University of Melbourne
Parkville Victoria 3052
Australia

J. Weaver
Department of Chemical Engineering and Materials Science
University of Minnesota
Minneapolis, MN 55455

H. W. Weinberg
Department of Chemical and Nuclear Engineering
University of California, Santa Barbara
Santa Barbara, CA 93106

J. C. Weisshaar
Department of Chemistry
University of Wisconsin
1101 University Avenue
Madison, WI 53706

K. B. Whaley
Department of Chemistry
University of California
Berkeley, CA 94720

No. of Copies

R. L. Whetten
School of Chemistry and Biochemistry
Boggs Chemistry Building
Georgia Institute of Technology
Atlanta, GA 30332-0400

T. Whitaker
Department of Chemistry
BG-10
University of Washington
Seattle, WA 98105

M. G. White
Department of Chemistry
Brookhaven National Laboratory
Upton, NY 11973

K. Wiberg
Yale University
225 Prospect Street
New Haven, CT 06511

R. Willitt
Department of Chemistry
Washington State University
Pullman, WA 99164

M. W. Windsor
Department of Chemistry
Washington State University
Pullman, WA 99164

C. Wittig
Department of Chemistry, SSC-403
University of Southern California
Los Angeles, CA 90089-0482

S. M. Wolf
EM-542, 413/TREV
U.S. Department of Energy
12800 Middlebrook Road
Germantown, MD 20874

No. of Copies

J. C. Wooley
Office of Health and Environmental Research
Office of Energy Research
U.S. Department of Energy
Washington, D.C. 20545

J. T. Yates
Director, Pittsburgh Surface Science Center
Department of Chemistry
University of Pittsburgh
Pittsburgh, PA 15260

W. A. Yee
Department of Chemistry
Santa Clara University
Santa Clara, CA 95053

R. N. Zare
Department of Chemistry
Stanford University
Stanford, CA 94305-5080

A. H. Zewail
Department of Chemistry
Cal Tech
Pasadena, CA 91125

L. D. Ziegler
Department of Chemistry
Northeastern University
Boston, MA 02115

T. S. Zwier
Department of Chemistry
Purdue University
West Lafayette, IN 47907

No. of Copies

ONSITE

5 **DOE Richland Operations Office**

H. E. Bell A5-90
P. W. Kruger K8-50
J. P. Neath K8-50
J. J. Sutey K8-50
D. E. Trader K8-50

257 **Pacific Northwest Laboratory**

W. J. Apley P7-75
J. F. Bagley K1-66
R. A. Bair K1-87
S. E. Barlow K2-14
J. W. Bixler K9-56
T. A. Blake K3-58
S. D. Colson (50) K2-14
C. A. Counts (50) K2-20
J. P. Cowin K2-14
T. H. Dunning, Jr. (5) K2-20
P. D. Ellis P7-55
T. Foley K2-18
T. R. Fox K6-48
D. M. Friedrich K2-14
B. C. Garrett K1-83
M. J. Graham K9-38
J. S. Hartman K5-25
A. C. Hess K1-83
W. P. Hess K2-14
G. R. Holtom K2-14

No. of Copies

J. Janata K2-12
A. G. Joly K2-14
D. R. Jones K1-96
S. A. Joyce K2-14
B. D. Kay K2-14
M. L. Knotek K1-48
W. W. Laity K2-50
W. J. Madia K1-46
R. S. McDowell (100) K2-14
G. L. McVay K2-45
R. L. Ornstein K2-01
E. W. Pearson K1-72
G. R. Petersen K1-71
R. K. Quinn K9-69
D. Ray K2-14
J.T.A. Roberts K9-78
S. Rawson K9-34
S. W. Sharpe K3-58
A. A. Shepherd K1-33
B. D. Shipp K9-01
R. L. Skaggs K9-34
C. S. Sloane K9-34
R. S. Smith K2-14
J. D. Spencer K1-41
G. M. Stokes K1-74
B. R. Stults K1-65
R. G. Tonkyn K2-14
R. A. Walters K1-50
L. S. Wang K2-14
W. R. Wiley K9-95
G. L. Work K1-52
Technical Report Files (5)